

**Associate Editor Decision: Publish subject to minor revisions (review by editor) (18 Dec 2019)**

**by Wiebke Frey**

Comments to the Author:

Dear Fan Mei et al.,

thanks for your revisions. Following up on these, I have a some more comments, see below.

**Response: We sincerely appreciate the comments and suggestions from our associate editor Wiebke Frey. Thank you very much for considering the publication of our manuscript. We address your comments below (also in blue). Note that the included line number is based on the mark-up version, which may be different from the final version.**

Main comments:

1) With regard to the last reviewers comments about ground comparisons, I have the impression that you did not fully address the question. From how I understand your answer, comparisons to ground instrumentation had not been carried out, right? Why not? You refer to the ground site a number of times in your manuscript (e.g lines 31-33, lines 66-71, l 83/84, l 563-565, l 581-584) which makes me wonder why there was no comparison of ground based and airborne data. Such comparison might have given an even more comprehensive view on the reliability of the airborne data. Please also add a comment on the (missing?) comparison in the manuscript (and possibly a recommendation in the summary?).

**Response: The last reviewer's comments are on the comparison of the similar instruments deployed on G1 and HALO side by side on the ground, as in a typical setting of a lab-based comparison study. We clarified that we did not perform such a comparison due to logistic difficulties. It would also be beneficial to compare similar instruments deployed at the ground site and those aboard aircraft side by side. Unfortunately, we did not get a chance to do that either.**

**We agree with the editor that a comparison of the aircraft measurements with similar measurements from the ground site (i.e., when aircraft overflew the site) might provide a more comprehensive view of the reliability of the airborne data. However, such a comparison will also be influenced by the spatial variations (both vertical and horizontal). We found that how we define the "flew over" area would affect the comparison results. A comprehensive comparison between the aircraft and ground measurements will go beyond the scope of the current study. We appreciate the excellent suggestion from the editor and added the below recommendation in the summary section (line 803-805). "A side-by-side comparison among the similar instruments deployed at different platforms, including those at ground sites is highly recommended and will provide a comprehensive view of the data reliability."**

2) Numbering:

There are several instances where I find the numbering does not follow the usual order. Starting with the numbering of author affiliations - the third affiliation that appears in the author list is number 13

and not, as I would expect, number 3.

Table S2 and S3 are mentioned in the manuscript before S1. Also some of the figures in the supplement are at higher numbers than others that get mentioned later.

So please check numbering of author affiliations, Figures, and Tables, also in the supplement.

**Response: We have revised the manuscript and the supplement. For example, we revised the order of the author's affiliations and the supplemental tables (in the manuscript line 122).**

3) Supplement:

The supplement reads as if the collection of sections/figures/tables was not always updated after an iteration of the review. Please treat the supplement with the same care as the main manuscript, keep in mind, that the supplement is published along with the final paper.

For some Sections of the supplement, I could not find references to it in the main manuscript. Either include references (e.g. to Section S1) in the main manuscript, or remove from the supplement. Actually, I could only find references to the flight on October 1 (without mentioning the exact position/section in the supplement), Table S2 and S3, and Figures S13 and S14.

**Response: We have revised the content and the figures in the supplement. We removed the section S3 and included more details with the below responses for each specific comment.**

Further comments:

I 115: trace gases concentrations -> trace gas concentrations

**Response: Corrected in the current Line 117.**

I 141: this comparson -> the comparison

**Response: Corrected in the current Line 143.**

I 242: number of small shattered particles (remove brackets)

**Response: Corrected in the current Line 244.**

I 269: developed by Weigel et al. (2016) -> move opening bracket

**Response: Corrected in the current Line 271.**

I 299: The other coordinated flight on October 1 is included in the supplemental document. -> Please include references to specific text/Section and Figures in supplement.

**Response: The reference to Figure S1 and S2 is in line 302 of the main manuscript. The reference to Figure S3-S5 is in line 418 of the main manuscript. The reference to Figure S6 is in line 121 and 130 of the supplemental material. The reference to Figure S7 and S8 is in both lines 302 and 547 of the main manuscript. The reference to Figure S9 is in line 167-168 of the supplemental material. The reference to Figure S10 is in line 172 of the supplemental material. The reference to Figure S11 and S12 is in line 590 of the main manuscript. The**

reference to Figure S13 is in line 652 of the main manuscript. The reference to Figure S14 is in line 674 of the main manuscript. The reference to section S1 is in line 302. The reference to section S2 is in line 546. The reference to section S3 is in line 566. The reference to the table S1 and S2 is in line 123. The reference to the table S3 is in line 717.

I 360/361: variation of the G1 altitude flight legs when the G1 flew around 50m/s higher...  
Do you mean 'altitude' and 'higher' or 'flight speed' and 'faster'?

**Response: Changed to “faster” in the current Line 364.**

I 362/363: You argue that the G1 has a larger standard deviation in pressure due to the faster flight speed than normal - but HALO flew slower than normal (lines 304/305), would that not also be a possible source for increased errors in HALO observations?

**Response: When the G1 flew at a faster airspeed, it did not maintain the altitude as good as HALO, which flew at a slower airspeed. Thus, the substantial variation of the G1 altitude contributed to the larger standard deviation in the G1 pressure measurements.**

I 374: Two regression results in Table 4 doesn't -> don't

**Response: Changed to “don’t” in the current Line 377.**

I 377: Figure 4 - see comment 2)

**Response: Figure 3 is in line 315. Figure 4 is in the current line 381. And figure 5 is in line 411.**

I 385: chilled mirror hydrometer - hygrometer?

**Response: Changed to “hygrometer” in the current Line 389.**

I 395: different saturations: How do you think will saturations impact on wind speed measurements?

**Response: The different saturations during the evaporation-condensation processes will affect the ambient temperature measurement and differential pressure measurements. Then due to the error propagation, it will affect the derived wind speed.**

I 447: The first criterion is the same criterion - maybe repeat it here with a few words.

**Response: Changed to “The first criterion is the same criterion described in the previous section that makes sure all the compared measurements happen in less than 30 minutes apart.” in the current line 452-453.**

I 454: Should the references in brackets be in the sentence? Move point back.

**Response: Corrected in the current Line 459.**

I 488: You sometimes say 'cloud-free flight' and sometimes you say the dates of the flights, please be consistent.

**Response: changed to “cloud-free flight on September 9” in the current line 303, 402, 443, and 493.**

I 566: 0.17+-0.06 derived -> space missing

**Response: Corrected in the current Line 571.**

I 582: Figure 3, two aircraft -> both aircraft...

**Response: Changed to “both” in the current line 588.**

I 584: see comment 2)

**Response: Changed to “Figure S11 and Figure S12”.**

I 636: You used a correction for coincidences on the FCDP data? In lines 596-598 you explicitly say that coincidence bias should not be considered for the cloud probe measurements to avoid deviations caused by application of different corrections!

**Response: for the G1 flights, we applied the coincidence correction to the final FCDP data product, which the user can access online. However, for the comparison in this paper, we used the FCDP data without applying the coincidence correction. We added “in the final data product” to line 642.**

I 701: This will lead to a considerable uncertainty ... -> add 'to'?

**Response: added “to” in the current Line 708.**

I 702-704: Can you elaborate why "especially for the regional or small scale modelling work"? For example, if someone does a modelling case study of a specific convective cloud, wouldn't more routine or long term measurements smear out the specifics/characteristics of that particular case study storm?

**Response: We try to point out that the modeling evaluation should not be based on the data from a single flight, but the data from more routine and long-term flights. To confirm any physical features in the regional model should require more flights over the region. Changed to “Thus, to evaluate or constrain atmospheric modeling work, more routine and long-term airborne measurements should be used to provide statistically sufficient observation.” In the current line 709-712.**

I 730: The UHSAS measurements ... (plural - two instruments being compared), same for CPC measurements.

**Response: Corrected in the current Line 738-739.**

Supplement:

Figures: Please move the Figures to the appropriate text within the Supplement, e.g. Figure 3 to Section S2 - CCN closure.

**Response: We revised the whole document and rearranged the figures.**

I 24: described by Mei et al. (2013b). -> brackets missing

**Response: Corrected in the current Line 165.**

I 24: CCN number concentration (typo)

**Response: Corrected in the current Line 166.**

I 26/27: Figures S3(a) and S3(b) (not Figure 3S...)

**Response: Corrected in the current Line 167 and 168.**

Figures S3 and S4: Please include 1:1 lines for guidance.

**Response: Revised the current figure S9.**

Section S3:

I have to admit, that I am highly skeptical about this section: Extrapolation of aerosol size distributions towards the smaller sizes should in my opinion not be done. The extrapolation is extremely uncertain, as you have to make assumptions about whether sources (particle formation events!) or sinks are present. As I cannot find a link to this section from the main manuscript, I suggest removing this section.

**Response: Removed the aerosol size distribution section.**

I 104: What is "AB, IE, and RIE"?

**Response: Corrected in the current Line 102 -103 .**

I 107-114: Sorry, but this part sounds like copy & paste from an email. Please keep in mind that the supplement will be part of the published manuscript and should be written like such. Please rephrase!

**Response: We are sorry that we sent a wrong version of the supplemental material to Lorena after the first version crashed. We included the revised version in the current line 98 – 114.**

I 117: the inlet flow was kept constant -> keep tense as in the other sentences before/after.

**Response: Corrected in the current Line 117.**

I 134: (Molleker, S., in prep.) -> still in preparation or submitted in meantime?

**Response: Yes, it is still in preparation, but close to submit.**

Figures:

Please check for consistency in axis labelling (N, #/cc vs N, cm<sup>-3</sup> for example), and for full axis labelling (some axes do not have labels at all).

**Response: Revised figure S3-S5, S11 and S12.**

S5-7: Occurrence not occurrence, why Frequency and not Occurrence in Fig 6a?

**Response: Corrected the current figure S3-S5.**

S11: Would be better to plot similar to S3 (N vs N with altitude as colour code), including 1:1 line.

**Response: Removed the previous S11 with the section S3.**

Table S2 and S3, cloud probes: In the manuscript you state that the G1 cloud probes were calibrated biweekly, in the supplement you write weekly calibration. For HALO cloud probes (e.g. the two CIPgs instruments) you state spinning disk calibrations before or after each flight, again, weekly calibration stated in the table. Please be consistent! What is the real frequency of calibration?

**Response: Corrected the errors in the previous table S2 and S3 (now table S1, S2), and the main manuscript in the current line 123 and 246.**

## Comparison of Aircraft Measurements during GoAmazon2014/5 and ACRIDICON-CHUVA

Fan Mei<sup>1</sup>, Jian Wang<sup>2, 156</sup>, Jennifer M. Comstock<sup>1</sup>, Ralf Weigel<sup>3</sup>, Martina Krämer<sup>4, 3</sup>, Christoph Mahnke<sup>3, 5</sup>, John E. Shilling<sup>1</sup>, Johannes Schneider<sup>5</sup>, Christiane Schulz<sup>5</sup>, Charles N. Long<sup>6</sup>, Manfred Wendisch<sup>7</sup>, Luiz A. T. Machado<sup>8</sup>, Beat Schmid<sup>1</sup>, Trismono Krisna<sup>7</sup>, Mikhail Pekour<sup>1</sup>, John Hubbe<sup>1</sup>, Andreas Giez<sup>9</sup>, Bernadett Weinzierl<sup>109</sup>, Martin Zoeger<sup>9</sup>, Mira L. Pöhlker<sup>5</sup>, Hans Schlager<sup>9</sup>, Micael A. Cecchini<sup>101</sup>, Meinrat O. Andreae<sup>5, 124</sup>, Scot T. Martin<sup>133</sup>, Suzane, S. de Sá<sup>123</sup>, Jiwen Fan<sup>1</sup>, Jason Tomlinson<sup>1</sup>, Stephen Springston<sup>2</sup>, Ulrich Pöschl<sup>5</sup>, Paulo Artaxo<sup>143</sup>, Christopher Pöhlker<sup>5</sup>, Thomas Klimach<sup>5</sup>, Andreas Minikin<sup>124</sup>, Armin Afchine<sup>4</sup>, Stephan Borrmann<sup>3, 5</sup>

1. Pacific Northwest National Laboratory, Richland, WA, United States.
2. Brookhaven National Laboratory, Upton, NY, United States.
3. Institute for Physics of the Atmosphere, Johannes Gutenberg University, Mainz, Germany
4. Research Centre Jülich, Institute for Energy and Climate Research 7: Stratosphere (IEK-7), Jülich, Germany
5. Max Planck Institute for Chemistry, Mainz, Germany
6. NOAA ESRL GMD/CIRES, Boulder, CO, United States
7. University of Leipzig, Leipzig, Germany
8. National Institute for Space Research (INPE), São Paulo, Brazil
9. Deutsches Zentrum für Luft- und Raumfahrt (DLR), Oberpfaffenhofen, Germany
- 9-10. University of Vienna, Vienna, Austria
- 10-11. University of São Paulo (USP), São Paulo, Brazil
- 11-12. Scripps Institution of Oceanography, University of California San Diego, La Jolla, California, USA
- 12-13. Harvard University, Cambridge, MA, United States
- 13-14. Instituto de Física, Universidade de São Paulo, São Paulo, Brazil
- 14-15. DLR Oberpfaffenhofen, Flight Experiments Facility, Wessling, Germany
- 15-16. Center for Aerosol Science and Engineering, Department of Energy, Environmental and Chemical Engineering, Washington University in St. Louis, St. Louis, Missouri, USA

Correspondence to: Fan Mei (fan.mei@pnnl.gov)

**Abstract.** The indirect effect of atmospheric aerosol particles on the Earth's radiation balance remains one of the most uncertain components affecting climate change throughout the industrial period. The large uncertainty is partly due to the incomplete understanding of aerosol-cloud interactions. One objective of the GoAmazon2014/5 and ACRIDICON-CHUVA projects was to

understand the influence of ~~the~~ emissions from the tropical megacity of Manaus (Brazil) on the surrounding atmospheric environment of the rainforest and to investigate its role in the life cycle of convective clouds. During one of the intensive observation periods (IOPs) in the dry season from September 1 to October 10, 2014, comprehensive measurements of trace gases and aerosol properties were carried out at several ground sites. In a coordinated way, the advanced suites of sophisticated in situ instruments were deployed aboard both the U.S. Department of Energy Gulfstream-1 (G1) aircraft and the German High Altitude and Long-Range Research Aircraft (HALO) during three coordinated flights on September 9, 21, and October 1. Here we report on the comparison of measurements collected by the two aircraft during these three flights. Such comparisons are challenging but essential for assessing the data quality from the individual platforms and quantifying their uncertainty sources. Similar instruments mounted on the G1 and HALO collected vertical profile measurements of aerosol particles number concentrations and size distribution, cloud condensation nuclei concentrations, ozone and carbon monoxide mixing ratios, cloud droplet size distributions, and downward solar irradiance. We find that the above measurements from the two aircraft agreed within the measurement uncertainties. The relative fraction of the ~~a~~aerosol chemical composition measured by instruments on HALO agreed with the corresponding G1 data, although the total mass loadings only have a good agreement at high altitudes. Furthermore, possible causes of the discrepancies between measurements on the G1 and HALO are examined in this paper. Based on these results, criteria for meaningful aircraft measurement comparisons are discussed.

## 1. Introduction

Dominated by biogenic sources, the Amazon basin is one of the few remaining continental regions where atmospheric conditions realistically represent those of the pristine or pre-industrial era (Andreae et al., 2015). As a natural climatic “chamber”, the area around the urban region of Manaus in central Amazonia is an ideal location for studying the atmosphere under natural conditions as well as under conditions influenced by human activities and biomass burning events (Andreae et al., 2015; Artaxo et al., 2013; Davidson et al., 2012; Keller et al., 2009; Kuhn et al., 2010; Martin et al., 2016b; Pöhlker et al., 2018; Poschl et al., 2010; Salati and Vose, 1984). The Observations and Modeling of the Green Ocean Amazon (GoAmazon2014/5) campaign was



conducted in 2014 and 2015 (Martin et al., 2017; Martin et al., 2016b). The primary objective of GoAmazon2014/5 was to improve the quantitative understanding of the effects of anthropogenic influences on atmospheric chemistry and aerosol-cloud interactions in the tropical rainforest area. During the dry season in 2014, the ACRIDICON (Aerosol, Cloud, Precipitation, and Radiation Interactions and Dynamics of Convective Cloud Systems)-CHUVA (Cloud Processes of the Main Precipitation Systems in Brazil) campaign also took place to study tropical convective clouds and precipitation over Amazonia (Wendisch et al., 2016).

A feature of the GoAmazon 2014/5 field campaign was the design of the ground sites' location, which uses principles of Lagrangian sampling to align the sites with the Manaus pollution plume (Figure 1: Source location – Manaus (T1 site), and downwind location – Manacapuru (T3 site)). The ground sites were overflown with the low-altitude U.S. Department of Energy (DOE) Gulfstream-1 (G1) aircraft and the German High Altitude and Long Range Research Aircraft (HALO). These two aircraft are among the most advanced in atmospheric research, deploying suites of sophisticated and well-calibrated instruments (Schmid et al., 2014; Wendisch et al., 2016). The pollution plume from Manaus was intensively sampled during the G1 and HALO flights and also by the DOE Atmospheric Radiation Measurement (ARM) program Mobile Aerosol Observing System and ARM Mobile Facility located at one of the downwind surface sites (T3 site- 70 km west of Manaus). The routine ground measurements with coordinated and intensive observations from both aircraft provided an extensive data set of multi-dimensional observations in the region, which serves i) to improve the scientific understanding of the influence of the emissions of the tropical megacity of Manaus (Brazil) on the surrounding atmospheric environment of the rainforest and ii) to understand the life cycle of deep convective clouds and study open questions related to their influence on the atmospheric energy budget and hydrological cycle.

As more and more data sets are merged to link the ground-based measurements with aircraft observations, and as more studies focus on the spatial variation and temporal evolution of the atmospheric properties, it is critical to quantify the uncertainty ranges when combining the data collected from the different platforms. Due to the challenges of airborne operations, especially when two aircraft are involved in data collection in the same area, direct comparison studies are rare. However, this type of research is critical for further combining the datasets between the ground sites and aircraft. Thus, the main objectives of the study herein are to demonstrate how to

achieve meaningful comparisons between two moving platforms, to conduct detailed comparisons between data collected by two aircraft, to identify the potential measurement issues, to quantify reasonable uncertainty ranges of the extensive collection of measurements, and to evaluate the measurement sensitivities to the temporal and spatial variance. The comparisons and the related uncertainty estimations quantify the current measurement limits, which provide realistic measurement ranges to climate models as initial conditions to evaluate their output.

The combined GoAmazon2014/5 and ACRIDICON-CHUVA field campaigns not only provide critical measurements of aerosol and cloud properties in an under-sampled geographic region but also offer a unique opportunity to understand and quantify the quality of these measurements using carefully orchestrated comparison flights. The comparisons between the measurements from similar instruments on the two research aircraft can be used to identify potential measurement issues and quantify the uncertainty range of the field measurements, which include primary meteorological variables (Section 3.1), trace gases concentrations (Section 3.2), aerosol particle properties (number concentration, size distribution, chemical composition, and microphysical properties) (Section 3.3), cloud properties (Section 3.4), and downward solar irradiance (Section 3.5). We evaluate the consistency between the measurements aboard the two aircraft for a nearly full set of gas, aerosol particle, and cloud variables. Results from this comparison study provide the foundation not only for assessing and interpreting the observations from multiple platforms (from the ground to low altitude, and then to high altitude) but also for providing high-quality data to improve the understanding of the accuracy of the measurements related to the effects of human activities in Manaus on local air quality, terrestrial ecosystems in rainforest, and tropical weather.

## **2. Measurements**

### **2.1 Instruments**

The ARM Aerial Facility deployed several in situ instruments on the G1 to measure atmospheric state parameters, trace gases concentrations, aerosol particle properties, and cloud characteristics (Martin et al., 2016b; Schmid et al., 2014). The instruments installed on HALO covered measurements of meteorological, chemical, microphysical, and radiation parameters. Details of measurements aboard HALO are discussed in the ACRIDICON-CHUVA campaign overview paper (Wendisch et al., 2016). The measurements compared between the G1 and HALO

are listed in Table 1. Details on maintenance and calibration of the involved instrumentation can be found in the supplement (Table S12 and Table S23).

#### 2.1.1 Atmospheric parameters

All G1 and HALO meteorological sensors were routinely calibrated to maintain measurement accuracy. The G1 primary meteorological data were provided at one-second time resolution based on the standard developed by the Inter-Agency Working Group for Airborne Data and Telemetry Systems (Webster and Freudinger, 2018). For static temperature measurement, the uncertainty given by the manufacturer (Emerson) is  $\pm 0.1$  K, and the uncertainty of the field data is  $\pm 0.5$  K. The static pressure had a measurement uncertainty of 0.5 hPa. The standard measurement uncertainties were  $\pm 2$  K for the chilled mirror hygrometer and  $0.5 \text{ ms}^{-1}$  for wind speed.

On HALO, primary meteorological data were obtained from the Basic HALO Measurement and Sensor System (BAHAMAS) at one-second time resolution. The system acquired data from airflow and thermodynamic sensors and from the aircraft avionics and a high-precision inertial reference system to derive the basic meteorological parameters like pressure, temperature, the 3D wind vector, aircraft position, and attitude. Water vapor mixing ratio and further derived humidity quantities were measured by the Sophisticated Hygrometer for Atmospheric Research (SHARC) based on direct absorption measurement by a tunable diode laser (TDL) system. The absolute accuracy of the primary meteorological data was 0.5 K for air temperature, 0.3 hPa for air pressure,  $0.4\text{--}0.6 \text{ ms}^{-1}$  for wind, and 5% ( $\pm 1$  ppm) for water vapor mixing ratio. All sensors were routinely calibrated and traceable to national standards (Giez et al., 2017; Krautstrunk and Giez, 2012).

#### 2.1.2 Gas phase

Constrained by data availability, ~~this~~the comparison of trace gas measurements is focused on carbon monoxide (CO) and ozone (O<sub>3</sub>) concentrations. Those measurements were made aboard the G1 by a CO/N<sub>2</sub>O/H<sub>2</sub>O instrument (Los Gatos Integrated Cavity Output Spectroscopy instrument model 907-0015-0001), and an Ozone Analyzer (Thermo Scientific, Model 49i), respectively. The G1 CO analyzer was calibrated for response daily by NIST-traceable commercial standards before the flight. Due to the difference between laboratory and field conditions, the uncertainty of the CO measurements is about  $\pm 5\%$  for one-second sampling periods. An ultra-fast carbon monoxide monitor (Aero Laser GmbH, AL5002) was deployed on HALO. The detection

151 of CO is based on a vacuum-ultraviolet-fluorimetry, employing the excitation of CO at 150 nm,  
152 and the precision is 2 ppb, and the accuracy is about 5%. The ozone analyzer measures ozone  
153 concentration based on the absorbance of ultraviolet light at a wavelength of 254 nm. The ozone  
154 analyzer (Thermo Scientific, Model 49c) in the HALO payload is very similar to the one on the  
155 G1 (Model 49i), with an accuracy greater than 2 ppb or about  $\pm 5\%$  for four-second sampling  
156 periods. The G1 ozone monitor was calibrated at the New York State Department of  
157 Environmental Conservation testing laboratory at Albany.

### 158 2.1.3 Aerosol

159 Aerosol number concentration was measured by different condensation particle counters  
160 (CPCs) on the G1 (TSI, CPC 3010) and HALO (Grimm, CPC model 5.410). Although two CPCs  
161 were from different manufacturers, they were designed using the same principle, which is to detect  
162 particles by condensing butanol vapor on the particles to grow them to a large enough size that  
163 they can be counted optically. Both CPCs were routinely calibrated in the lab and reported the data  
164 at one-second time resolution. The HALO CPC operated at  $0.6\text{--}1\text{ L min}^{-1}$ , with a nominal cutoff  
165 of 4 nm. Due to inlet losses, the effective cutoff diameter increases to 9.2 nm at 1000 hPa, and  
166 11.2 nm at 500 hPa (Andreae et al., 2018; Petzold et al., 2011). The G1 CPC operated at  $1\text{ L min}^{-1}$   
167 volumetric flow rate and the nominal cut-off diameter  $D_{50}$  measured in the lab was  $\sim 10\text{ nm}$ .  
168 During a flight, the cut-off diameter may vary due to tubing losses, which contributes less than 10  
169 % uncertainty to the comparison between two CPC concentrations.

170 Two instruments deployed on the G1 measured aerosol particle size distribution. a Fast  
171 Integrated Mobility Spectrometer (FIMS) inside of the G1 cabin measured the aerosol mobility  
172 size from 15 to 400 nm (Kulkarni and Wang, 2006a, b; Olfert et al., 2008; Wang, 2009). The  
173 ambient aerosol particles were charged after entering the FIMS inlet and then separated into  
174 different trajectories in an electric field based on their electrical mobility. The spatially separated  
175 particles grow into super-micrometer droplets in a condenser where supersaturation of the working  
176 fluid is generated by cooling. At the exit of the condenser, a high-speed charge-coupled device  
177 camera captures the image of an illuminated grown droplet at high resolution. In this study, we  
178 used the FIMS 1 Hz data for comparison. The size distribution data from FIMS were smoothed.  
179 Aside from the FIMS, the airborne version of the Ultra High Sensitivity Aerosol Spectrometer  
180 (UHSAS) was deployed on G1 and HALO. The G1 and HALO UHSAS were manufactured by

the same company, and both were mounted under the wing on a pylon. UHSAS is an optical-scattering, laser-based particle spectrometer system. The size resolution is around 5% of the particle size. The G1 UHSAS typically covered a size range of 60 nm to 1000 nm. HALO UHSAS covered 90 nm to 500 nm size range for the September 9 flight.

Based on operating principles, FIMS measures aerosol electrical mobility size and UHSAS measures the aerosol optical equivalent size. Thus, the difference in the averaged size distributions from those two types of instruments might be linked to differences in their underlying operating principles, such as the assumption in the optical properties of aerosol particles. The data processing in the G1 UHSAS assumed that the particle refractive index is similar to ammonium sulfate (1.55), which is larger than the average refractive index (1.41-0.013i) from a previous Amazon study (Guyon et al., 2003). The HALO UHSAS was calibrated with polystyrene latex spheres, which have a refractive index about 1.572 for the UHSAS wavelength of 1054 nm. The uncertainty due to the refraction index can lead to up to 10% variation in UHSAS measured size (Kupc et al., 2018). Also, the assumption of spherical particles affects the accuracy of UHSAS sizing of ambient aerosols.

The chemical composition of submicron non-refractory (NR-PM<sub>1</sub>) organic and inorganic (sulfate, nitrate, ammonium) aerosol particles was measured using a high-resolution time-of-flight aerosol mass spectrometer (HR-ToF-AMS) aboard the G1 (DeCarlo et al., 2006; Jayne et al., 2000; Shilling et al., 2018; Shilling et al., 2013). Based on the standard deviation of observed aerosol mass loadings during filter measurements, the HR-ToF-AMS detection limits for the average time of thirteen seconds are approximately 0.13, 0.01, 0.02, 0.01 (3 $\sigma$  values)  $\mu\text{g m}^{-3}$  for organic, sulfate, nitrate, and ammonium, respectively (DeCarlo et al., 2006). A Compact Time-of-flight Aerosol Mass Spectrometer (C-ToF-AMS) was operated aboard HALO to investigate the aerosol composition. Aerosol particles enter both the C-ToF-AMS and HR-ToF-AMS via constant pressure inlets controlling the volumetric flow into the instrument, although the designs of the inlets are somewhat different (Bahreini et al., 2008). The details about the C-ToF-AMS operation and data analysis are reported in Schulz's paper (Schulz et al., 2018). The overall accuracy has been reported as ~30 % for both AMS instruments (Alfarra et al., 2004; Middlebrook et al., 2012). Data presented in this section were converted to the same condition as the HALO AMS data, which is 995 hPa and 300 K. Both AMS instruments were calibrated before and after the field deployment and also once a week during the field campaign.

212 The number concentration of cloud condensation nuclei (CCN) was measured aboard both  
213 aircraft using the same type of CCN counter from Droplet Measurement Technologies (DMT,  
214 model 200). This CCN counter contains two continuous-flow, thermal-gradient diffusion  
215 chambers for measuring aerosols that can be activated at constant supersaturation. The  
216 supersaturation is created by taking advantage of the different diffusion rates between water vapor  
217 and heat. After the supersaturated water vapor condenses on the CCN in the sample air, droplets  
218 are formed, counted, and sized by an Optical Particle Counter (OPC). The sampling frequency is  
219 one second for both deployed CCN counters. Both CCN counters were calibrated using ammonium  
220 sulfate aerosol particles in the diameter range of 20-200 nm. The uncertainty of the effective water  
221 vapor supersaturation was  $\pm 5\%$ . (Rose et al., 2008)

#### 222 2.1.4 Clouds

223 Aircraft-based measurements are an essential method for in situ samplings of cloud properties  
224 (Brenguier et al., 2013; Wendisch and Brenguier, 2013). Over the last 50–60 years, hot-wire probes  
225 have been the most commonly used devices to estimate liquid water content (LWC) in the cloud  
226 from research aircraft. Since the 1970s, the most widely used technique for cloud droplet spectra  
227 measurements has been developed based on the light-scattering effect. This type of instrument  
228 provides the cloud droplet size distribution as the primary measurement. By integrating the cloud  
229 droplet size distribution, additional information, such as LWC can be derived from the high-order  
230 data product.

231 Three cloud probes from the G1 are discussed in this manuscript. The Cloud Droplet Probe  
232 (CDP) is a compact, lightweight forward-scattering cloud particle spectrometer that measures  
233 cloud droplets in the 2 to 50  $\mu\text{m}$  size range (Faber et al., 2018). Using state-of-the-art electro-optics  
234 and electronics, Stratton Park Engineering (SPEC Inc.) developed a Fast Cloud Droplet Probe  
235 (FCDP), which also use forward-scattering to determine cloud droplet distributions and  
236 concentrations in the same range as CDP with up to 100 Hz sampling rate. The G1 also carried a  
237 two-dimensional stereo probe (2DS, SPEC Inc.), which has two 128-photodiode linear arrays  
238 working independently. The 2DS electronics produce shadowgraph images with 10  $\mu\text{m}$  pixel  
239 resolution. Two orthogonal laser beams cross in the middle of the sample volume, with the sample  
240 cross section for each optical path of 0.8  $\text{cm}^2$ . The manufacturer claims the maximum detection

size is up to 3000  $\mu\text{m}$  for the 2DS. However, due to the counting statistic issue, the data used in this study is from 10–1000  $\mu\text{m}$  only (Lawson et al., 2006). 2DS was upgraded with modified probe tips, and an arrival time algorithm was applied to the 2DS data processing. Both efforts effectively reduced the number of small ~~(shattered)~~ particles (Lawson, 2011). For G1 cloud probes, the laboratory calibrations of the sample area and droplet sizing were performed before the field deployment. During the deployment, ~~bi~~weekly calibrations with glass beads were performed with the size variation of less than 5%, which were consistent with the pre-campaign and after-campaign calibrations. Comparison between the LWC derived from cloud droplet spectra with hot-wire LWC measurement was made to estimate/eliminate the coincidence errors in cloud droplet concentration measurements (Lance et al., 2010; Wendisch et al., 1996)

On board of HALO, two cloud probes were operated and discussed in this manuscript, each consisting of a combination of two instruments: Cloud Combination Probe (CCP) and a Cloud Aerosol Precipitation Spectrometer (CAPS, denoted as NIXE-CAPS; NIXE: Novel Ice Experiment). The CCP is a combination of a CDP (denoted as CCP-CDP) with a CIPgs (Cloud Imaging Probe with greyscale, DMT, denoted as CCP-CIPgs). NIXE-CAPS consists of a CAS-Dpol (Cloud and Aerosol Spectrometer, DMT, denoted as NIXE-CAS) and a CIPgs (denoted as NIXE-CIPgs). CIPgs is an optical array probe comparable to the 2DS operated on the G1. CIPgs obtains images of cloud elements using a 64-element photodiode array (15 $\mu\text{m}$  resolution) to generate two-dimensional images with nominal detection diameter size range from 15 to 960  $\mu\text{m}$  (Klingebiel et al., 2015; Molleker et al., 2014). The CCP-CDP detects the forward-scattered laser light by cloud particles in the size range of 2.5 to 46  $\mu\text{m}$ . The sample area of the CCP- CDP was determined to be  $0.27\pm0.025\text{ mm}^2$  with an uncertainty of less than 10% (Klingebiel et al., 2015). CAS-Dpol (or NIXE-CAS) is a light scattering probe comparable to the CDP but covers the size range of 0.6 to 50  $\mu\text{m}$  in diameter, thus including the upper size range of the aerosol particle size spectrum (Luebke et al., 2016). Furthermore, CAS-Dpol measures the polarization state of the particles (Costa et al., 2017). Correspondingly to the G1 CDP, the performance of the CCP-CDP and NIXE-CAS were frequently examined by glass beads calibrations. Prior to or after each HALO flight, CCP-CIPgs and NIXE-CIPgs calibrations were performed by using a mainly transparent spinning disc that carries opaque spots of different but known size. The data of the CCP measured particle concentration on board of HALO are corrected to gain ambient conditions using a

thermodynamic approach developed by Weigel et al. (2016). For NIXE-CAPS, the size distributions were provided where NIXE-CAS was merged with the NIXE-CIPs at 20  $\mu\text{m}$ .

#### 2.1.5 Solar radiation

The G1 radiation suite included shortwave (SW, 400 - 2,700 nm) broadband total upward and downward irradiance measurements using Delta-T Devices model SPN-1 radiometers. The radiation data were corrected for aircraft tilt from the horizontal reference plane. A methodology has been developed (Long et al., 2010) for using measurements of total and diffuse shortwave irradiance and corresponding aircraft navigation data (latitude, longitude, pitch, roll, heading) to calculate and apply a correction for platform tilt to the broadband hemispheric downward SW measurements. Additionally, whatever angular offset there may be between the actual orientation of each radiometer's detector and what the navigation data say is level has also been determined for the most accurate tilt correction.

The Spectral Modular Airborne Radiation measurement system (SMART-Albedometer) was installed aboard HALO. Depending on the scientific objective and the configuration, the optical inlets determining the measured radiative quantities can be chosen. The SMART-Albedometer has been utilized to measure the spectral upward and downward irradiances; thereby, it is called as an albedometer, as well as to measure the spectral upward radiance. The SMART-Albedometer is designed initially to cover measurements in the solar spectral range between 300 and 2,200 nm (Krisna et al., 2018; Wendisch et al., 2001; Wendisch et al., 2016). However, due to decreasing sensitivity of the spectrometer at large wavelengths, the use of the wavelengths was restricted to 300 – 1,800 nm. The spectral resolution is defined by the full width at half maximum (FWHM), which is between 2 and 10 nm. In this case, the instruments were mounted on an active horizontal stabilization system for keeping the horizontal position of the optical inlets during aircraft movements (up to  $\pm 6$  degrees from the horizontal plane).

#### 2.2 Flight patterns

During the dry season IOP (September 1 – October 10, 2014), two types of coordinated flights were carried out: one flight in cloud-free condition (September 9) and two flights with clouds present (September 21 and October 1). In this study, we compare the measurements for both coordinated flight patterns. The discussion is mainly focused on the flights under cloud-free



conditions on September 9 and the flight with clouds present on September 21, as shown in figure 1. The other coordinated flight on October 1 is included in the supplemental document ([section S1, Figure S1, S2, S7, and S8](#)).

For the cloud-free coordinated flight [on September 9](#), the G1 took off first and orbited around an area from the planned rendezvous point until HALO arrived in sight. It then coordinated with HALO and performed a wing-to-wing maneuver along straight legs around 500 m above sea level, as shown in Figure 2. The normal G1 average sampling speed is  $100 \text{ m s}^{-1}$ , and the normal HALO average sampling speed is  $200 \text{ m s}^{-1}$ . During the coordinated flight on September 9, both aircraft also adjusted their normal sampling speed by about  $50 \text{ m s}^{-1}$  so that they could fly side by side.

For the second type of coordinated flights, the G1 and HALO flew the stacked pattern at their own typical airspeed. On September 21, the G1 also took off from the airport first, followed by HALO 15 minutes later. Then, both aircraft flew above the T3 ground site and subsequently flew several flight legs stacked at different altitudes. The two aircraft were vertically separated by about 330 m and sampled below, inside, and above clouds. Due to the different aircraft speeds, the time difference between two aircraft visiting the same part of the flight paths varied, increasing up to 1 hour at the end of the flight path, as shown in Figure 3. On October 1, the G1 focused on the cloud microphysical properties and contrasting polluted versus clean clouds. HALO devoted the flight to the cloud vertical evolution and life cycle and also probed the cloud processing of aerosol particles and trace gases. The G1 and HALO coordinated two flight legs between 950–1250 m above the T3 site under cloud-free conditions. Following that, HALO flew to the south of Amazonia, and the G1 continued sampling plume-influenced clouds above the T3 site, and then flew above the Rio Negro area.

In this study, to perform a meaningful comparison of in situ measurements, all the data from instruments were time-synchronized with the aircraft (G1 or HALO) navigation system. For AMS and CPC data, the time shifting due to tubing length and instrument flow had been corrected. For the coordinated flight on Sep. 9, the data compared was from the same type of measurements with the same sampling rate. For the measurements with the different sampling rate, the data were binned to the same time interval for comparison. For the flight with the cloud present (Sep.21 and Oct. 1), the following criteria are used: 1) the data collected by the two aircraft must be less than 30 mins apart from each other; 2) the comparison data were binned to 200 m altitude intervals; 3) the cloud flag was applied to the aerosol measurements, and the data affected by the cloud

shattering are eliminated from the comparisons of aerosol measurements. Moreover, additional comparison criteria are specified for individual measurements in the following section. Table 2 shows the total number of points used for the comparison.

### 3. Results

#### 3.1 Comparison of the G1 and HALO measurements of atmospheric state parameters

The atmospheric state parameters comprise primary variables observed by the research aircraft. The measurements provide essential meteorological information not only for understanding the atmospheric conditions but also for providing the sampling conditions for other measurements, such as those of aerosol particles, trace gases, and cloud microphysical properties.

For cloud-free coordinated flights, the comparison focused on the near side-by-side flight leg at around 500 m, as shown in Figure 2. Table 3 shows the basic statistics of the data for primary atmospheric state parameters, assuming that two measurements from the G1 and HALO have a proportional relationship without any offset ( $Y=m0*X$ ). In general, the atmospheric state parameters observed from both aircraft were in excellent agreement. The linear regression achieved a slope that was near 1 for four individual measurements. The regression is evaluated using the equation below.

$$R^2 = 1 - \frac{SS_{regression}}{SS_{Total}} \quad (1)$$

Where the sum squared regression error is calculated by  $SS_{regression} = \sum(y_i - y_{regression})^2$ , and the sum squared total error is calculated by  $SS_{Total} = \sum(y_i - \bar{y})^2$ ,  $y_i$  is the individual data point,  $\bar{y}$  is the mean value, and  $y_{regression}$  is the regression value. When the majority of the data points are in a narrow value range, using the mean is better than the regression line, and the  $R^2$  will be negative (Neg in Table 3).

The difference between the average ambient temperatures on the two aircraft was 0.5 K, and the difference between the average dew point temperatures was about 1 K. For temperature and humidity, the G1 data were slightly higher than the HALO data. The main contributions to the observed differences include the error propagation in the derivation of the ambient temperature from the measured temperature, instrumental-measurement uncertainty, and the temporal and spatial variability. The average horizontal wind speed measured by HALO is 0.4 m s<sup>-1</sup> higher than the average horizontal wind speed measured by the G1. The uncertainty source of wind estimation

is mainly due to the error propagation from the indicated aircraft speed measurement and the aircraft ground speed estimation from GPS. The static pressure distribution measured aboard HALO showed a smaller standard deviation (0.9 hPa) compared to the value of the G1 (1.5 hPa). Part of the reason for this difference is a more substantial variation of the G1 altitude during level flight legs when the G1 flew at around 50 m/s ~~higher-faster~~ than its normal airspeed. Thus, any biases caused by their near side-by-side airspeeds being different from their typical airspeeds would be undetected during these coordinated flights.

For the coordinated flights under cloudy conditions, we used the criteria from Section 2 to compare ambient conditions measured by the G1 and HALO aircraft. In addition to the ordinary linear regression, we also used the orthogonal regression to minimize the perpendicular distances from the data points to the fitted line. The ordinary linear regression assumes only the response (Y) variable contains measurement error but not the predictor (X), which remains unknown when we start the comparison between the measurements from the G1 and HALO. Thus, the additional orthogonal regression examines the assumption in the least square regression and makes sure the roles of the variables have little influence on the results. In Table 4, two equations were used for the orthogonal regression. One assumes that two measurements have a proportional relationship ( $Y=m_1*X$ ). The other one assumes a linear relationship, which can be described with the slope-intercept equation  $Y=m*X+b$ . Two regression results in Table 4 ~~does~~n't show a significant difference. The regression using the slope-intercept equation shows different level of improvement in each individual measurement and will be discussed in the corresponding sections.

As shown in Figure 4, the linear regression slopes for ambient temperature ([Figure 4\(a\)](#)), ~~pressure (Figure 4 (b))~~~~dew point temperature~~, and ~~dew point temperature pressure~~ were also close to 1 between the G1 and HALO measurements during the September 21 coordinated flight. The  $R^2$  value is also close to 1. These results suggest that the G1 and HALO measurements achieved excellent agreements. Note that the dew point temperature from the G1 measurement was erroneous and removed from the comparison the data points between 2200–2700 m and above 3700 m (Figure 4(c)) because the G1 sensor was skewed by wetting in the cloud. The HALO dew point temperature was calculated from the total water mixing ratio measured by TDL, and that measurement in the cloud was more accurate than the measurement made by the chilled mirror ~~hydrometer-hygrometer~~ aboard the G1.

The lower value of the  $R^2$  value in horizontal wind speed means the ratio of the regression error and total error in wind measurement is much higher than the temperature and pressure measurements. The main contributions to this difference are the error propagation during the horizontal wind speed estimation and the temporal and spatial variance between two aircraft sampling location. We observed differences between the two aircraft data of up to  $2 \text{ m s}^{-1}$ , caused by the increasing sampling distance as the two aircraft were climbing up. For example, the G1 flew a level leg above T3 around 2500 m between 16:20-16:30, while HALO stayed around 2500 m for a short period and kept climbing to a higher altitude. Due to strong vertical motion, turbulence, and different saturations (evaporation-condensation processes), the variances in the horizontal wind speed (Figure 4(d)) were also more significant compared to the variances of temperature and pressure measurements.

### 3.2 Comparison of trace gas measurements

For the cloud-free coordinated flight on September 9, ozone is the only trace gas measurement available on both aircraft. The linear regression slope shows that the HALO ozone concentration was about 8% higher than the G1 concentration. The difference between the averaged ozone concentrations was 4.1 ppb. As mentioned in section 2.1.2, each instrument has a 2 ppb accuracy (or 5%) on the ground based on a direct photometric measurement measuring the ratio between a sample and ozone-free cell. The in-flight calibration suggested that the accuracy of each instrument could raise to 5-7% (or 2-3.5 ppb). Thus, the difference between the averaged ozone concentrations – 4.1 ppb is within the instrument variation. The primary source of bias is probably the different ozone loss in the sampling and transfer lines.

The comparison made on September 21 flight in Figure 5 shows good agreement for the vertically averaged ozone measurements. Comparing the statistics data from September 9, the ozone measurement is not sensitive to the temporal and spatial changes. Although we do not have the comparison data on September 9, the G1 and HALO CO measurements comparison show a higher correlation than the ozone data comparison at different altitudes on September 21. Note that the data points with more substantial variance in CO concentration were excluded because the G1 and HALO were sampling different air masses between 2000-3000 m, as indicated in Figure S3-S57. The CO plot in Figure (5b) shows the real atmospheric variability. Around 4000 m, the CO reading from the G1 and HALO has the minimum variation and is averaged around 85 ppb,

Formatted: Indent: First line: 0.2"

420 which is at the atmospheric background level. At lower altitudes and higher CO concentrations,  
421 the local contribution is not well-mixed, and the inhomogeneity expresses as the more substantial  
422 variations observed in the plot.

### 423 3.3 Comparison of aerosol measurements

424 Aerosol particles exhibited substantial spatial variations, both vertically and horizontally, due  
425 to many aerosol sources and complex atmospheric processes in the Amazon basin, especially with  
426 the local anthropogenic sources in Manaus. Thus, spatially resolved measurements are critical to  
427 characterizing the properties of the Amazonian aerosols. The cloud-free coordinated flights allow  
428 us to compare the G1 and HALO aerosol measurements and thus will facilitate further studies that  
429 utilize the airborne measurements. The vertical profiles obtained using the G1 and HALO in  
430 different aerosol regimes of the Amazon basin have contributed to many studies (Fan et al., 2018;  
431 Martin et al., 2017; Wang et al., 2016).

432 The design and performance of the aircraft inlets can strongly influence measured aerosol  
433 particle number concentration, size distribution, and chemical composition (Wendisch et al.,  
434 2004). Therefore, they need to be taken into consideration when comparing the measurements  
435 aboard two aircraft. The G1 aerosol inlet is a fully automated isokinetic inlet. Manufacturer wind  
436 tunnel test and earlier studies show that this inlet operates for aerosol particles with diameter up to  
437 5  $\mu\text{m}$ , with transmission efficiency around 50 % at 1.5  $\mu\text{m}$  (Dolgos and Martins, 2014; Kleinman  
438 et al., 2007; Zaveri et al., 2010). The HALO sub-micrometer Aerosol Inlet (HASI) was explicitly  
439 designed for HALO. Based on the numerical flow modeling, optical particle counter  
440 measurements, and field study evaluation, HASI has a cut-off size of 3  $\mu\text{m}$ , with transmission  
441 efficiency larger than 90 % at 1  $\mu\text{m}$  (Andreae et al., 2018; Minikin et al., 2017).

#### 442 3.3.1 Aerosol particle number concentration

443 For the cloud-free coordinated flight [on September 9](#), the linear regression of CPC and UHSAS  
444 between the G1 and HALO measurements are also included in Table 3. The total number  
445 concentration measured by HALO CPC was about 20 % lower than that by the G1 CPC, as shown  
446 in Figure 6 (a). The CPC measurement is critically influenced by the isokinetic inlet operation and  
447 performance. During the flights, the aircraft attitude, such as the pitch and roll angles will cause  
448 the isokinetic sampling under non-axial condition. The non-axial flow at the probe inlet may result

in flow separation, turbulence, and particle deposition. Therefore, the quantitative particle measurements have a more substantial uncertainty. As shown in Figure 6 (b), we compared the CPC data by applying three different data quality criteria. The first criterion is the same criterion described in the previous section that makes sure all the compared measurements happen in less than 30 minutes apart, and the linear regression is included in Table 3. The second criterion constrains the data under the isokinetic and iso-axial condition and the plot in Figure 6(b) shows the iso-axial criteria reduced the broadness of the scattered data, but no significant change to the linear regression. We further constrained the data with the averaging. Based on the average wind speed and distance between two aircraft, we averaged the data into 10 seconds interval and found that the regression  $R^2$  increase to 0.9392. The typical uncertainty between two CPCs is 5-10% on the well-controlled environment (Gunthe et al., 2009; Liu and Pui, 1974). Although both CPCs from the G1 and HALO were characterized in the lab to be within 10% with its respective lab standard, we observed 20% variance during the flight. This result suggests the challenging condition of airborne measurement can significantly increase the systematic uncertainties of CPC measurements, such as systematic instrument drifts, different aerosol particle losses inside of the two CPCs, and different inlet transmission efficiencies in the two aircraft.

The CPC data in Figure 6 are color-coded with UTC time. The general trend is that the aerosol number concentration increased with time through the Manaus plume between 15:30 and 15:40. A similar trend was observed in aerosol particle number concentration (Figure 7) measured by the Ultra-High Sensitivity Aerosol Spectrometer (UHSAS)-Airborne version (referred to as UHSAS). The total number concentration data given by UHSAS (Figure 7) is integrated over the overlapping size range (90 – 500 nm for the September 9 flight) for both the G1 and HALO UHSAS. The linear regression shows that the total aerosol particle number concentration from HALO UHSAS is about 16.5% higher than that from the G1 UHSAS. The discrepancy between the two UHSAS measurements is mainly due to the error propagation in the sampling flow, the differential pressure transducer reading, the instrument stability, and calibration repeatability, consistent with the other UHSAS study (Kupc et al., 2018). In the airborne version of UHSAS, mechanical vibrations have a more significant impact on the pressure transducer reading than the case for the bench version of UHSAS.

For the coordinated flight on September 21, the G1 and HALO data are averaged to 200 m vertical altitude intervals (Figure 8). The data points with an altitude between 2000 – 3000 m

altitude were excluded from the comparisons, because the G1 and HALO sampled different airmasses, as evidenced from trace gas and aerosol chemical composition data (detailed in Section 3.2 and 3.3.3). The UHSAS size range was integrated from 100 to 700 nm on September 21. The variation of the size range was because the overlap of size distributions from both UHSAS instruments was changed. Both the CPC and UHSAS measurement comparisons show stronger variation at the low altitude, especially below 2000 m. Above 3500 m, the variations on the CPC and UHSAS measured concentration became significantly smaller than the variation at the lower altitude. This result is consistent with the observation from the trace gas measurement and confirms that the variability of aerosol properties changes significantly with time and space. It is noticeable that the discrepancy observed in the UHSAS measurements comparison is larger than that from the CPC comparison. That is because the aerosol flow control inside the UHSAS can't respond quickly enough to the rapid change of the altitude and caused significant uncertainty in the data.

### 3.3.2 Aerosol particle size distribution

For the cloud-free coordinated flight on September 9, the averaged aerosol size distributions measured by FIMS, G1 UHSAS, and HALO UHSAS during one flight leg are compared in Figure 9. For particle diameter below 90 nm, the G1 UHSAS overestimated the particle concentration, which is due to the uncertainty in counting efficiency correction. The UHSAS detection efficiency is close to 100% for particles larger than 100 nm and concentrations below 3000 cm<sup>-3</sup> but decreases considerably for both smaller particles and higher concentrations (Cai et al., 2008). The aerosol counting efficiency correction developed under the lab conditions does not necessarily apply under the conditions during the flight. Between 90 nm and 250 nm, FIMS agreed well with the G1 UHSAS, whereas HALO UHSAS was about 30 % higher than the two instruments. For the size range of 250–500 nm, FIMS had good agreement with HALO UHSAS and was about 30-50 % higher than the G1 UHSAS depending on the particle size. Because the UHSAS has a simplified “passive” inlet, the large size aerosol particle loss in the UHSAS inlet was expected to increase with the increasing of the aircraft speed. Thus, the lower G1 UHSAS concentrations at a larger aerosol particle size are likely related to the particle loss correction.

For the September 21 flight, the vertical profiles of aerosol size distributions are averaged into 100 m altitude intervals (Figure 10). Overall, all size distribution measurements captured the mode near 100 nm between 800–1000 m at the top of the convective boundary layer, as indicated by the

potential temperature (Figure 10(d)), which starts from a maximum near the ground and then becomes remarkably uniform across the convective boundary layer. The peak of the aerosol size distribution shifted from 100 nm to 150 nm with increasing altitude. Note that due to data availability, the aerosol size distribution data from the HALO UHSAS has a reduced vertical resolution.

### 3.3.3 Aerosol particle chemical composition

Figure 11 shows the vertical profiles of the aerosol mass concentrations measured by the two AMS on September 21. The upper panel shows the medians and interquartile ranges of the different species (organics, nitrate, sulfate, ammonium) and the total mass concentration for the G1 (circles) and HALO (triangles). The lower panel shows the difference between the medians of G1 and HALO. The error bars were calculated using error propagation from the error of the median (interquartile range divided by  $2\sqrt{N}$ ). The data were grouped into 400 m altitude bins. The total mass concentration is the highest in the lower altitudes between 100 m and 2000 m with a median value of  $5 \mu\text{g m}^{-3}$  (G1-AMS). At altitudes between 2000 m and 3800 m, the aerosol mass concentration decreased to a median value of  $1.2 \mu\text{g m}^{-3}$  (G1-AMS).

The most significant difference was observed at altitudes below 1800 m. The aerosol mass concentration measured by HALO-AMS is less than that measured by G1-AMS, likely due to particle losses in the constant pressure inlet (CPI) used on the HALO-AMS. Between 1800 m and 3000 m, the mass concentrations measured by the HALO-AMS exceed those measured by the G1-AMS. This is most likely because the G1 was sampling different air masses than the HALO as indicated by the differences in CO mixing ratios and the CPC concentrations for this altitude region (see Fig. 5 and 8). Above 3000 m altitude, both instruments agree within the uncertainty range.

Among individual species, the largest difference above 2000 m is observed for ammonium. The deployed G1 AMS is a high-resolution mass spectrometer (HR-ToF), whereas the HALO-AMS has a lower resolution (C-ToF). The higher resolution of the G1-AMS allows for a better separation of interfering ions at  $m/z$  15, 16, and 17 ( $\text{NH}^+$ ,  $\text{NH}^{2+}$ ,  $\text{NH}^{3+}$ ) and thereby a more reliable calculation of the ammonium mass concentration.

Overall the aerosol chemical composition is dominated by organics, as is evident from the vertical profiles of the relative fractions (Fig. 12). Both AMS show a dominant contribution of



organics to the total mass concentration with values around 70 %. This contribution is constant at altitudes between 100 m and 3500 m and decreases to 50 % at 3800 m altitude. The inorganic fraction has the highest contribution from sulfate (20 %), followed by ammonium (7 %) and nitrate (2 – 4 %). For organics, ammonium, and sulfate both instruments give similar relative fractions, only for nitrate where a discrepancy is observed between 1000 and 3000 m. Although the absolute aerosol mass concentration measured by the HALO-AMS was affected by the constant pressure inlet below 1800 m altitude, the relative fractions of both instruments generally agree well. Similar results were found for a second comparison flight on October 1, 2014 (see supplemental [section 2](#) and plots [S713](#), [S148](#)).

#### 3.3.4 CCN number concentration

These measurements provide key information about the aerosol's ability to form cloud droplets and thereby modify the microphysical properties of clouds. Numerous laboratory and field studies have improved the understanding of the connections among aerosol particle size, chemical composition, mixing states and CCN activation properties (Bhattu and Tripathi, 2015; Broekhuizen et al., 2006b; Chang et al., 2010; Duplissy et al., 2008; Lambe et al., 2011; Mei et al., 2013a; Mei et al., 2013b; Pöhlker et al., 2016; Thalman et al., 2017). In addition, based on the simplified chemical composition and internal mixing state assumption, various CCN closure studies have achieved success within  $\pm 20\%$  uncertainty for ambient aerosols (Broekhuizen et al., 2006a; Mei et al., 2013b; Rissler et al., 2004; Wang et al., 2008).

According to earlier studies (Gunthe et al., 2009; Pöhlker et al., 2016; Roberts et al., 2001; Roberts et al., 2002; Thalman et al., 2017), the hygroscopicity ( $\kappa_{\text{CCN}}$ ) of CCN in the Amazon basin is usually dominated by organic components ( $\kappa_{\text{org}}$ ). Long-term ground-based measurements at the Amazon Tall Tower Observatory also suggest low temporal variability and lack of pronounced diurnal cycles in hygroscopicity only under natural rainforest background conditions (Pöhlker et al., 2018; Pöhlker et al., 2016).

Using FIMS and CCN data from both the G1 and HALO collected during the coordinated flight leg on September 9, the critical activation dry diameter ( $D_{50}$ ) was determined by integrating FIMS size distribution to match the CCN total number concentration ([section S3](#)). Then, the effective particle hygroscopicity was derived from  $D_{50}$  and the CCN-operated supersaturation using the  $\kappa$ -

Köhler theory. The histogram plots based on the density of the estimated hygroscopicity ( $\kappa_{\text{est}}$ ) from both aircraft were compared for the flight leg above T3. The  $\kappa_{\text{est}}$  values derived from the G1 and HALO measurements during the flight leg above the T3 site are  $0.19 \pm 0.07$  and  $0.19 \pm 0.08$ , respectively. Those values agree very well with the overall mean value of  $0.17 \pm 0.06$  derived from long-term measurements at the Amazon Tall Tower Observatory (Pöhlker et al., 2016; Thalman et al., 2017).

A comparison of the vertical profiles of the CCN concentrations at 0.5% supersaturation on September 21 is shown in Figure 13 as an example. The difference between the CCN measurements on the two aircraft is about 20% on average. The linear regression slope would increase to 0.9120 if we focused on the data above 2500 m. The main contributions to the difference include the difference in aerosol inlet structure, aerosol particle loss correction in the main aircraft inlet and the constant pressure inlet, the systematic inlet difference below 2500 m as shown in AMS data, as well as the error propagation of CCN measurements.

### 3.4 Comparison of cloud measurements

In situ cloud measurements help to capture the diversity of different cloud forms and their natural temporal and spatial variability. The G1 CDP and FCDP were deployed under the different wing pylons, and also on the different side of the aircraft. The G1 2DS was deployed on the same side of FCDP. The HALO cloud combination probe (CCP-CDP and CCP-CIPgs) and NIXE-CAPS (NIXE-CAS and NIXE-CIPgs) were deployed under the different wing pylons but on the same side of the aircraft. On September 21, 2014, based on the aircraft location and elevation information as shown in Figure 1(b) and Figure 3, ~~two~~ both aircraft were sampling above T3 site and passing through the same cloud field at ~1600 m flight leg and ~1900 m flight leg as shown in Figure S118 and Figure S129. We used the cloud probes data from ~1900 m flight leg for the cloud droplet number concentration comparison. Two size ranges were considered: 3-20  $\mu\text{m}$  from light scattering probes (CDP vs. FCDP on the G1, CCP-CDP vs. NIXE-CAS on HALO) and 2-960  $\mu\text{m}$  from combined cloud probes.

#### 3.4.1 Comparison of cloud droplet number concentration between 3-20 $\mu\text{m}$

595 For underwing cloud probes, such as the CDP and the CAS, Lance (Lance, 2012) suggests an  
596 undercounting bias of measured particle number concentration by up to 44% due to coincidence  
597 as soon as the ambient cloud particle density rises to 1000 per cm<sup>3</sup>. At identical cloud particle  
598 densities, an earlier study (Baumgardner et al., 1985) estimates the coincidence bias for underwing  
599 cloud probes to the range at 20%. Factually, the coincidence correction depends on the  
600 instruments' individual detection volume, the air's volume flow rate through the detector and the  
601 cloud particles' residence time within the detection volume (Hermann and Wiedensohler, 2001;  
602 Jaenicke, 1972). For this comparison, coincidence bias remained unconsidered for each of the  
603 cloud probe measurements to avoid deviations that are caused by the application of different  
604 corrections.

605 The primary cloud layer was observed by both the G1 and HALO between 1000-2500 m above  
606 ground. Although the two aircraft have sampled along the same flight path, the instruments  
607 probably observed different sets of the cloud due to cloud movement with the prevailing wind or  
608 different cloud evolution stages. Thus, an initial comparison focuses on the redundant instruments  
609 on the same aircraft, that measured truly collocated and synchronous on board of HALO and of  
610 the G1, respectively. In Figure 14 (a), the data of the CCP-CDP and of the NIXE-CAS are  
611 juxtaposed sampled over about 13 minutes for particles detection size ranges which were  
612 considered as most equivalent. The comparison reveals two ranges of particle number  
613 concentrations at which densification of agreeing measurements become visible. At very low  
614 number concentrations (about 10<sup>-1</sup> – 10 per cm<sup>3</sup>) the presence of inactivated (interstitial) aerosols  
615 in the clear air space between the very few cloud elements should be considered. Over specific  
616 ranges, however, the fine structure of varying cloud droplet number concentration may cause the  
617 regression's scattering, indicated by cloud particle measured by one instrument whilst respective  
618 antagonist seems to measure within almost clear air – and vice versa. At higher number  
619 concentrations, i.e., between 10<sup>2</sup> and 10<sup>3</sup> per cm<sup>3</sup>, the comparison of the highly resolved data  
620 constitutes increasing compactness with respect to the 1:1 line. The overall data scatter of this  
621 comparison, however, may indicate the highly variable structure within clouds as those  
622 investigated over the Amazon basin. The data of the G1 CDP and the FCDP are juxtaposed as the  
623 same as HALO cloud probes. However, the sampled cloud period was much shorter – about 3  
624 minutes. Similar to the HALO cloud probes comparison, we observe two ranges of particle number  
625 concentrations at which densification of agreeing measurements become visible, especially for the

lower number concentrations (Figure 14(b)). At higher number concentrations, only a few cloud elements were observed by the G1 cloud probes. That is because the G1 was about 7-23 minutes later to pass the same location as HALO, and experienced much fewer cloud elements.

#### 3.4.2 Comparison of cloud droplet size distribution between 2-960 $\mu\text{m}$ from both aircraft

Comparing the cloud probes from the G1 and HALO, the size distributions from the HALO CCP and NIXE-CAPS probes are in remarkably good agreement between 2-960  $\mu\text{m}$ , and both peaked around 10  $\mu\text{m}$ , as shown in Figure 15. That is because the potential effects of cloud elements shattering on the probe measurements were considered similarly for the HALO-deployed CCP and NIXE instruments. On the G1, the CDP and FCDP had a more significant difference in the size range less than 8  $\mu\text{m}$ , although both of them peaked between 10-20  $\mu\text{m}$ . The difference between the G1 CDP and FCDP is mainly due to the data post-processing. The G1 CDP used an old data acquisition system from the Science Engineering Associates, which limited its capability to store the particle-by-particle (PBP) data for further processing. The CDP had placed an 800- $\mu\text{m}$ -diameter pinhole in front of the sizing detector to minimize the coincidence up to  $1850\text{ cm}^{-3}$ . On the other side, the FCDP was equipped with new electronics and PBP data was locally stored in a flash drive onboard the Linux machine. For the G1 flights, a constant probe-dependent adjustment factor was applied to FCDP to adjust the coincidence further in the final data product. The G1 CDP and FCDP operated with a redesigned probe tip to minimize the shattering effect. An additional algorithm was applied to the FCDP data to eliminate particles with short interarrival times.

For cloud droplets larger than 20  $\mu\text{m}$ , the difference between the obtained cloud particle size distributions from two aircraft becomes substantial (up to two orders of magnitude) which indicated the observations of two different stages within the progressing development of a precipitation cloud. The precipitation cloud developing process is evidently expressed in elevated number concentrations of larger cloud elements observed during the G1 measurement that happened later. We also observed that the general cloud characteristic is similar at different altitude levels, as shown in Figure S139. The first two of three averaged periods were chosen during the flight leg of  $\sim 1600\text{ m}$  and the last average period is for the flight leg  $\sim 1900\text{ m}$  compared in Figure 15. Due to the averaging, the fine in-cloud structure gets suppressed. The small scale

variabilities inside a cloud which are illustrated by the scattering of the highly resolved measurement data from the instrument comparison (cf. Figure 14) and the temporal evolution of in-cloud microphysics are not ascertainable and furthermore are beyond the scope of this study.

### 3.5 Comparison of radiation measurements

In this study, the downward irradiance measured by the SPN-1 unshaded center detector was compared with the integrated downward irradiance from the SMART-Albedometer between 300–1,800 nm wavelengths in Figure 16. Only measurements from flight legs, where the G1 and HALO flew near side-by-side and at the same altitude were taken into consideration for analysis. In Figure 16, the top panel shows the time series of SPN-1 measurements, and the bottom panel shows the time series of SMART-Albedometer measurements. The black dots represented all data, and the blue circles identified data when the navigation condition was within  $\pm 1$  degree from the horizontal level. The large scatter in the data between 15:12-15:28 and 15:35-15:40 is mainly due to the different sensor trajectories during the maneuvering of the aircraft to get to the coordinated flight position. Because of the difference of each aircraft position from horizontal, the measured signal varied from the signal of the direct component of sunlight. Each sensor might look at different directions of the sky or different parts of the clouds. In addition, both aircraft flew under scattered clouds, and this uneven sunlight blocking is another contribution to the “drop-off” behavior in the time series plots of the downward irradiance.

Comparing the G1 and HALO measurements between 15:15-15:55 using the restricted navigation criteria in Figure S154, we observed that the G1 SPN1 irradiance is slightly higher than the integrated irradiance from the SMART-Albedometer. We used the NCAR tropospheric ultraviolet and visible (TUV) radiation model estimated the weighted irradiance at 15:42:00 on Sep 9, 2014 and confirm that the spectral variation in the instruments is the main contribution to the difference in the comparison.

## 4 Uncertainty assessment

As mentioned in the introduction, a low-flying G1 and a high-flying HALO cover the sampling area from the atmospheric boundary layer to the free troposphere, and the sampling period from the dry and wet seasons (Martin et al., 2016a). This spatial coverage provides the user community

683 with abundant atmospheric-related data sets for their further studies, such as for remote sensing  
684 validation and modeling evaluation. However, one critical step to bridge the proper usage of the  
685 observation with further atmospheric science study is to understand the measurement uncertainty  
686 in this data set, especially the variation between the coexisting measurements due to the temporal  
687 and spatial difference.

688 For the majority of the measurements during this field study, three primary sources contribute  
689 to the measurement variation between the two aircraft: the temporal and spatial variations, the  
690 difference in the inlet characterization, and the limitation of the instrument capability. We used  
691 both ordinary least squares (OLS) linear regression and the orthogonal distance regression (ODR)  
692 to correlate the measurements from the G1 and HALO and confirmed that the slope and  $R^2$  are  
693 very similar for the measurements made on September 9. The results from Table 2 confirmed that  
694 the G1 and HALO measurements should be in a linear relationship without an offset if there is no  
695 altitude variation. It also shows the minimum discrepancy between two aerosol instruments (CPC  
696 or UHSAS) could be around 20%, which will include the error caused by the difference in the inlet  
697 characterization and the limitation of the instrument capability. If we assume those two  
698 measurement variation sources are not affected by the altitude, then by comparing the linear  
699 regression data from Table 3 to Table 2, we can estimate the temporal and spatial variation between  
700 two aircraft in a stack flight pattern. Three linear regression approaches were assessed, and the  
701 results are listed in Table 3. If we assume that two measurements from the G1 and HALO should  
702 not have any offsets, the OLS and ODR regressions show similar results. For the meteorological  
703 parameters, this assumption is valid. In addition, good correlations also indicate that there is no  
704 significant temporal or spatial variation during the stack pattern flight. As expected, the wind speed  
705 and the aerosol measurements show that the correlations between the measurements from the G1  
706 and HALO significantly improved with the offset assumption. This result suggests that the  
707 temporal and spatial variation in a half-hour will add an additional 20% variance to the measured  
708 aerosol properties. This will lead to a considerable uncertainty when we combine the observation  
709 data between the ground station and airborne platform. Thus, to evaluate or constrain atmospheric  
710 modeling work, more routine and long-term airborne measurements should be used ~~to evaluate or~~  
711 ~~constrain atmospheric modeling work to provide statistically sufficient observation, especially for~~  
712 ~~the regional or small scale modeling work.~~

## 5 Summary

In situ measurements made by well-characterized instruments installed on two research aircraft (the G1 and HALO) during the GoAmazon 2014/5 and ACRIDICON-CHUVA campaigns were compared (Table S3). Overall, the analysis shows good agreement between the G1 and HALO measurements for a relatively broad range of atmospheric-related variables in a challenging lower troposphere environment. Measured variables included atmospheric state parameters, aerosol particles, trace gases, clouds, and radiation properties. This study outlines the well-designed coordinated flights for achieving a meaningful comparison between two moving platforms. The high data quality was ensured by the most sophisticated instruments aboard two aircraft used the most advanced techniques, assisted with the best-calibrated/characterized procedures. The comparisons and the related uncertainty estimations quantify the current measurement limits, which provide the guidance to the modeler to realistically quantify the modeling input value and evaluate the variation between the measurement and the model output. The comparison also identified the measurement issues, outlined the associated reasonable measurement ranges, and evaluated the measurement sensitivities to the temporal and spatial variance.

The comparisons presented here were mainly from two coordinated flights. The flight on September 9 was classified as a cloud-free flight. During this flight, the G1 and HALO flew nearly side-by-side within a “polluted” leg, which was above the T3 site and across the downwind pollution plume from Manaus, and a “background” leg, which was outbound from Manaus to the west and could be influenced by the regional biomass burning events during the dry season. Both legs were at 500 m altitude and showed linear regression slopes of ambient temperature and pressure, horizontal wind speed and dew point temperature near to 1 between the G1 and HALO measurements. These comparisons provide a solid foundation for further evaluation of aerosol, trace gas, cloud, and radiation properties. The total aerosol concentration from CPC and UHSAS were compared for the 500 m flight leg above the T3 site. The UHSAS measurements had a better agreement than the CPC measurements. That is because of the minor difference in the inlet structure and instrument design between two UHSAS aboard the two aircraft. The average size distribution from both UHSAS and one FIMS in the G1 suggests that UHSAS had an over-counting issue at the size range between 60-90 nm, which was probably due to electrical noise and

743 small signal-to-noise ratio in that size range. Good agreement in the aerosol size distribution  
744 measurement provides a “sanity” check for AMS measurements. A CCN closure study suggested  
745 that FIMS provides valuable size coverage for better CCN number concentration estimation. Based  
746 on the  $\kappa$ -Köhler parameterization,  $\kappa_{\text{est}}$  observed at 500 m above the T3 site is  $0.19 \pm 0.08$ , which is  
747 similar to the overall mean kappa from long-term ATTO measurements -  $0.17 \pm 0.06$  (Pöhlker et  
748 al., 2016). This similarity suggests that there is no significant spatial variability along the  
749 downwind transect, although the freshly emitted aerosol particles may have much less  
750 hygroscopicity. The difference in the ozone measurement comparison is about 4.1 ppb, which  
751 suggests that the bias due to the sampling line loss inside of the G1 gas inlet. The irradiance from  
752 the SPN1 unshaded center detector in the G1 was compared with the HALO integrated downward  
753 irradiance between 300–1800 nm and achieved a very encouraging agreement with a variance of  
754 less than 10%.

755 During the second type of coordinated flights on September 21 (with cloudy conditions),  
756 HALO followed the G1 after take-off from Manus airport; then the two aircraft flew stacked legs  
757 relative to each other at different altitudes above the T3 site. For atmospheric state parameters,  
758 nearly linear correlations between the G1 and HALO were observed for ambient pressure,  
759 temperature, and dew point temperature measurements at an altitude range from ground to around  
760 5000 m. The horizontal wind had more variation than the rest of the meteorological properties,  
761 which is mainly due to the temporal and spatial variability. The aerosol number concentration and  
762 the trace gas measurements both suggest inhomogeneous aerosol distribution between 2000-3000  
763 m altitude. The integrated aerosol number concentration from UHSAS showed consistent  
764 discrepancy at different altitudes. This considerable uncertainty in the UHSAS measurements is  
765 caused by the significant aerosol sample flow variations due to the slow and unstable flow control.  
766 Although the aircraft-based UHSAS is a challenging instrument to operate, a reasonable size  
767 distribution profile comparison was made between both UHSAS and FIMS on the G1. Overall the  
768 chemical composition of the aerosol is dominated by organics. Around 70% of the AMS measured  
769 mass is organic, and this fractional contribution is maintained from the surface to 3500 m, then  
770 decreases to 50% at higher altitudes. The most substantial difference among all the species is  
771 observed for ammonium due to the different mass resolution of the AMS instruments, and more  
772 reliable ammonium mass concentration can be achieved with high resolution mass spectrometer.  
773 Although the absolute aerosol mass concentration measured by the HALO AMS was affected



below 1800 m altitude by the constant pressure inlet, the relative fractions of both instruments from the G1 and HALO agree well.

Cloud probe comparisons were made for the cloud droplet number concentration between 3–20  $\mu\text{m}$  for the initial comparison between the redundant instruments on the same aircraft. Then the comparison of cloud droplet size distribution between 2–960  $\mu\text{m}$  for a flight leg around 1900 m showed a remarkably good agreement. The major cloud appearance was captured by both aircraft, although the cloud elements observed were affected by the cloud movement with the prevailing wind and the different cloud evolution stages. Furthermore, the relatively short time delay of 7–23 minutes between the independent measurements may give a hint for the time scales in which the cloud droplet spectra develop within a convective cloud over the Amazon basin.

The above results provide additional information about the reasonableness of measurements for each atmospheric variable. This study confirms the high-quality spatial and temporal dataset with clearly identified uncertainty ranges had been collected from two aircraft and builds a good foundation for further studies on the remote sensing validation and the spatial and temporal evaluation of modeling representation of the atmospheric processing and evolution.

Several efforts made by both airborne measurement teams have significantly contributed to the overall success of this comparison study, and we recommend them for ~~the~~ future field operations.

- 1) Characterize instruments following the same established guideline. For example, the aerosol instruments can follow the guideline from the World Calibration Centre for Aerosol Physics (WCCAP).
- 2) Periodically compare measurements from different instruments for consistency in the field. For example, we found that comparing the integrated aerosol volume distribution from the aerosol sizer with the converted total aerosol mass from the AMS measurement can help check both the instrument performances and the inlet operation condition. Additionally, measurements from different cloud probes should be compared in the overlapping size ranges.
- 3) Daily calibration would be valuable but likely unrealistic to perform in the field. One alternative is to daily even hourly monitor the variation of the critical instrument parameters, such as the aerosol sample flow of the individual aerosol instruments.

4) For the cases with minor variations in the calibration results, the typical practice is to use the average calibration results for the variation period. However, we also recommend documenting the corresponding uncertainty with the data product.

4)5) A side-by-side comparison among the similar instruments deployed at different platforms, including those at ground sites, is highly recommended and will provide a comprehensive view of the data reliability.

**Acknowledgments:** This study was supported by the U.S. DOE, Office of Science, Atmospheric System Research Program, and used data from Atmospheric Radiation Measurement Aerial Facility, a DOE Office of Science User Facility. The Pacific Northwest National Laboratory (PNNL) is operated for DOE by Battelle under contract DE-AC05-76RL01830. This work was also supported by the Max Planck Society, the DFG (Deutsche Forschungsgemeinschaft, German Research Foundation) HALO Priority Program SPP 1294, the German Aerospace Center (DLR), the FAPESP (São Paulo Research Foundation) Grants 2009/15235-8 and 2013/05014-0, and a wide range of other institutional partners. The contributions from Micael A. Cecchini were funded by FAPESP grant number 2017/04654-6.

## References:

Alfarra, M. R., Coe, H., Allan, J. D., Bower, K. N., Boudries, H., Canagaratna, M. R., Jimenez, J. L., Jayne, J. T., Garforth, A. A., and Li, S.-M.: Characterization of urban and rural organic particulate in the lower Fraser valley using two aerodyne aerosol mass spectrometers, *Atmos Environ*, 38, 5745-5758, 2004.

Andreae, M. O., Acevedo, O. C., Araujo, A., Artaxo, P., Barbosa, C. G. G., Barbosa, H. M. J., Brito, J., Carbone, S., Chi, X., Cintra, B. B. L., da Silva, N. F., Dias, N. L., Dias, C. Q., Ditas, F., Ditz, R., Godoi, A. F. L., Godoi, R. H. M., Heimann, M., Hoffmann, T., Kesselmeier, J., Konemann, T., Kruger, M. L., Lavric, J. V., Manzi, A. O., Lopes, A. P., Martins, D. L., Mikhailov, E. F., Moran-Zuloaga, D., Nelson, B. W., Nolscher, A. C., Nogueira, D. S., Piedade, M. T. F., Pöhlker, C., Poschl, U., Quesada, C. A., Rizzo, L. V., Ro, C. U., Ruckteschler, N., Sa, L. D. A., Sa, M. D., Sales, C. B., dos Santos, R. M. N., Saturno, J., Schongart, J., Sorgel, M., de Souza, C. M., de Souza, R. A. F., Su, H., Targhetta, N., Tota, J., Trebs, I., Trumbore, S., van Eijck, A., Walter, D., Wang, Z., Weber, B., Williams, J., Winderlich, J., Wittmann, F., Wolff, S., and Yanez-Serrano, A. M.: The Amazon Tall Tower Observatory (ATTO): overview of pilot measurements on ecosystem ecology, meteorology, trace gases, and aerosols, *Atmos Chem Phys*, 15, 10723-10776, 2015.

Andreae, M. O., Afchine, A., Albrecht, R., Holanda, B. A., Artaxo, P., Barbosa, H. M. J., Borrmann, S., Cecchini, M. A., Costa, A., Dollner, M., Fütterer, D., Järvinen, E., Jurkat, T., Klimach, T., Konemann, T., Knote, C., Krämer, M., Krisna, T., Machado, L. A. T., Mertes, S., Minikin, A., Pöhlker, C., Pöhlker, M. L., Pöschl, U., Rosenfeld, D., Sauer, D., Schlager, H.,

839 Schnaiter, M., Schneider, J., Schulz, C., Spanu, A., Sperling, V. B., Voigt, C., Walser, A., Wang,  
840 J., Weinzierl, B., Wendisch, M., and Ziereis, H.: Aerosol characteristics and particle production  
841 in the upper troposphere over the Amazon Basin, *Atmos. Chem. Phys.*, 18, 921-961, 2018.  
842 Artaxo, P., Rizzo, L. V., Brito, J. F., Barbosa, H. M. J., Arana, A., Sena, E. T., Cirino, G. G.,  
843 Bastos, W., Martin, S. T., and Andreae, M. O.: Atmospheric aerosols in Amazonia and land use  
844 change: from natural biogenic to biomass burning conditions, *Faraday Discuss*, 165, 203-235,  
845 2013.  
846 Bahreini, R., Dunlea, E. J., Matthew, B. M., Simons, C., Docherty, K. S., DeCarlo, P. F.,  
847 Jimenez, J. L., Brock, C. A., and Middlebrook, A. M.: Design and operation of a pressure-  
848 controlled inlet for airborne sampling with an aerodynamic aerosol lens, *Aerosol Sci Tech*, 42,  
849 465-471, 2008.  
850 Baumgardner, D., Strapp, W., and Dye, J. E.: Evaluation of the Forward Scattering Spectrometer  
851 Probe. Part II: Corrections for Coincidence and Dead-Time Losses, 2, 626-632, 1985.  
852 Bhattu, D. and Tripathi, S. N.: CCN closure study: Effects of aerosol chemical composition and  
853 mixing state, *J Geophys Res-Atmos*, 120, 766-783, 2015.  
854 Brenguier, J. L., Bachalo, W. D., Chuang, P. Y., Esposito, B. M., Fugal, J., Garrett, T., Gayet, J.  
855 F., Gerber, H., Heymsfield, A., and Kokhanovsky, A.: In situ measurements of cloud and  
856 precipitation particles, *Airborne Measurements for Environmental Research: Methods and*  
857 *Instruments*, 2013. 225-301, 2013.  
858 Broekhuizen, K., Chang, R.-W., Leaitch, W., Li, S.-M., and Abbatt, J.: Closure between  
859 measured and modeled cloud condensation nuclei (CCN) using size-resolved aerosol  
860 compositions in downtown Toronto, *Atmos Chem Phys*, 6, 2513-2524, 2006a.  
861 Broekhuizen, K., Chang, R. Y. W., Leaitch, W. R., Li, S. M., and Abbatt, J. P. D.: Closure  
862 between measured and modeled cloud condensation nuclei (CCN) using size-resolved aerosol  
863 compositions in downtown Toronto, *Atmos Chem Phys*, 6, 2513-2524, 2006b.  
864 Cai, Y., Montague, D. C., Mooiweer-Bryan, W., and Deshler, T.: Performance characteristics of  
865 the ultra high sensitivity aerosol spectrometer for particles between 55 and 800 nm: Laboratory  
866 and field studies, *J Aerosol Sci*, 39, 759-769, 2008.  
867 Chang, R. Y. W., Slowik, J. G., Shantz, N. C., Vlasenko, A., Liggio, J., Sjostedt, S. J., Leaitch,  
868 W. R., and Abbatt, J. P. D.: The hygroscopicity parameter ( $\kappa$ ) of ambient organic aerosol at  
869 a field site subject to biogenic and anthropogenic influences: relationship to degree of aerosol  
870 oxidation, *Atmos Chem Phys*, 10, 5047-5064, 2010.  
871 Costa, A., Meyer, J., Afchine, A., Luebke, A., Günther, G., Dorsey, J. R., Gallagher, M. W.,  
872 Ehrlich, A., Wendisch, M., and Baumgardner, D.: Classification of Arctic, midlatitude and  
873 tropical clouds in the mixed-phase temperature regime, *Atmos Chem Phys*, 17, 12219-12238,  
874 2017.  
875 Davidson, E. A., de Araujo, A. C., Artaxo, P., Balch, J. K., Brown, I. F., Bustamante, M. M. C.,  
876 Coe, M. T., DeFries, R. S., Keller, M., Longo, M., Munger, J. W., Schroeder, W., Soares, B. S.,  
877 Souza, C. M., and Wofsy, S. C.: The Amazon basin in transition (vol 481, pg 321, 2012), *Nature*,  
878 483, 232-232, 2012.  
879 DeCarlo, P. F., Kimmel, J. R., Trimborn, A., Northway, M. J., Jayne, J. T., Aiken, A. C., Gonin,  
880 M., Fuhrer, K., Horvath, T., Docherty, K. S., Worsnop, D. R., and Jimenez, J. L.: Field-  
881 deployable, high-resolution, time-of-flight aerosol mass spectrometer, *Anal Chem*, 78, 8281-  
882 8289, 2006.  
883 Dolgos, G. and Martins, J. V.: Polarized Imaging Nephelometer for in situ airborne  
884 measurements of aerosol light scattering, *Optics express*, 22, 21972-21990, 2014.

885 Duplissy, J., Gysel, M., Alfarra, M. R., Dommen, J., Metzger, A., Prevot, A. S. H., Weingartner,  
 886 E., Laaksonen, A., Raatikainen, T., Good, N., Turner, S. F., McFiggans, G., and Baltensperger,  
 887 U.: Cloud forming potential of secondary organic aerosol under near atmospheric conditions,  
 888 *Geophys Res Lett*, 35, 2008.  
 889 Faber, S., French, J. R., and Jackson, R.: Laboratory and in-flight evaluation of measurement  
 890 uncertainties from a commercial Cloud Droplet Probe (CDP), *Atmos Meas Tech*, 11, 3645-3659,  
 891 2018.  
 892 Fan, J., Rosenfeld, D., Zhang, Y., Giangrande, S. E., Li, Z., Machado, L. A., Martin, S. T., Yang,  
 893 Y., Wang, J., and Artaxo, P.: Substantial convection and precipitation enhancements by ultrafine  
 894 aerosol particles, *Science*, 359, 411-418, 2018.  
 895 Giez, A., Mallaun, C., Zöger, M., Dörnbrack, A., and Schumann, U.: Static pressure from aircraft  
 896 trailing-cone measurements and numerical weather-prediction analysis, *J Aircraft*, 54, 1728-  
 897 1737, 2017.  
 898 Gunthe, S., King, S., Rose, D., Chen, Q., Roldin, P., Farmer, D., Jimenez, J., Artaxo, P.,  
 899 Andreae, M., and Martin, S.: Cloud condensation nuclei in pristine tropical rainforest air of  
 900 Amazonia: size-resolved measurements and modeling of atmospheric aerosol composition and  
 901 CCN activity, *Atmos Chem Phys*, 9, 7551-7575, 2009.  
 902 Guyon, P., Boucher, O., Graham, B., Beck, J., Mayol-Bracero, O. L., Roberts, G. C., Maenhaut,  
 903 W., Artaxo, P., and Andreae, M. O.: Refractive index of aerosol particles over the Amazon  
 904 tropical forest during LBA-EUSTACH 1999, *J Aerosol Sci*, 34, 883-907, 2003.  
 905 Hermann, M. and Wiedensohler, A. J. J. o. A. S.: Counting efficiency of condensation particle  
 906 counters at low-pressures with illustrative data from the upper troposphere, 32, 975-991, 2001.  
 907 Jaenicke, R. J. J. o. A. S.: The optical particle counter: cross-sensitivity and coincidence, 3, 95-  
 908 111, 1972.  
 909 Jayne, J. T., Leard, D. C., Zhang, X. F., Davidovits, P., Smith, K. A., Kolb, C. E., and Worsnop,  
 910 D. R.: Development of an aerosol mass spectrometer for size and composition analysis of  
 911 submicron particles, *Aerosol Sci Tech*, 33, 49-70, 2000.  
 912 Keller, M., Bustamante, M., Gash, J., and Dias, P. S. (Eds.): Amazonia and Global Change,  
 913 American Geophysical Union, Washington, DC, 2009.  
 914 Kleinman, L. I., Daum, P. H., Lee, Y. N., Senum, G. I., Springston, S. R., Wang, J., Berkowitz,  
 915 C., Hubbe, J., Zaveri, R. A., and Brechtel, F. J.: Aircraft observations of aerosol composition and  
 916 ageing in New England and Mid-Atlantic States during the summer 2002 New England Air  
 917 Quality Study field campaign, *Journal of Geophysical Research: Atmospheres*, 112, 2007.  
 918 Klingebiel, M., de Lozar, A., Molleker, S., Weigel, R., Roth, A., Schmidt, L., Meyer, J., Ehrlich,  
 919 A., Neuber, R., Wendisch, M., and Borrmann, S.: Arctic low-level boundary layer clouds: in situ  
 920 measurements and simulations of mono- and bimodal supercooled droplet size distributions at  
 921 the top layer of liquid phase clouds, *Atmos Chem Phys*, 15, 617-631, 2015.  
 922 Krautstrunk, M. and Giez, A.: The transition from FALCON to HALO era airborne atmospheric  
 923 research. In: *Atmospheric Physics*, Springer, 2012.  
 924 Krisna, T. C., Wendisch, M., Ehrlich, A., Jäkel, E., Werner, F., Weigel, R., Borrmann, S.,  
 925 Mahnke, C., Pöschl, U., Andreae, M. O., Voigt, C., and Machado, L. A. T.: Comparing airborne  
 926 and satellite retrievals of cloud optical thickness and particle effective radius using a spectral  
 927 radiance ratio technique: two case studies for cirrus and deep convective clouds, *Atmos. Chem.*  
 928 *Phys.*, 18, 4439-4462, 2018.  
 929 Kuhn, U., Ganzeveld, L., Thielmann, A., Dindorf, T., Schebeske, G., Welling, M., Sciare, J.,  
 930 Roberts, G., Meixner, F. X., Kesselmeier, J., Lelieveld, J., Kolle, O., Ciccioli, P., Lloyd, J.,

931 Trentmann, J., Artaxo, P., and Andreae, M. O.: Impact of Manaus City on the Amazon Green  
 932 Ocean atmosphere: ozone production, precursor sensitivity and aerosol load, *Atmos Chem Phys*,  
 933 10, 9251-9282, 2010.

934 Kulkarni, P. and Wang, J.: New fast integrated mobility spectrometer for real-time measurement  
 935 of aerosol size distribution - I: Concept and theory, *J Aerosol Sci*, 37, 1303-1325, 2006a.

936 Kulkarni, P. and Wang, J.: New fast integrated mobility spectrometer for real-time measurement  
 937 of aerosol size distribution: II. Design, calibration, and performance characterization, *J Aerosol*  
 938 *Sci*, 37, 1326-1339, 2006b.

939 Kupc, A., Williamson, C., Wagner, N. L., Richardson, M., and Brock, C. A.: Modification,  
 940 calibration, and performance of the Ultra-High Sensitivity Aerosol Spectrometer for particle size  
 941 distribution and volatility measurements during the Atmospheric Tomography Mission (ATom)  
 942 airborne campaign, *Atmos. Meas. Tech.*, 11, 369-383, 2018.

943 Lambe, A. T., Onasch, T. B., Massoli, P., Croasdale, D. R., Wright, J. P., Ahern, A. T.,  
 944 Williams, L. R., Worsnop, D. R., Brune, W. H., and Davidovits, P.: Laboratory studies of the  
 945 chemical composition and cloud condensation nuclei (CCN) activity of secondary organic  
 946 aerosol (SOA) and oxidized primary organic aerosol (OPOA), *Atmos Chem Phys*, 11, 8913-  
 947 8928, 2011.

948 Lance, S.: Coincidence Errors in a Cloud Droplet Probe (CDP) and a Cloud and Aerosol  
 949 Spectrometer (CAS), and the Improved Performance of a Modified CDP, *J Atmos Ocean Tech*,  
 950 29, 1532-1541, 2012.

951 Lance, S., Brock, C. A., Rogers, D., and Gordon, J. A.: Water droplet calibration of the Cloud  
 952 Droplet Probe (CDP) and in-flight performance in liquid, ice and mixed-phase clouds during  
 953 ARCPAC, *Atmospheric Measurement Techniques*, 3, 1683-1706, 2010.

954 Lawson, R.: Effects of ice particles shattering on the 2D-S probe, *Atmos Meas Tech*, 4, 1361-  
 955 1381, 2011.

956 Lawson, R. P., O'Connor, D., Zmarzly, P., Weaver, K., Baker, B., Mo, Q., and Jonsson, H.: The  
 957 2D-S (stereo) probe: Design and preliminary tests of a new airborne, high-speed, high-resolution  
 958 particle imaging probe, *J Atmos Ocean Tech*, 23, 1462-1477, 2006.

959 Liu, B. Y. and Pui, D. Y.: A submicron aerosol standard and the primary, absolute calibration of  
 960 the condensation nuclei counter, *Journal of Colloid and Interface Science*, 47, 155-171, 1974.

961 Long, C. N., Bucholtz, A., Jonsson, H., Schmid, B., Vogelmann, A., and Wood, J.: A Method  
 962 of Correcting for Tilt from Horizontal in Downwelling Shortwave Irradiance Measurements on  
 963 Moving Platforms, *The Open Atmospheric Science Journal*, 4, 78-87, 2010.

964 Luebke, A. E., Afchine, A., Costa, A., Grooss, J. U., Meyer, J., Rolf, C., Spelten, N., Avallone,  
 965 L. M., Baumgardner, D., and Kramer, M.: The origin of midlatitude ice clouds and the resulting  
 966 influence on their microphysical properties, *Atmos Chem Phys*, 16, 5793-5809, 2016.

967 Martin, S., Artaxo, P., Machado, L., Manzi, A., Souza, R., Schumacher, C., Wang, J., Andreae,  
 968 M., Barbosa, H., and Fan, J.: Introduction: observations and modeling of the Green Ocean  
 969 Amazon (GoAmazon2014/5), *Atmos Chem Phys*, 16, 2016a.

970 Martin, S. T., Artaxo, P., Machado, L., Manzi, A. O., Souza, R. A. F., Schumacher, C., Wang, J.,  
 971 Biscaro, T., Brito, J., Calheiros, A., Jardine, K., Medeiros, A., Portela, B., de Sa, S. S., Adachi,  
 972 K., Aiken, A. C., Albrecht, R., Alexander, L., Andreae, M. O., Barbosa, M. J., Buseck, P.,  
 973 Chand, D., Comstock, J. M., Day, D. A., Dubey, M., Fan, J., Fast, J., Fisch, G., Fortner, E.,  
 974 Giangrande, S., Gilles, M., Goldstein, A. H., Guenther, A., Hubbe, J., Jensen, M., Jimenez, J.  
 975 L., Keutsch, F. N., Kim, S., Kuang, C., Laskin, A., McKinney, K., Mei, F., Miller, M.,  
 976 Nascimento, R., Pauliquevis, T., Pekour, M., Peres, J., Petaja, T., Pohlker, C., Poschl, U., Rizzo,

977 L., Schmid, B., Shilling, J. E., Dias, M. A. S., Smith, J. N., Tomlinson, J. M., Tota, J., and  
 978 Wendisch, M.: The Green Ocean Amazon Experiment (GoAmazon2014/5) Observes Pollution  
 979 Affecting Gases, Aerosols, Clouds, and Rainfall over the Rain Forest, *B Am Meteorol Soc*, 98,  
 980 981-997, 2017.  
 981 Martin, S. T., Artaxo, P., Machado, L. A. T., Manzi, A. O., Souza, R. A. F., Schumacher, C.,  
 982 Wang, J., Andreae, M. O., Barbosa, H. M. J., Fan, J., Fisch, G., Goldstein, A. H., Guenther, A.,  
 983 Jimenez, J. L., Poschl, U., Dias, M. A. S., Smith, J. N., and Wendisch, M.: Introduction:  
 984 Observations and Modeling of the Green Ocean Amazon (GoAmazon2014/5), *Atmos Chem*  
 985 *Phys*, 16, 4785-4797, 2016b.  
 986 Mei, F., Hayes, P. L., Ortega, A., Taylor, J. W., Allan, J. D., Gilman, J., Kuster, W., de Gouw, J.,  
 987 Jimenez, J. L., and Wang, J.: Droplet activation properties of organic aerosols observed at an  
 988 urban site during CalNex-LA, *J Geophys Res-Atmos*, 118, 2903-2917, 2013a.  
 989 Mei, F., Setyan, A., Zhang, Q., and Wang, J.: CCN activity of organic aerosols observed  
 990 downwind of urban emissions during CARES, *Atmos Chem Phys*, 13, 12155-12169, 2013b.  
 991 Middlebrook, A. M., Bahreini, R., Jimenez, J. L., and Canagaratna, M. R.: Evaluation of  
 992 composition-dependent collection efficiencies for the aerodyne aerosol mass spectrometer using  
 993 field data, *Aerosol Sci Tech*, 46, 258-271, 2012.  
 994 Minikin, A., Sauer, D., Ibrahim, A., Franke, H., Rösenthaller, T., Fütterer, D. A., and Petzold,  
 995 A.: The HALO Submicrometer Aerosol Inlet (HASI): Design concept and first characterization,  
 996 1st HALO symposium: Airborne Research with HALO: Achievements and Prospects,  
 997 Oberpfaffenhofen, Deutschland, 2017. 2017.  
 998 Molleker, S., Borrmann, S., Schlager, H., Luo, B., Frey, W., Klingebiel, M., Weigel, R., Ebert,  
 999 M., Mitev, V., Matthey, R., Woiwode, W., Oelhaf, H., Dornbrack, A., Stratmann, G., Grooss, J.  
 1000 U., Gunther, G., Vogel, B., Müller, R., Kramer, M., Meyer, J., and Cairo, F.: Microphysical  
 1001 properties of synoptic-scale polar stratospheric clouds: in situ measurements of unexpectedly  
 1002 large HNO<sub>3</sub>-containing particles in the Arctic vortex, *Atmos Chem Phys*, 14, 10785-10801,  
 1003 2014.  
 1004 Olfert, J. S., Kulkarni, P., and Wang, J.: Measuring aerosol size distributions with the fast  
 1005 integrated mobility spectrometer, *J Aerosol Sci*, 39, 940-956, 2008.  
 1006 Petzold, A., Marsh, R., Johnson, M., Miller, M., Sevcenco, Y., Delhaye, D., Ibrahim, A.,  
 1007 Williams, P., Bauer, H., Crayford, A., Bachalo, W. D., and Raper, D.: Evaluation of Methods for  
 1008 Measuring Particulate Matter Emissions from Gas Turbines, *Environ Sci Technol*, 45, 3562-  
 1009 3568, 2011.  
 1010 Pöhlker, M. L., Ditas, F., Saturno, J., Klimach, T., de Angelis, I. H., Araujo, A. C., Brito, J.,  
 1011 Carbone, S., Cheng, Y. F., Chi, X. G., Ditz, R., Gunthe, S. S., Holanda, B. A., Kandler, K.,  
 1012 Kesselmeier, J., Konemann, T., Kruger, O. O., Lavric, J. V., Martin, S. T., Mikhailov, E., Moran-  
 1013 Zuloaga, D., Rizzo, L. V., Rose, D., Su, H., Thalman, R., Walter, D., Wang, J., Wolff, S.,  
 1014 Barbosa, H. M. J., Artaxo, P., Andreae, M. O., Pöschl, U., and Pöhlker, C.: Long-term  
 1015 observations of cloud condensation nuclei over the Amazon rain forest - Part 2: Variability and  
 1016 characteristics of biomass burning, long-range transport, and pristine rain forest aerosols, *Atmos*  
 1017 *Chem Phys*, 18, 10289-10331, 2018.  
 1018 Pöhlker, M. L., Pöhlker, C., Ditas, F., Klimach, T., de Angelis, I. H., Araujo, A., Brito, J.,  
 1019 Carbone, S., Cheng, Y. F., Chi, X. G., Ditz, R., Gunthe, S. S., Kesselmeier, J., Konemann, T.,  
 1020 Lavric, J. V., Martin, S. T., Mikhailov, E., Moran-Zuloaga, D., Rose, D., Saturno, J., Su, H.,  
 1021 Thalman, R., Walter, D., Wang, J., Wolff, S., Barbosa, H. M. J., Artaxo, P., Andreae, M. O., and  
 1022 Poschl, U.: Long-term observations of cloud condensation nuclei in the Amazon rain forest - Part

1: Aerosol size distribution, hygroscopicity, and new model parametrizations for CCN prediction, *Atmos Chem Phys*, 16, 15709-15740, 2016.

Poschl, U., Martin, S. T., Sinha, B., Chen, Q., Gunthe, S. S., Huffman, J. A., Borrmann, S., Farmer, D. K., Garland, R. M., Helas, G., Jimenez, J. L., King, S. M., Manzi, A., Mikhailov, E., Pauliquevis, T., Petters, M. D., Prenni, A. J., Roldin, P., Rose, D., Schneider, J., Su, H., Zorn, S. R., Artaxo, P., and Andreae, M. O.: Rainforest aerosols as biogenic nuclei of clouds and precipitation in the Amazon, *Science*, 329, 1513-1516, 2010.

Rissler, J., Swietlicki, E., Zhou, J., Roberts, G., Andreae, M. O., Gatti, L., and Artaxo, P.: Physical properties of the sub-micrometer aerosol over the Amazon rain forest during the wet-to-dry season transition-comparison of modeled and measured CCN concentrations, *Atmos Chem Phys*, 4, 2119-2143, 2004.

Roberts, G. C., Andreae, M. O., Zhou, J., and Artaxo, P.: Cloud condensation nuclei in the Amazon Basin: "Marine" conditions over a continent?, *Geophys Res Lett*, 28, 2807-2810, 2001.

Roberts, G. C., Artaxo, P., Zhou, J., Swietlicki, E., and Andreae, M. O.: Sensitivity of CCN spectra on chemical and physical properties of aerosol: A case study from the Amazon Basin, *Journal of Geophysical Research: Atmospheres*, 107, LBA 37-31-LBA 37-18, 2002.

Rose, D., Gunthe, S., Mikhailov, E., Frank, G., Dusek, U., Andreae, M. O., and Pöschl, U.: Calibration and measurement uncertainties of a continuous-flow cloud condensation nuclei counter (DMT-CCNC): CCN activation of ammonium sulfate and sodium chloride aerosol particles in theory and experiment, *Atmos Chem Phys*, 8, 1153-1179, 2008.

Salati, E. and Vose, P. B.: Amazon basin: a system in equilibrium, *Science*, 225, 129-138, 1984.

Schmid, B., Tomlinson, J. M., Hubbe, J. M., Comstock, J. M., Mei, F., Chand, D., Pekour, M. S., Kluzek, C. D., Andrews, E., Biraud, S. C., and McFarquhar, G. M.: The Doe Arm Aerial Facility, *B Am Meteorol Soc*, 95, 723+, 2014.

Schulz, C., Schneider, J., Amorim Holanda, B., Appel, O., Costa, A., de Sá, S. S., Dreiling, V., Fütterer, D., Jurkat-Witschas, T., Klimach, T., Knote, C., Krämer, M., Martin, S. T., Mertes, S., Pöhlker, M. L., Sauer, D., Voigt, C., Walser, A., Weinzierl, B., Ziereis, H., Zöger, M., Andreae, M. O., Artaxo, P., Machado, L. A. T., Pöschl, U., Wendisch, M., and Borrmann, S.: Aircraft-based observations of isoprene-epoxydiol-derived secondary organic aerosol (IEPOX-SOA) in the tropical upper troposphere over the Amazon region, *Atmos. Chem. Phys.*, 18, 14979-15001, 2018.

Shilling, J. E., Pekour, M. S., Fortner, E. C., Artaxo, P., Sá, S. d., Hubbe, J. M., Longo, K. M., Machado, L. A., Martin, S. T., and Springston, S. R.: Aircraft observations of the chemical composition and aging of aerosol in the Manaus urban plume during GoAmazon 2014/5, *Atmos Chem Phys*, 18, 10773-10797, 2018.

Shilling, J. E., Zaveri, R. A., Fast, J. D., Kleinman, L., Alexander, M., Canagaratna, M. R., Fortner, E., Hubbe, J. M., Jayne, J. T., and Sedlacek, A.: Enhanced SOA formation from mixed anthropogenic and biogenic emissions during the CARES campaign, *Atmos Chem Phys*, 13, 2091-2113, 2013.

Thalman, R., de Sa, S. S., Palm, B. B., Barbosa, H. M. J., Pöhlker, M. L., Alexander, M. L., Brito, J., Carbone, S., Castillo, P., Day, D. A., Kuang, C. G., Manzi, A., Ng, N. L., Sedlacek, A. J., Souza, R., Springston, S., Watson, T., Pöhlker, C., Poschl, U., Andreae, M. O., Artaxo, P., Jimenez, J. L., Martin, S. T., and Wang, J.: CCN activity and organic hygroscopicity of aerosols downwind of an urban region in central Amazonia: seasonal and diel variations and impact of anthropogenic emissions, *Atmos Chem Phys*, 17, 11779-11801, 2017.

1068 Wang, J.: A fast integrated mobility spectrometer with wide dynamic size range: Theoretical  
 1069 analysis and numerical simulation, *J Aerosol Sci*, 40, 890-906, 2009.  
 1070 Wang, J., Krejci, R., Giangrande, S., Kuang, C., Barbosa, H. M., Brito, J., Carbone, S., Chi, X.,  
 1071 Comstock, J., Ditas, F., Lavric, J., Manninen, H. E., Mei, F., Moran-Zuloaga, D., Pohlker, C.,  
 1072 Pohlker, M. L., Saturno, J., Schmid, B., Souza, R. A., Springston, S. R., Tomlinson, J. M., Toto,  
 1073 T., Walter, D., Wimmer, D., Smith, J. N., Kulmala, M., Machado, L. A., Artaxo, P., Andreae, M.  
 1074 O., Petaja, T., and Martin, S. T.: Amazon boundary layer aerosol concentration sustained by  
 1075 vertical transport during rainfall, *Nature*, 539, 416-419, 2016.  
 1076 Wang, J., Lee, Y.-N., Daum, P. H., Jayne, J., and Alexander, M.: Effects of aerosol organics on  
 1077 cloud condensation nucleus (CCN) concentration and first indirect aerosol effect, *Atmos Chem*  
 1078 *Phys*, 8, 6325-6339, 2008.  
 1079 Webster, C. and Freudinger, L.: Interagency Working Group for Airborne Data and  
 1080 Telecommunications, 2018.  
 1081 Wendisch, M. and Brenguier, J.-L.: Airborne measurements for environmental research: methods  
 1082 and instruments, John Wiley & Sons, 2013.  
 1083 Wendisch, M., Coe, H., Baumgardner, D., Brenguier, J.-L., Dreiling, V., Fiebig, M., Formenti,  
 1084 P., Hermann, M., Krämer, M., Levin, Z., Maser, R., Mathieu, E., Nacass, P., Noone, K.,  
 1085 Osborne, S., Schneider, J., Schütz, L., Schwarzenböck, A., Stratmann, F., and Wilson, J. C.:  
 1086 Aircraft Particle Inlets: State-of-the-Art and Future Needs, *B Am Meteorol Soc*, 85, 89-92, 2004.  
 1087 Wendisch, M., Keil, A., and Korolev, A. V.: FSSP characterization with monodisperse water  
 1088 droplets, *Journal of Atmospheric and Oceanic Technology*, 13, 1152-1165, 1996.  
 1089 Wendisch, M., Müller, D., Schell, D., and Heintzenberg, J.: An airborne spectral albedometer  
 1090 with active horizontal stabilization, *J Atmos Ocean Tech*, 18, 1856-1866, 2001.  
 1091 Wendisch, M., Poschl, U., Andreae, M. O., Machado, L. A. T., Albrecht, R., Schlager, H.,  
 1092 Rosenfeld, D., Martin, S. T., Abdelmomonem, A., Afchine, A., Araujo, A. C., Artaxo, P.,  
 1093 Aufmhoff, H., Barbosa, H. M. J., Borrmann, S., Braga, R., Buchholz, B., Cecchini, M. A., Costa,  
 1094 A., Curtius, J., Dollner, M., Dorf, M., Dreiling, V., Ebert, V., Ehrlich, A., Ewald, F., Fisch, G.,  
 1095 Fix, A., Frank, F., Futterer, D., Heckl, C., Heidelberg, F., Huneke, T., Jakel, E., Jarvinen, E.,  
 1096 Jurkat, T., Kanter, S., Kastner, U., Kenntner, M., Kesselmeier, J., Klimach, T., Knecht, M., Kohl,  
 1097 R., Kolling, T., Kramer, M., Kruger, M., Krisna, T. C., Lavric, J. V., Longo, K., Mahnke, C.,  
 1098 Manzi, A. O., Mayer, B., Mertes, S., Minikin, A., Molleker, S., Munch, S., Nillius, B.,  
 1099 Pfeilsticker, K., Pohlker, C., Roiger, A., Rose, D., Rosenowow, D., Sauer, D., Schnaiter, M.,  
 1100 Schneider, J., Schulz, C., de Souza, R. A. F., Spanu, A., Stock, P., Vila, D., Voigt, C., Walser,  
 1101 A., Walter, D., Weigel, R., Weinzierl, B., Werner, F., Yamasoe, M. A., Ziereis, H., Zinner, T.,  
 1102 and Zoger, M.: ACRIDICON-CHUVA CAMPAIGN Studying Tropical Deep Convective  
 1103 Clouds and Precipitation over Amazonia Using the New German Research Aircraft HALO, *B*  
 1104 *Am Meteorol Soc*, 97, 1885-1908, 2016.  
 1105 Zaveri, R. A., Berkowitz, C. M., Brechtel, F. J., Gilles, M. K., Hubbe, J. M., Jayne, J. T.,  
 1106 Kleinman, L. I., Laskin, A., Madronich, S., and Onasch, T. B.: Nighttime chemical evolution of  
 1107 aerosol and trace gases in a power plant plume: Implications for secondary organic nitrate and  
 1108 organosulfate aerosol formation, NO<sub>3</sub> radical chemistry, and N<sub>2</sub>O<sub>5</sub> heterogeneous hydrolysis,  
 1109 *Journal of Geophysical Research: Atmospheres*, 115, 2010.

1110

1111





Table 1. List of compared measurements and corresponding instruments deployed aboard the G1 and HALO during GoAmazon2014/5. The acronyms are defined in a table at the end of this paper.  $D_p$  indicates the particle diameter.  $\Delta D_p$  refers to the size resolution.

Measurement Variables	Instruments deployed on the G1 (Martin et al., 2016; Schmid et al., 2014)	Instruments deployed on HALO (Wendisch et al., 2016)
Static Pressure	Rosemount (1201F1), 0-1400 hPa	Instrumented nose boom tray (DLR development), 0-1400 hPa
Static air temperature	Rosemount E102AL/510BF -50 to +50 °C	Total Air Temperature (TAT) inlet (Goodrich/Rosemount type 102) with an open wire resistance temperature sensor (PT100), -70 to +50 °C
Dewpoint temperature	Chilled mirror hygrometer 1011B -40 to +50 °C	Derived from the water-vapor mixing ratio, which is measured by a tunable diode laser (TDL) system (DLR development), 5-40000 ppmv
3-D wind	Aircraft Integrated Meteorological Measurement System 20 (AIMMS-20)	Instrumented nose boom tray (DLR development) with an air data probe (Goodrich/Rosemount) 858AJ and high-precision Inertial Reference System (IGI IMU-IIe)
Particle number concentration	CPC, cut off size ( $D_p$ ) =10 nm	CPC, cut off size ( $D_p$ ) =10 nm
Size distribution*	UHSAS-A, 60-1000 nm.	UHSAS-A, 60-1000 nm.
	FIMS, 20 nm – 500 nm	
Non-Refractory particle chemical composition	HR-ToF-AMS: Organics, Sulfate, Nitrate, Ammonium, Chloride, 60-1000 nm	C-ToF-AMS: Organics, Sulfate, Nitrate, Ammonium, Chloride, 60-1000 nm
CCN concentration	CCN-200, SS= 0.25, 0.5%	CCN-200, SS= 0.13-0.53%
Gas phase concentration	N2O/CO and Ozone Analyzer, CO, O <sub>3</sub> concentration, precision 2 ppb	N2O/CO and Ozone Analyzer, CO, O <sub>3</sub> concentration, precision 2 ppb
Cloud properties*	CDP, 2-50 $\mu$ m, $\Delta D_p$ =1-2 $\mu$ m	CCP-CDP, 2.5-46 $\mu$ m, $\Delta D_p$ =1-2 $\mu$ m
	FCDP, 2-50 $\mu$ m, $\Delta D_p$ =1-2 $\mu$ m	NIXE-CAS: 0.61 -52.5 $\mu$ m
	2DS, 10-1000 $\mu$ m	NIXE-CIPgs, 15-960 $\mu$ m
		CCP-CIPgs: 15-960 $\mu$ m
Radiation	SPN1 downward irradiance, 400-2700 nm	SMART Albedometer, downward spectral irradiance, 300-2200 nm

\*for an individual flight, the size range may vary.

Table 2. Summary of the total data points compared between the G1 and HALO instruments.

	SEP 9, 2014		SEP 21, 2014	
	G1	HALO	G1	HALO
<b>Atmospheric parameters</b>	2815	2815	7326	12065
<b>Gas phase, CO</b>	N/A	N/A	7326	12065
<b>Gas phase, Ozone</b>	2815	2815	7110	11766
<b>CPC</b>	2043	2043	8466	11646
<b>UHSAS (FIMS)</b>	2031	2031	5841 (9405)	828
<b>AMS</b>	N/A	N/A	587	818
<b>CCNc</b>	663	531	7982	4546
<b>G1: CDP(FCDP)</b>	N/A	N/A	3627(4439)	2051(2260)
<b>HALO: CCP-CDP</b>				
<b>(NIXE-CAS)</b>				
<b>G1: 2DS</b>	N/A	N/A	2280	2261 (2260)
<b>HALO: CCP-CIPgs</b>				
<b>(NIXE-CIPgs)</b>				
<b>RAD</b>	1355	1355	N/A	N/A

10

11

Table 3. Summary of basic statistics of data between in situ measurements on Sep 9.

<i>Comparison of the coordinated flight on Sep. 9</i>										
<i>Variables</i>	G1				HALO					
	min	max	mean	std	min	max	mean	std	slope	R <sup>2</sup>
<i>T, K</i>	297.7	300.2	298.9	0.5	297.2	299.4	298.4	0.4	1.002	Neg.
<i>P, hPa</i>	955	965	960.1	1.5	958	964.9	961.8	0.9	0.998	Neg.
<i>WSpd, m/s</i>	0.3	8.9	3.4	1.2	0.3	7.7	3.8	1.1	0.998	Neg.
<i>T<sub>dew</sub>, k</i>	293	296.5	295.0	0.5	292.9	294.9	294.0	0.3	0.996	Neg.
<i>O<sub>3</sub>, ppb</i>	10.5	58.8	22.2	9.3	18.3	50.8	26.3	6.6	1.082	0.9401
<i>CPC, cm<sup>-3</sup></i>	696.0	3480.6	1591.3	568.7	687.4	2639.4	1313.8	473.5	0.819	0.8508
<i>UHSAS, cm<sup>-3</sup></i>	78.2	1118.	645.5	116.3	504.1	1622.2	756.3	138.6	1.165	0.8193
<i>CCNc (κ)</i>	0.010	0.347	0.1855	0.067	0.012	0.394	0.1890	0.083	0.8937	Neg.

12

13

14

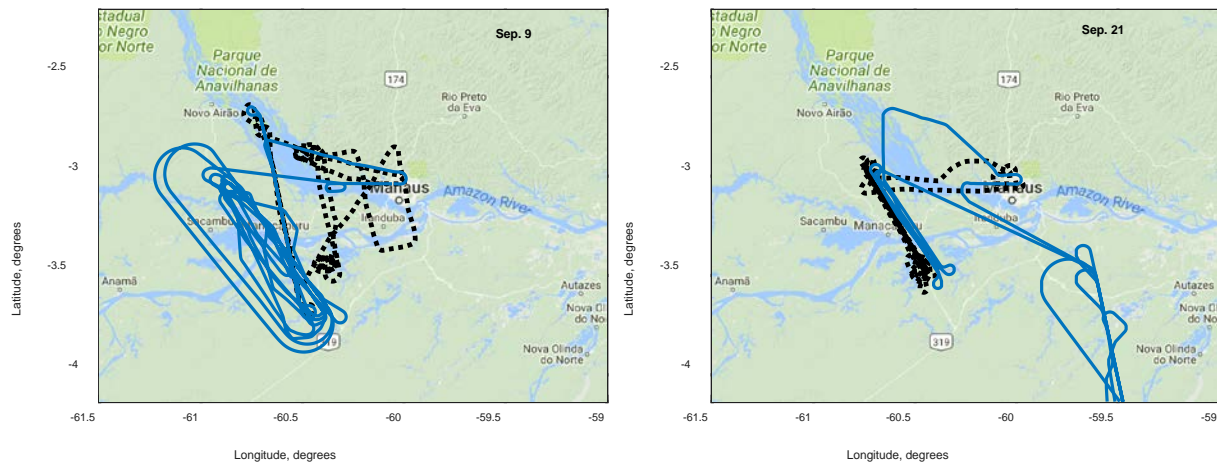
15 Table 4 Summary of three statistics analysis of data between in situ measurements on Sep 21

<i>Comparison of the coordinated flight on Sep. 21</i>							
	m	offset	R <sup>2</sup>	m0	R <sup>2</sup>	m1	R <sup>2</sup>
<i>T, K</i>	0.929	20.0	0.9992	0.999	0.9928	0.999	0.9928
<i>P, hPa</i>	1.001	0.929	0.9998	1.001	0.9998	1.001	0.9998
<i>WSpd, m/s</i>	0.885	1.0	0.7875	1.012	0.5076	1.023	0.5049
<i>T<sub>dew</sub>, k</i>	0.989	3.8	0.9963	1.003	0.9904	1.003	0.9904
<i>O<sub>3</sub>, ppb</i>	1.134	-1.5	0.9598	1.075	0.9369	1.101	0.9208
<i>CO, ppb</i>	0.922	5.4	0.9654	0.966	0.9254	0.967	0.9254
<i>CPC, cm<sup>-3</sup></i>	0.571	199.4	0.9482	0.635	0.8738	0.641	0.8735
<i>UHSAS, cm<sup>-3</sup></i>	1.126	178.0	0.8249	1.293	0.5070	1.384	0.4847
<i>CCNc (κ)</i>	0.766	55.3	0.8330	0.815	0.6544	0.829	0.6521

16

17

18  
19

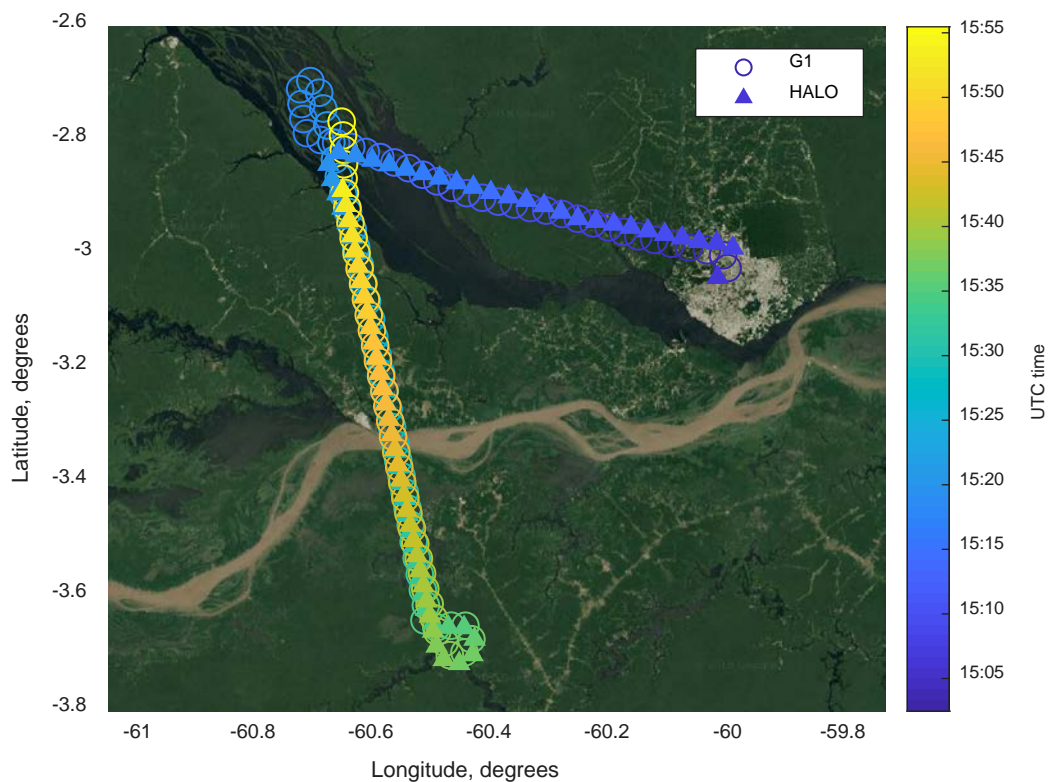


(a)

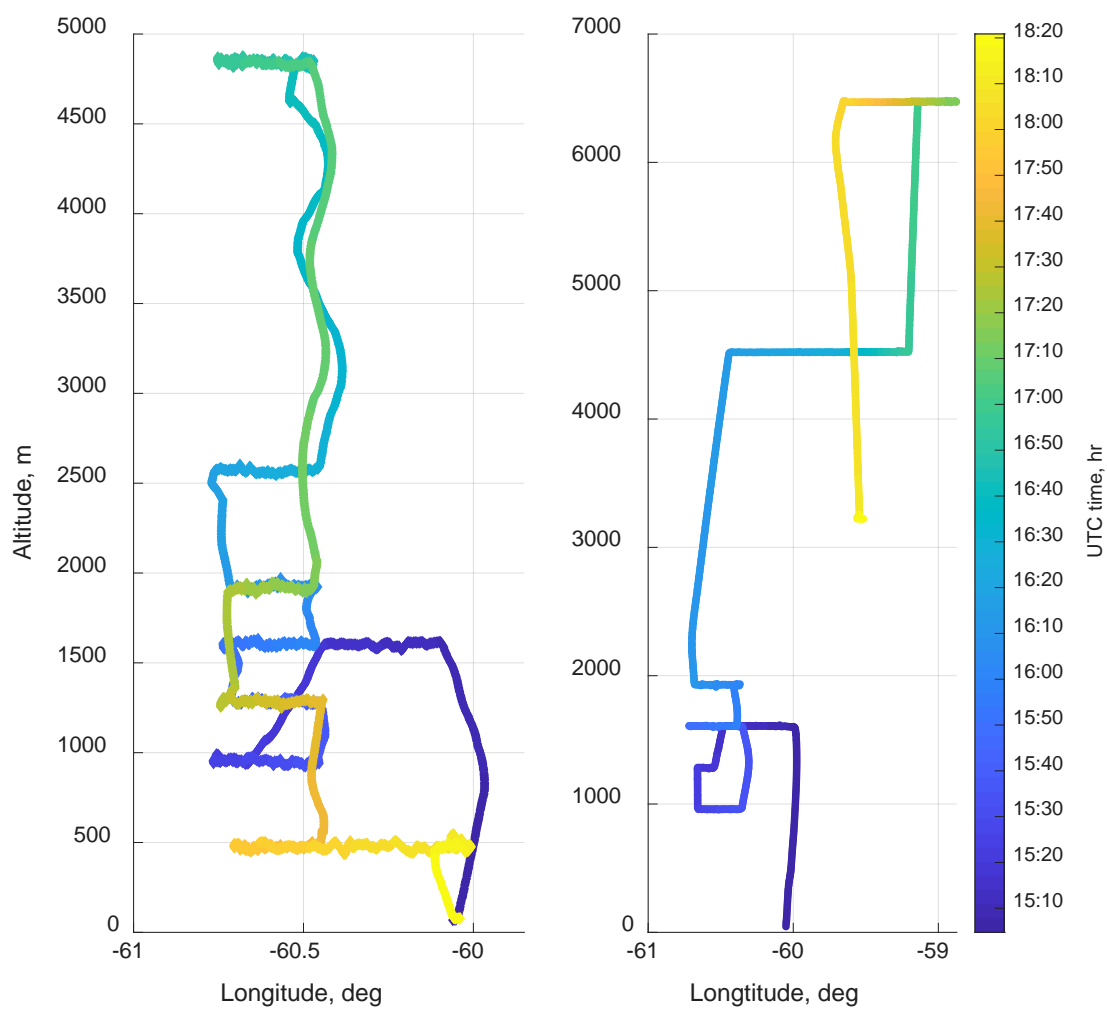
(b)

20  
21  
22  
23  
24

Figure 1. Coordinated flight tracks for September 9 (a) and September 21 (b). The black dotted line is the flight track of the G1, and the blue line is the flight track of HALO. (This figure was created using Mapping Toolbox™ © COPYRIGHT 1997–2019 by The MathWorks, Inc.)



25  
 26 Figure 2. Time-colored flight track of the G1 (circle) and HALO (triangle) on September 9 during  
 27 a cloud-free coordinated flight at 500 m above sea level (50 m apart as the closest distance). (This  
 28 figure was created using Mapping Toolbox™ © COPYRIGHT 1997–2019 by The MathWorks,  
 29 Inc.)



(a)

(b)

Figure 3. Time-colored flight profile of the G1 (a) and HALO (b) on September 21, during a coordinated flight.



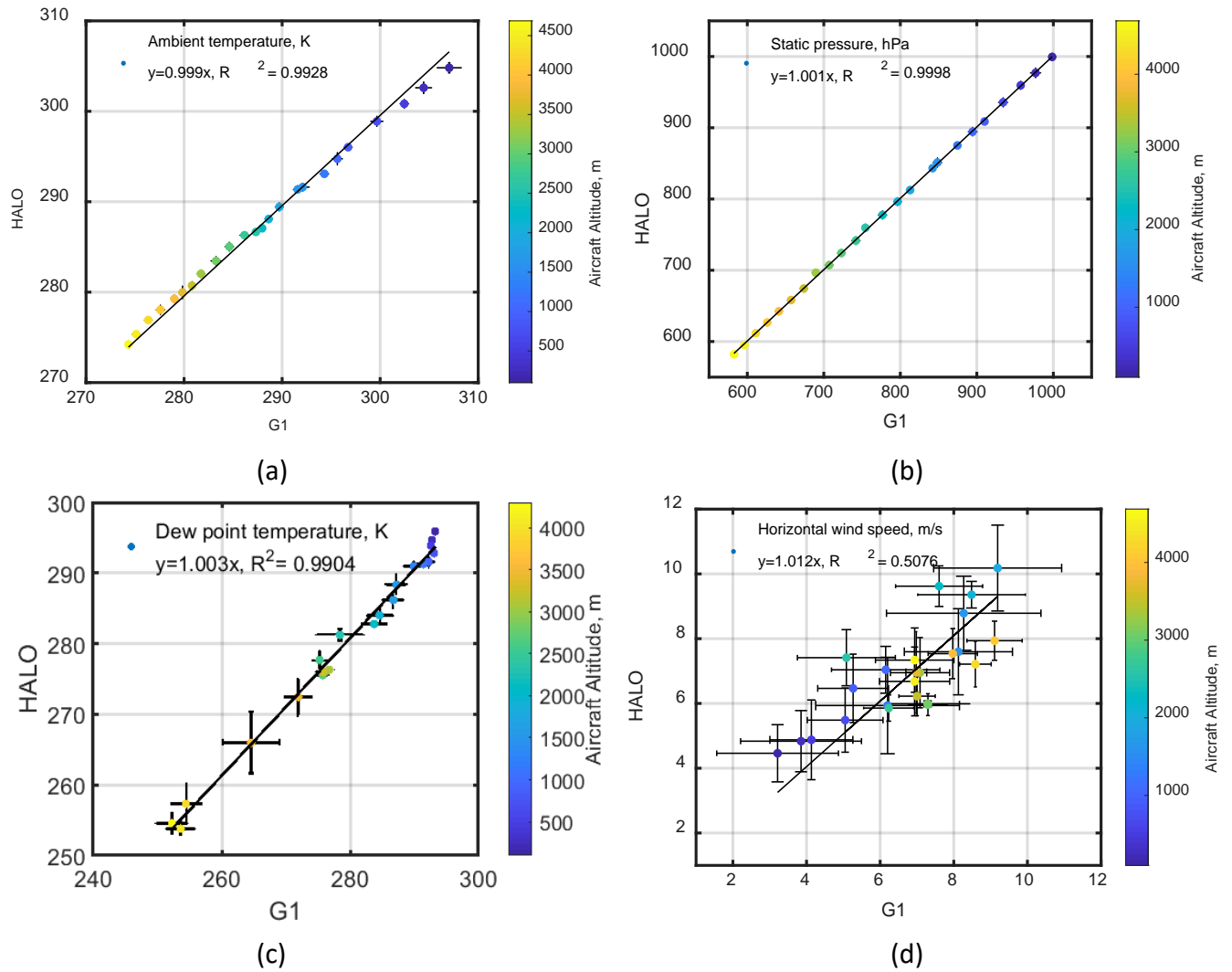


Figure 4. Aircraft altitude-colored plots of (a) ambient temperature, (b) static pressure, (c) dew point temperature, and (d) horizontal wind speed observed by the G1 and HALO on September 21.

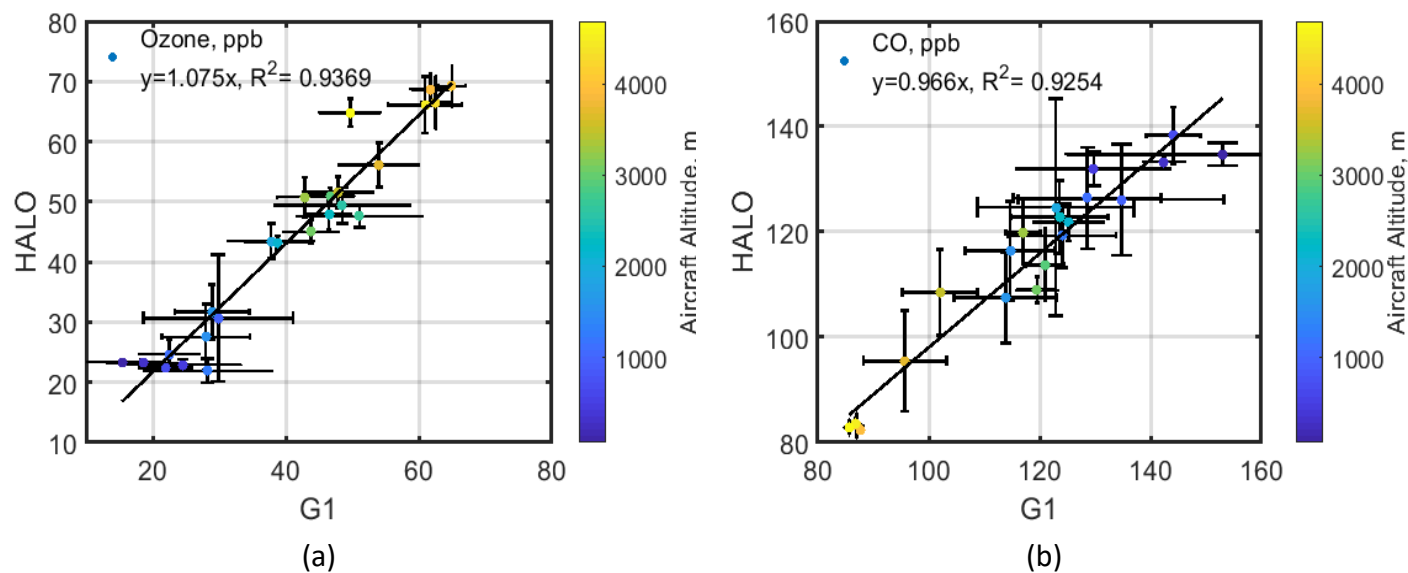


Figure 5. Aircraft altitude-colored plots of trace gas (a) Ozone, (b) CO, for the coordinated flight on September 21.

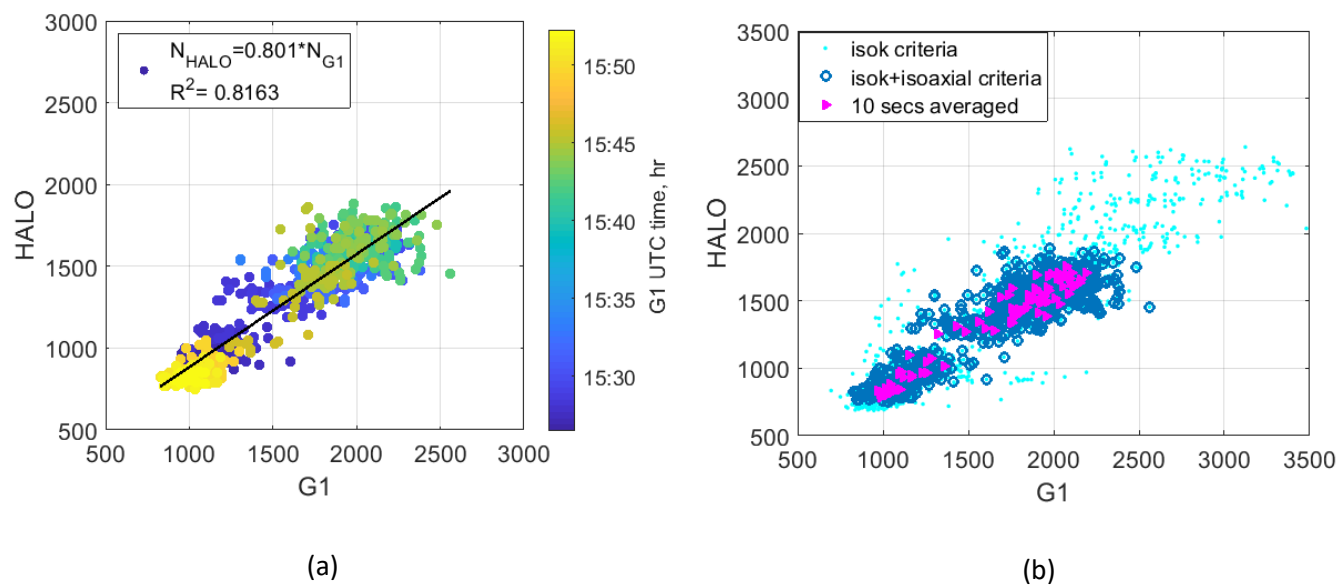


Figure 6. The G1 and HALO comparison for aerosol number concentration measured by CPC (>10 nm) on September 9: (a) with iso-kinetic inlet constrain; (b) with different criteria.

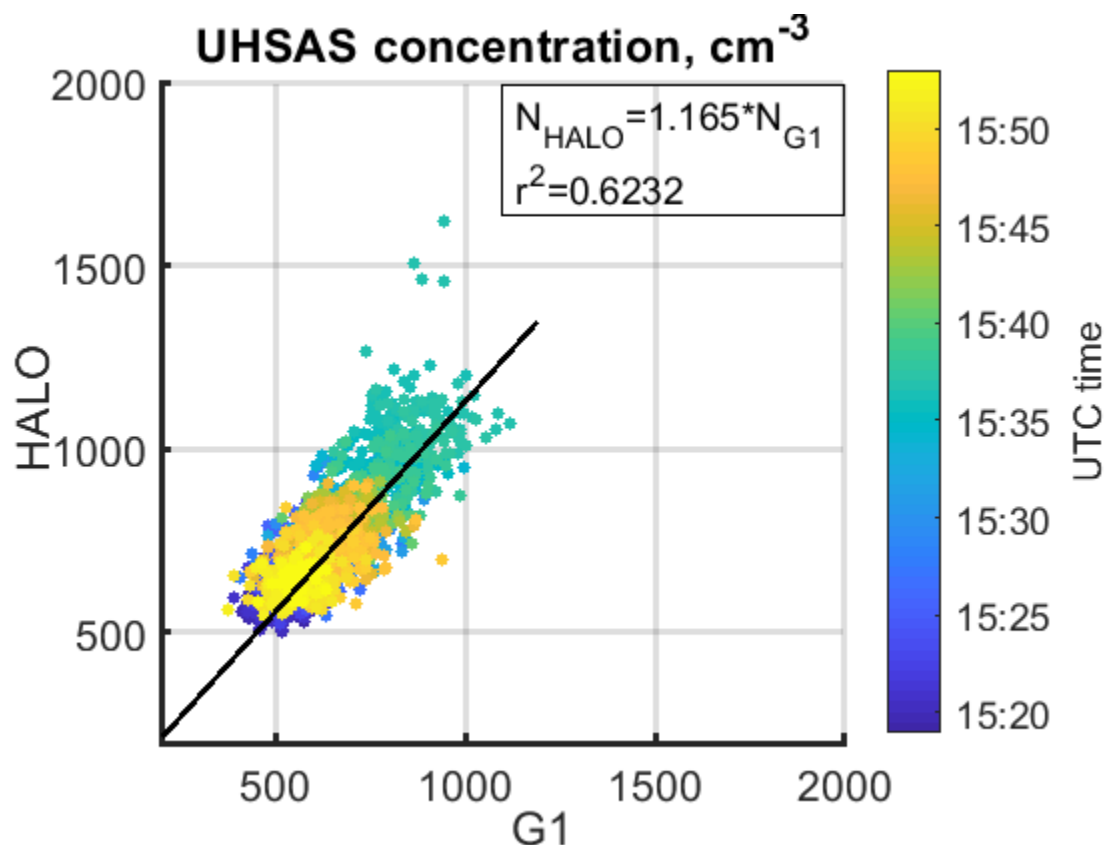


Figure 7. The G1 and HALO comparison for aerosol number concentration measured by UHSAS (90-500 nm) on September 9.

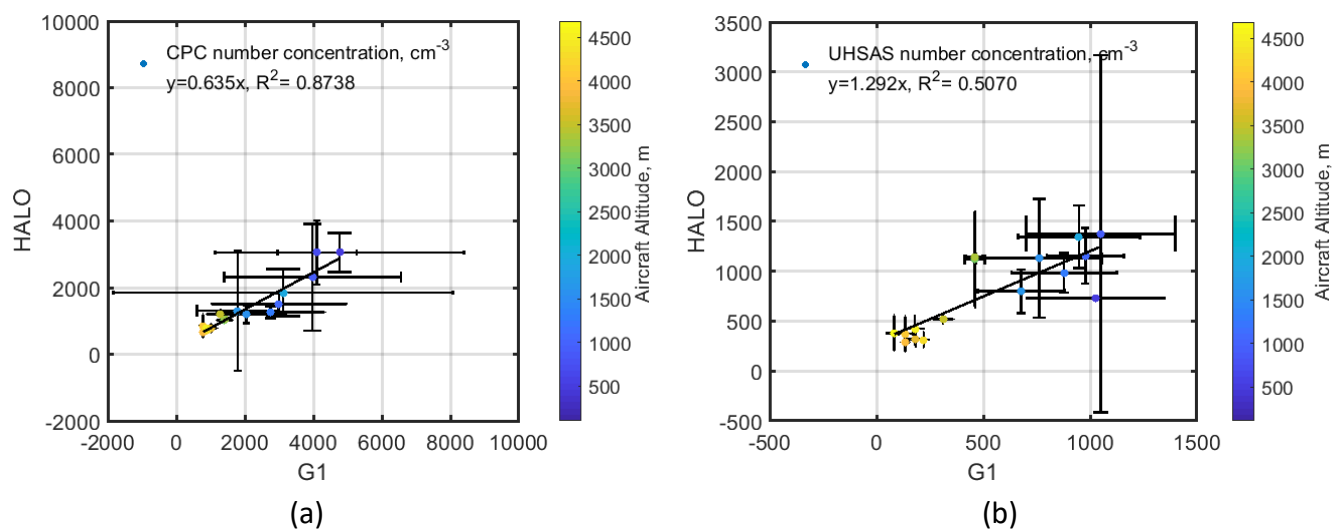


Figure 8. The G1 and HALO comparison for aerosol number concentration profiling measured by (a) CPC and (b) UHSAS (100-700 nm) on September 21.

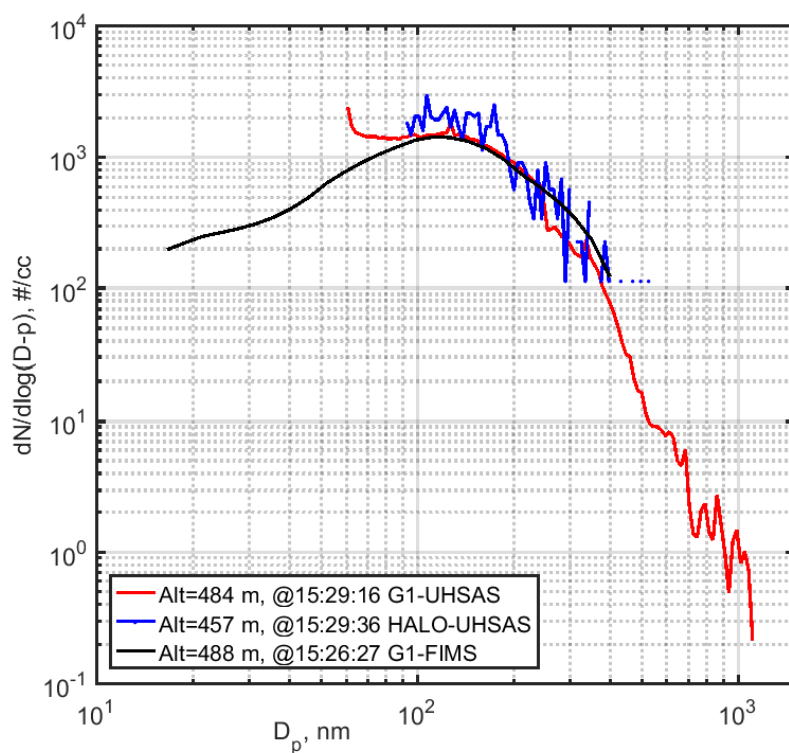
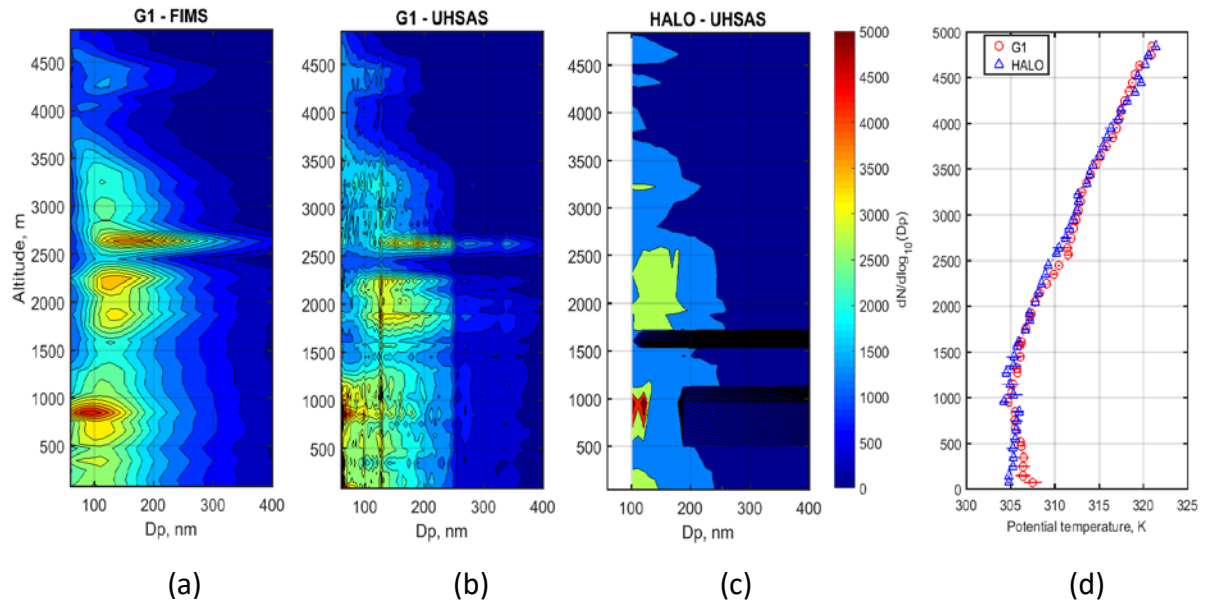


Figure 9. The G1 and HALO comparison for aerosol size distribution measured by UHSAS (from both aircraft) and FIMS (on the G1) on September 9.

56



57

58 Figure 10. Aerosol size distribution vertical profiles measured by (a) the G1 FIMS, (b) The G1  
 59 UHSAS, (c) the HALO UHSAS, (d) Potential temperature aboard the G1 and HALO on September  
 60 21.

61

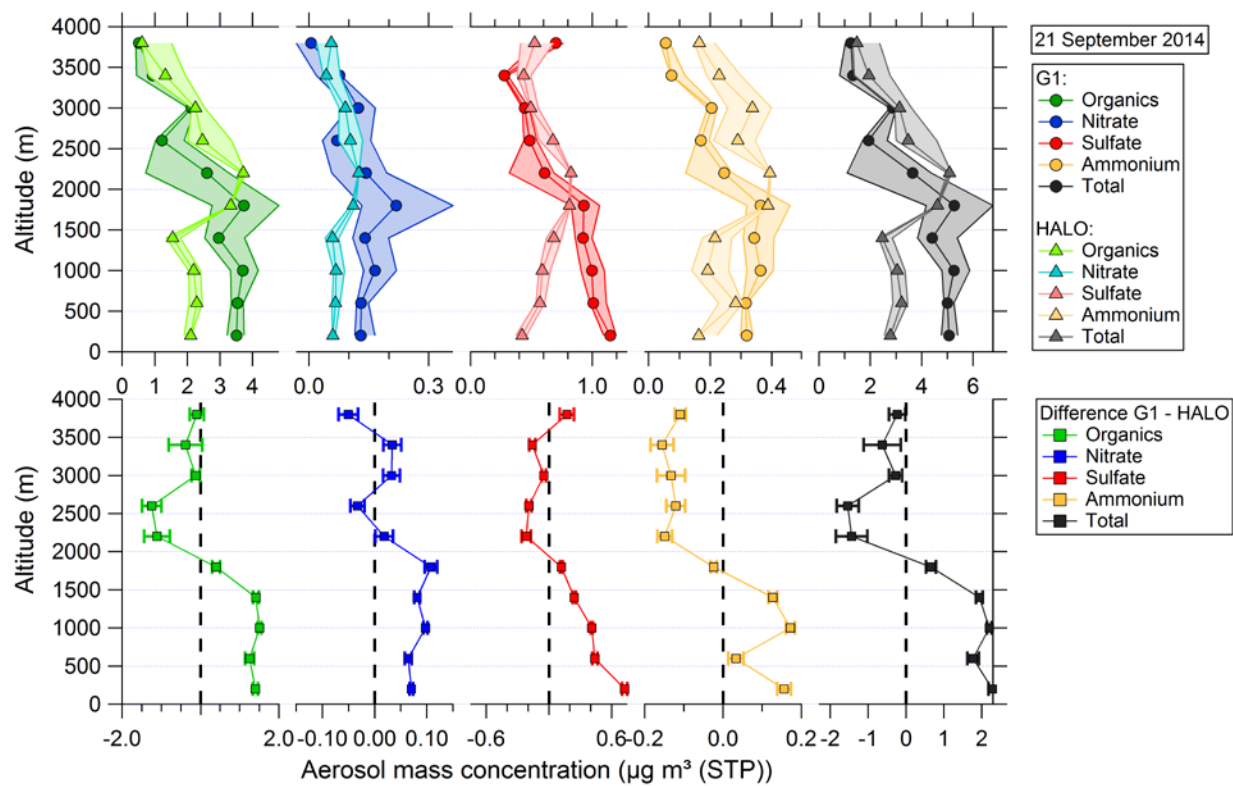


Figure 11. The vertical profile of aerosol mass concentration measured by the G1 and HALO AMS on September 21.

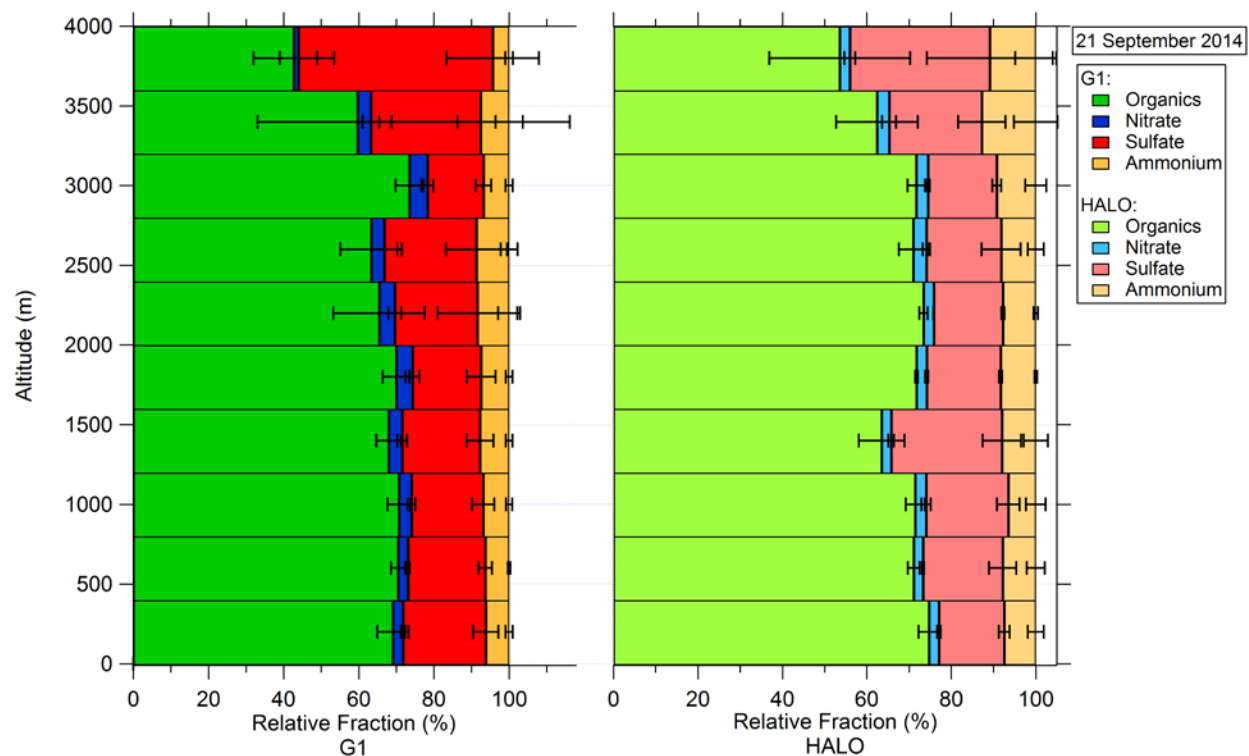
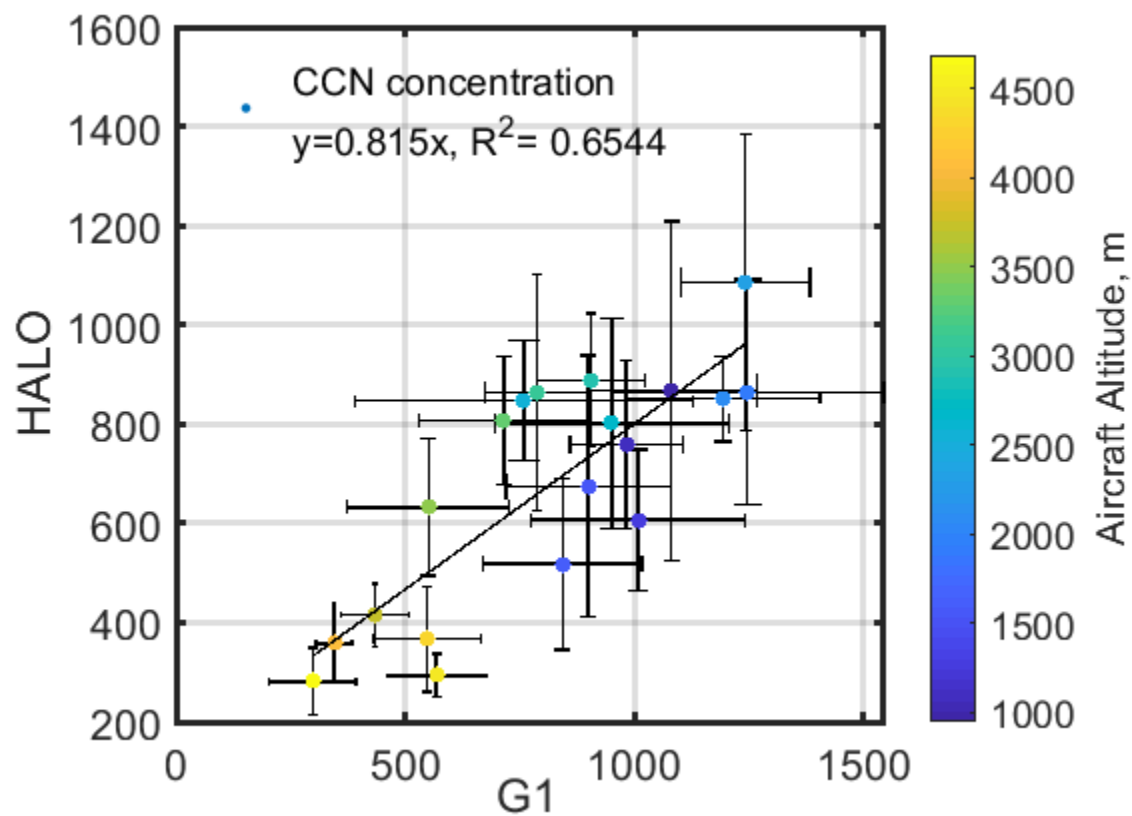


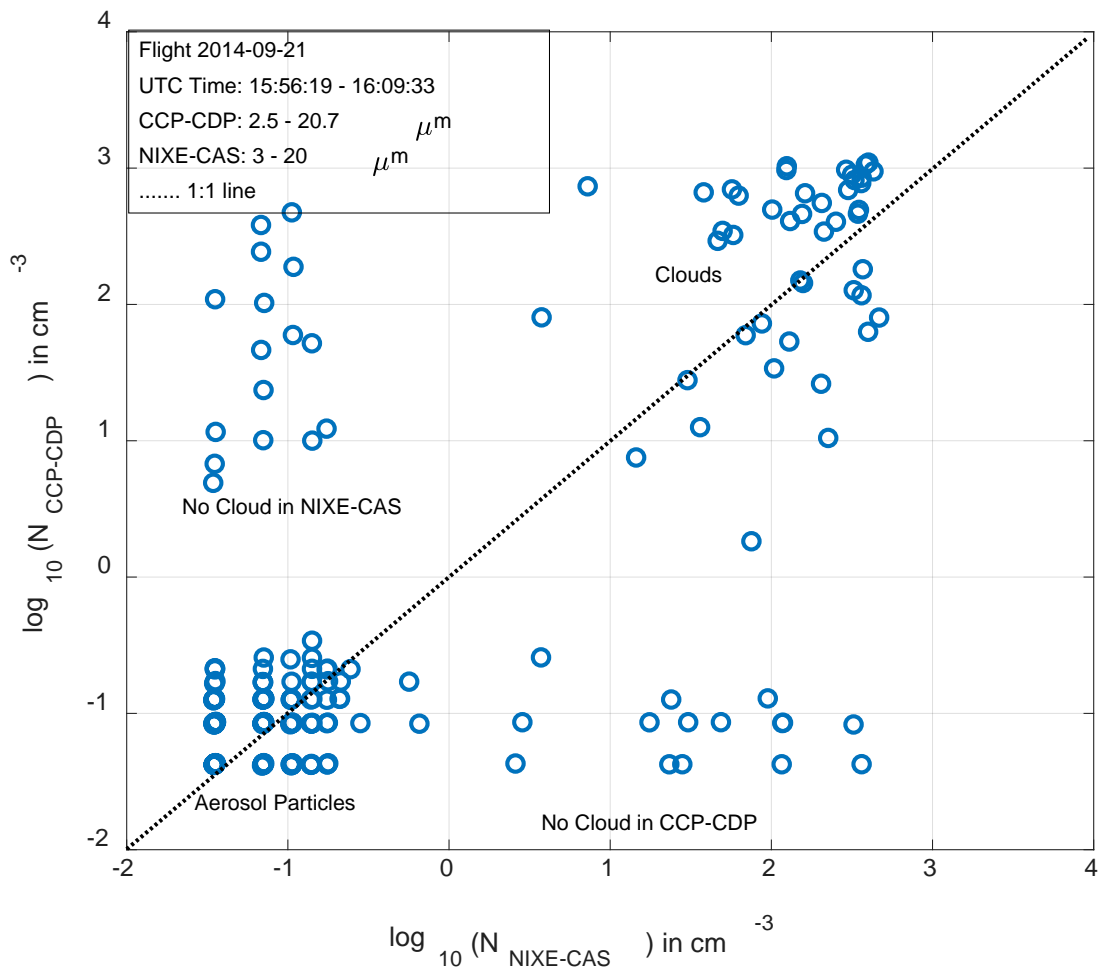
Figure 12. The vertical profile of relative mass fraction of major aerosol chemical species measured by the G1 and HALO AMS, respectively, on September 21



71

72 Figure 13. The G1 and HALO comparison of aerosol CCN concentration ( $S=0.5\%$ ) measured  
 73 on September 21.

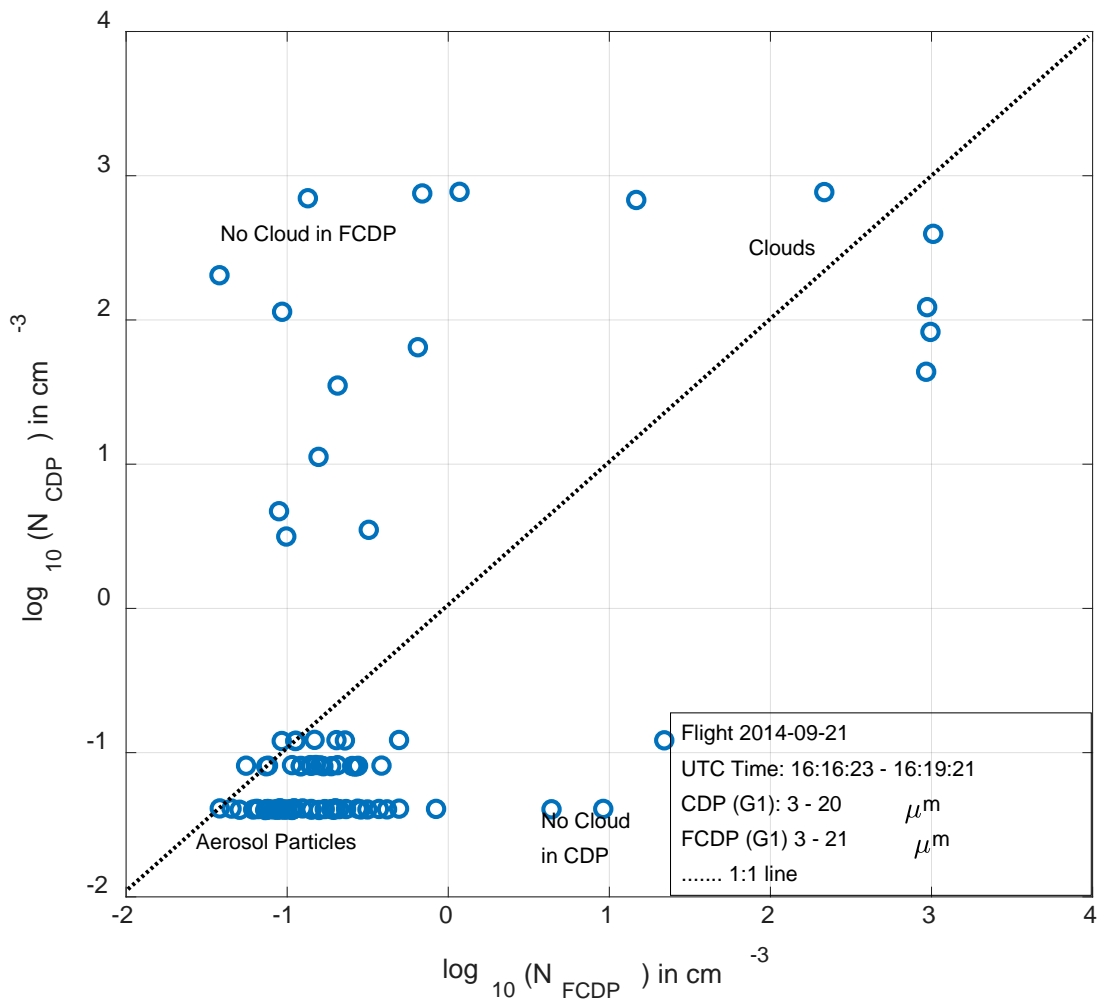




74

75

(a)



(b)

Figure 14 The comparison of cloud droplet concentrations in the same aircraft (a) between NIXE-CAS and CCP-CDP on board HALO; (b) between CDP and FCDP on board the G1.

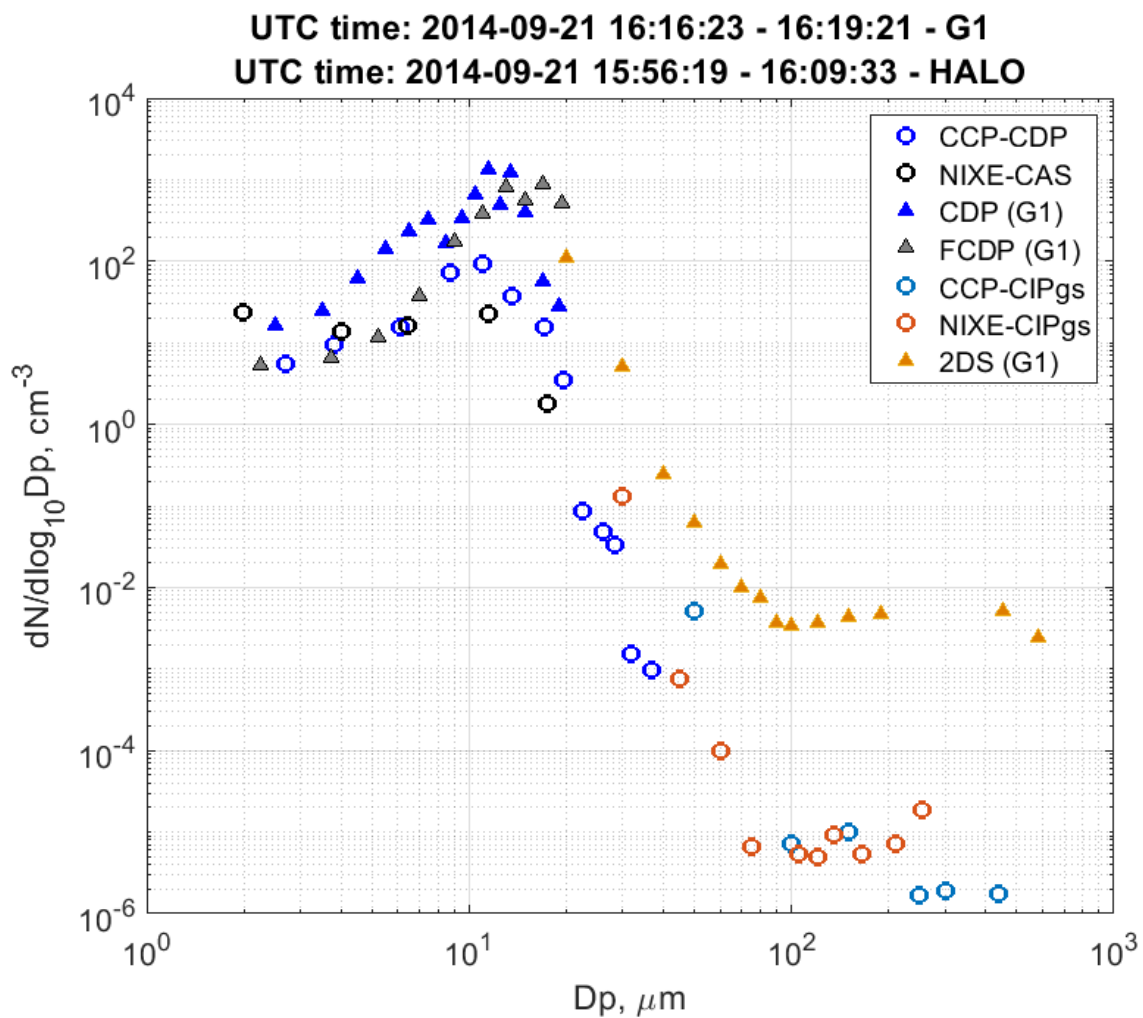


Figure 15. The cloud droplet size distribution from the cloud probes on the G1 and HALO.

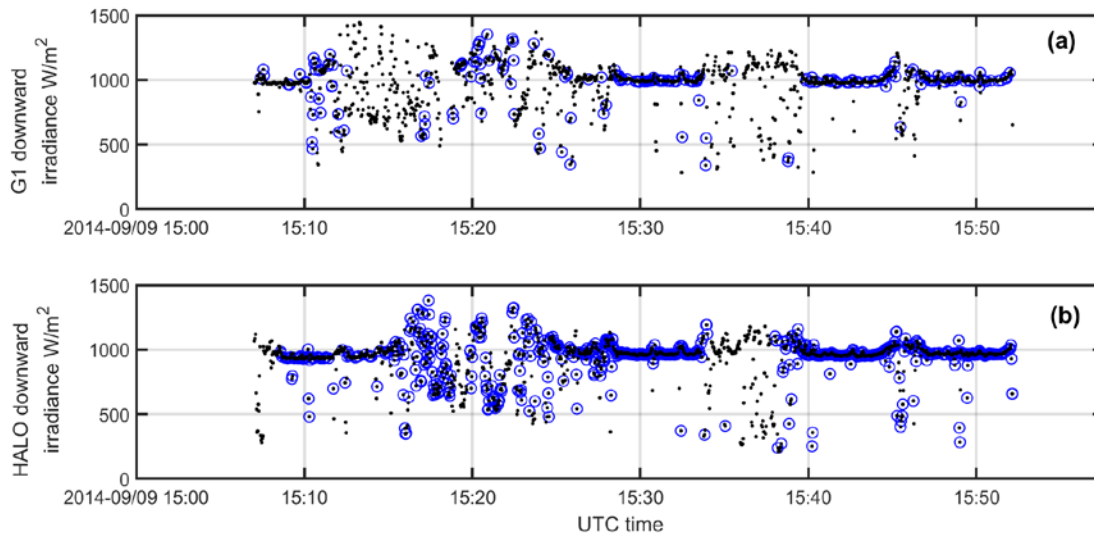


Figure 16. Time series of the G1 and HALO downward irradiance on September 9. The (a) by SPN-1 and (b) by SMART-Albedometer. Black dots represent all data under the general inter-comparison criteria. The blue circles represent the restricted navigation criteria.

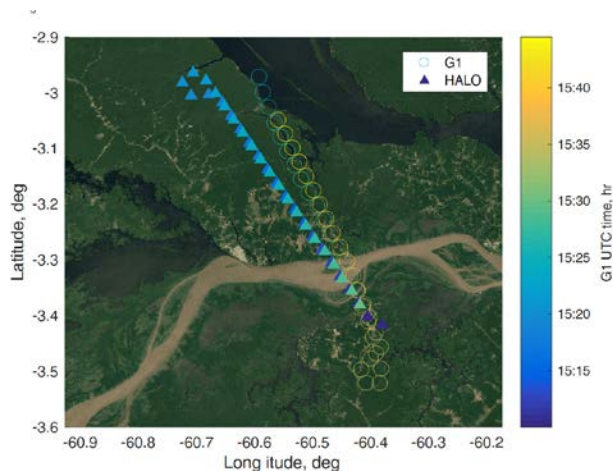
1 Supplemental material:

## 2 1. Pilot preparation for the comparison flight

3 Both aircraft cannot appear at the same location at the same time due to safety concerns.  
4 Thus, the approval of a formation (inter-comparison) flight was acquired six months before the  
5 campaign through DOE Pacific Northwest Site Office (PNSO) and the Office of Aviation  
6 Management (OAM). Essential risk mitigation was also discussed and approved by the Pacific  
7 Northwest National Laboratory Aviation Risk Management Committee (PNNL ARMC). During  
8 the IOP, both aircraft crew and scientists teams set up a meeting to discuss the potential flight plan.  
9 After the flight plan was formed, both pilots briefed the plan to the Brazilian Air Force (BAF) and  
10 Airport Traffic Control (ATC). The clear-sky flight would be under Visual Flight Rules (VFR),  
11 which means good weather and no cloud and pilots communicate with each other using an air-to-  
12 air frequency. For coordinated flights in cloudy condition, the G1 and the HALO were both on  
13 Instrument Flight Rules (IFR) flight plan.

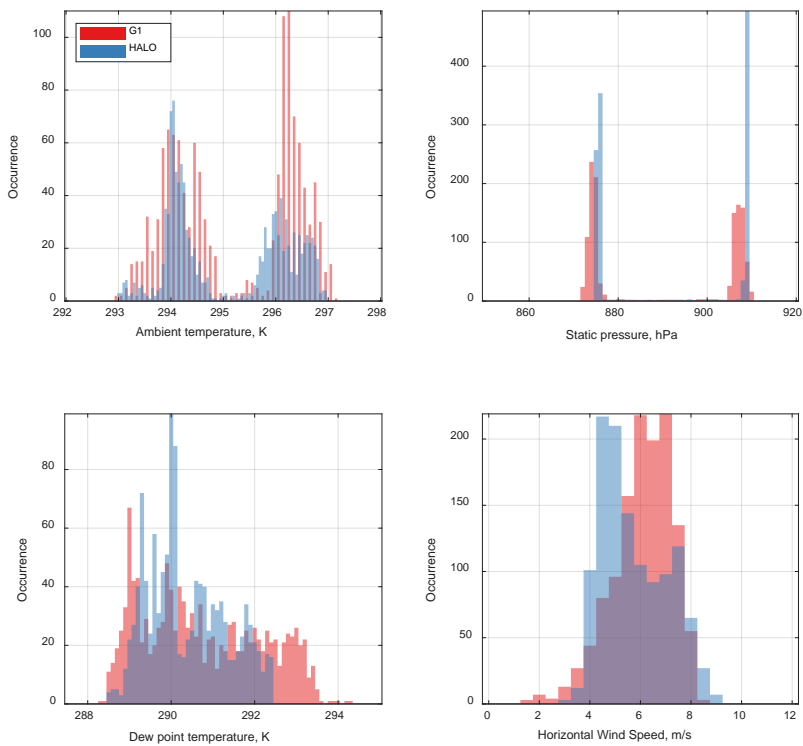
14 The coordinated flight on October 1, 2014, was initially designed to be a coordinated flight  
15 under a cloudy condition, which means the G1 and the HALO flew the same flight leg with at least  
16 300 m altitude offset and at least 5 minutes apart. However, the coordinated two flight legs (~900  
17 m and ~1200 m) are all below the cloud. Thus, the comparison focus on the correlation between  
18 two aircraft measurements, not vertical profiling.

19



20

21 Figure S1. Time colored flight track of the G1 (circle) and the HALO (triangle) on October 1,  
22 2014, during a cloudless coordinated flight (This figure was created using Mapping Toolbox™  
23 © COPYRIGHT 1997–2019 by The MathWorks, Inc).



24 Figure S2, Atmospheric parameters observed by the G1 and the HALO on October 1, 2014.  
25

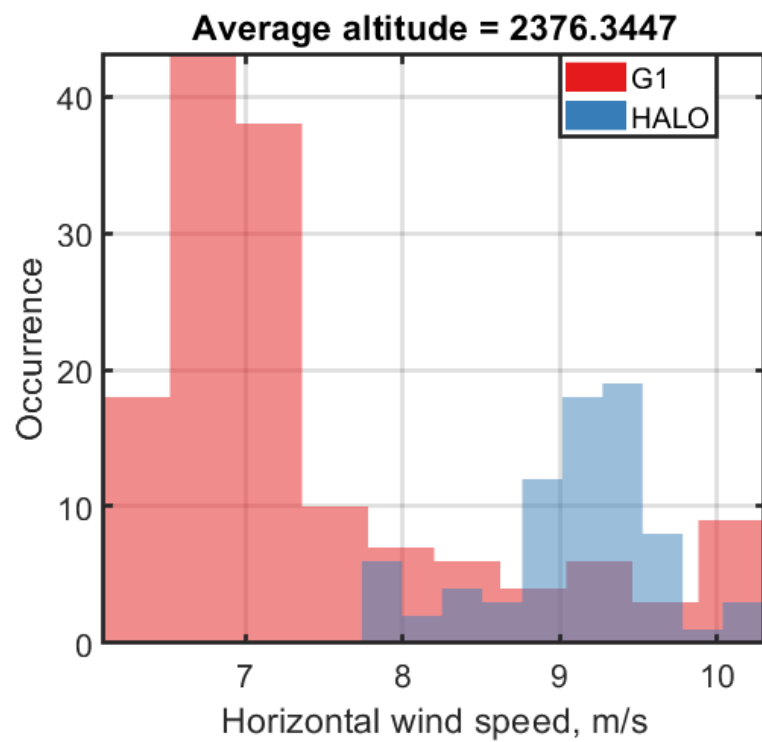
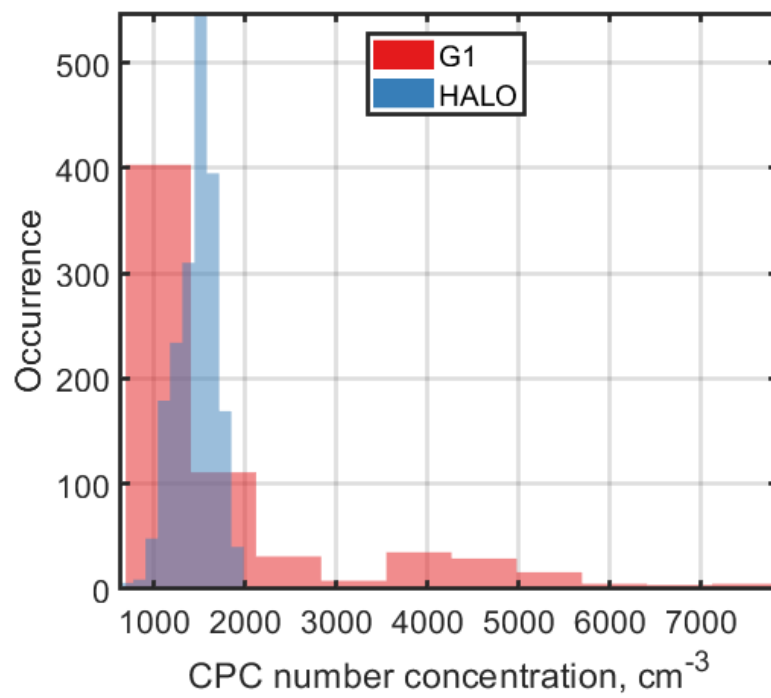


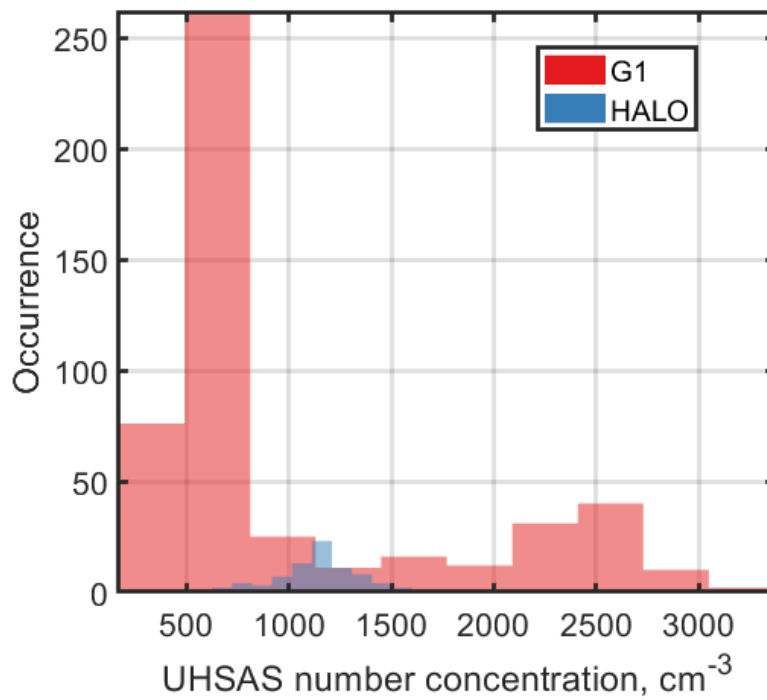
Figure S3. Horizontal wind speed between 2000-3000 m altitude on September 21, 2014.



(a)

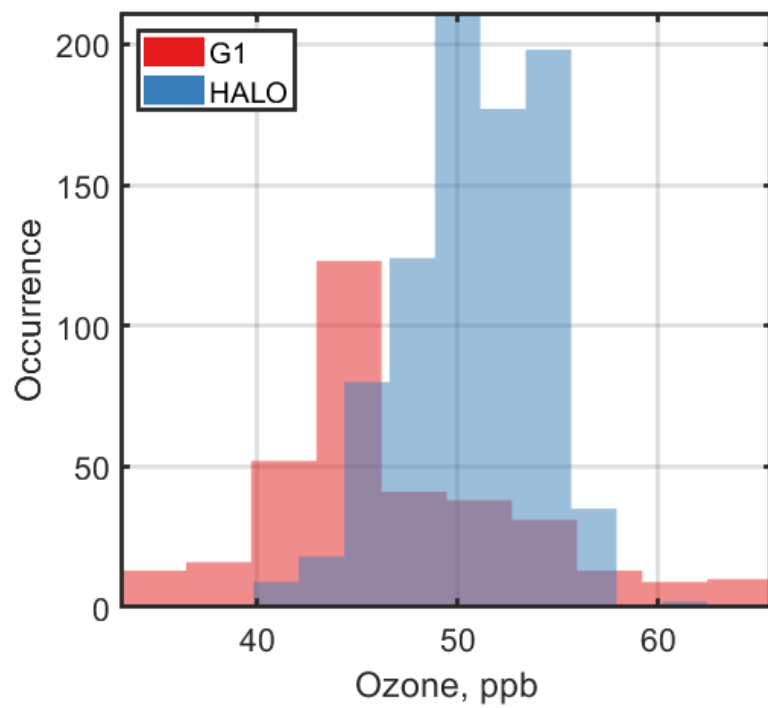
29  
30  
31



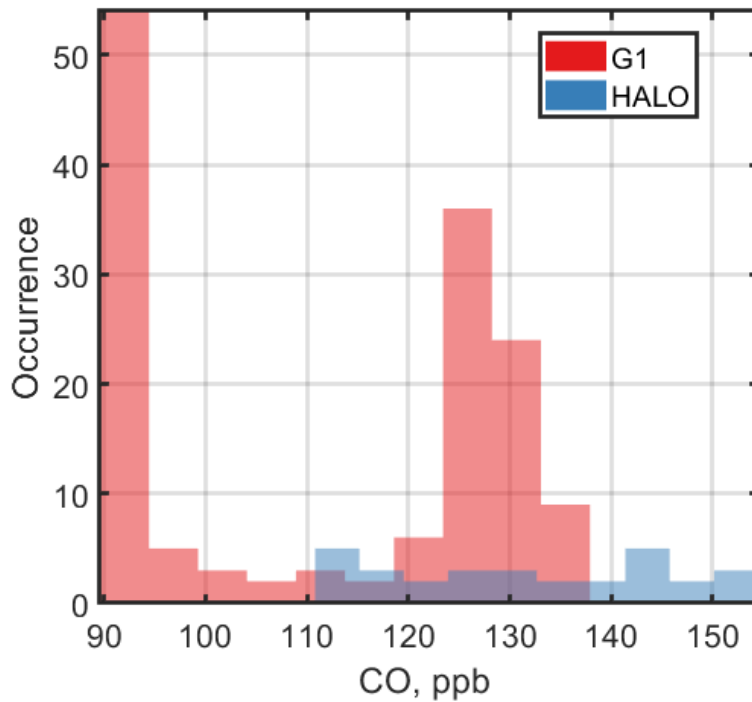


(b)

Figure S4. The total aerosol particles number concentration between 2000-3000 m altitude on September 21, 2014: (a) CPC measurement; (b) UHSAS measurement.



(a)



(b)

Figure S5. The trace gas concentration between 2000-3000 m altitude on September 21, 2014:  
(a) Ozone measurement; (b) CO measurement.

## 2. A significant contribution of small aerosol particles

Comprehensive characterization of aerosol particles, especially small ones (<50 nm) during GoAmazon2014/5 has demonstrated that high concentrations of those small particles in the lower free troposphere are transported from the free troposphere into the boundary layer by a strong convective downdraft and sustain the population of particles in the pristine Amazon boundary layer. This important observation improved the current understanding of the aerosol influence on cloud properties and climate under natural conditions (Fan et al., 2018; Wang et al., 2016). However, the aerosol particle size distribution measurement, especially for sizes less than

50 nm, is very rare due to the lack of high-frequency airborne measurements. The most common aerosol size spectrometer, UHSAS, covers aerosol particle sizes larger than 60 nm. The scanning mobility particle spectrometer cannot obtain size distribution in 1-Hz time resolution. The other approach is to estimate particle size distribution by extrapolating the UHSAS or Passive Cavity Aerosol Spectrometer Probe (size range 100–3000 nm) measured aerosol size distribution to smaller size ranges (down to 10 nm). The accuracy of the third approach is limited by the nature of the aerosol size distribution, and the aerosol particle concentration can be significantly underestimated if there is a dominant nucleation mode in the aerosol particle size distribution, such as during a new particle formation event.

As shown in Figure S11, we compared the integrated aerosol number concentrations between one wet season flight (on March 7), which was influenced by a long-range transport plume from Africa (Moran Zuloaga et al., 2018) and one typical dry season flight (September 21). The agreement of the small aerosol number concentration between the FIMS-measured size distribution and UHSAS/PCASP-estimated size distribution is reasonably good for the dry season flight when the accumulation mode dominated the aerosol particle size distribution. During the wet season, there was a strong vertical gradient in the particle size spectrum above central Amazonia under clean conditions. Thus, we can observe an increase of underestimation of the small size particle concentration both for the size ranges less than 50 nm and less than 100 nm, as the filled markers move away from each other with the increase of altitude. Because of the negligible mass contribution to the total aerosol loading, those ultrafine aerosol particles (< 50 nm) are conventionally considered too small to affect cloud formation. However, the new observational evidence and numerical simulation of deep convective clouds outlined a new mechanism, which suggests an energetic anthropogenic invigoration of deep convective clouds by those ultrafine aerosol particles in previously pristine regions of the world (Fan et al., 2018). Two newly published studies (Fan et al., 2018; Wang et al., 2016) emphasize the importance of the airborne observation and suggest the ultrafine aerosol particles (< 50 nm) measurement should be included as a baseline routine measurement in future airborne experiments.

For field studies without the deployment of FIMS, one option to assess the accuracy of UHSAS/PCASP-estimated size distribution is to compare the total number concentration based on the integration of the UHSAS/PCASP-estimated size distribution to the total number concentration

from CPC. For field study focusing on the high concentration and variability of sub-50 or sub-100 nm aerosol particles, such as new particle formation events, it is highly recommended to request the deployment of FIMS. Due to the limited availability of FIMS, one option is to use several well-characterized CPCs, which operate at the different cut off sizes, to measure the ambient aerosol simultaneously, and then use the data inversion technique to estimate the aerosol size distribution of sub-50 or sub-100 nm aerosol particles. One of examples of deploying such a fast time response measurements was discussed in detail by Williamson et al. (Williamson et al., 2018). Another reasonable substitute to the FIMS might be a Scanning Mobile Particle Sizer (SMPS), but it should be noted that on an airborne platform an SMPS does not nearly have the same time resolution as a FIMS. To better adapt the spatial change in aerosol concentration, a residence chamber similar to a system described in another study (Kotchenruther and Hobbs, 1998) should be deployed with SMPS.

Most of the details for the AMS measurements have been included in the separate AMS papers. (Schulz et al., 2018; Shilling et al., 2018) And we provide the summaries as below.

### 3.2. Additional information for AMS

Most of the details for the AMS measurements have been included in the separate AMS papers (Schulz et al., 2018; Shilling et al., 2018). Brief summaries are provided below.

The G-1 AMS was operated with a constant pressure inlet (CPI), which was set to a constant pressure during the campaign. The G1 AMS was calibrated approximately once a week during the deployment, typically on down days. One additional calibration was performed after the flight days and was all the calibrations were in agreement with the other calibrations each other. In total, 5 Based on five calibrations, the averaged parameters such as the airbeam signal (AB), the ionization efficiency (IE) and the relative ionization efficiency (RIE) were averaged and the average AB, IE, and RIE were applied to all of the data. The flow rate is directly controlled by the Pressure Controlled inlet and it was set constant (60 kpa) through the experiment. We make a  $\Delta$  real-time correction was made to account for the variations in the AB changes for changes in to improve the instrument sensitivity. Typically, this correction is small (<20%) in absolute magnitude. The correction typically is largest at the beginning of the flight and gradually stabilizes about 1 hour into the flight. Essentially, the AB correction stabilizes as the instrument warms up

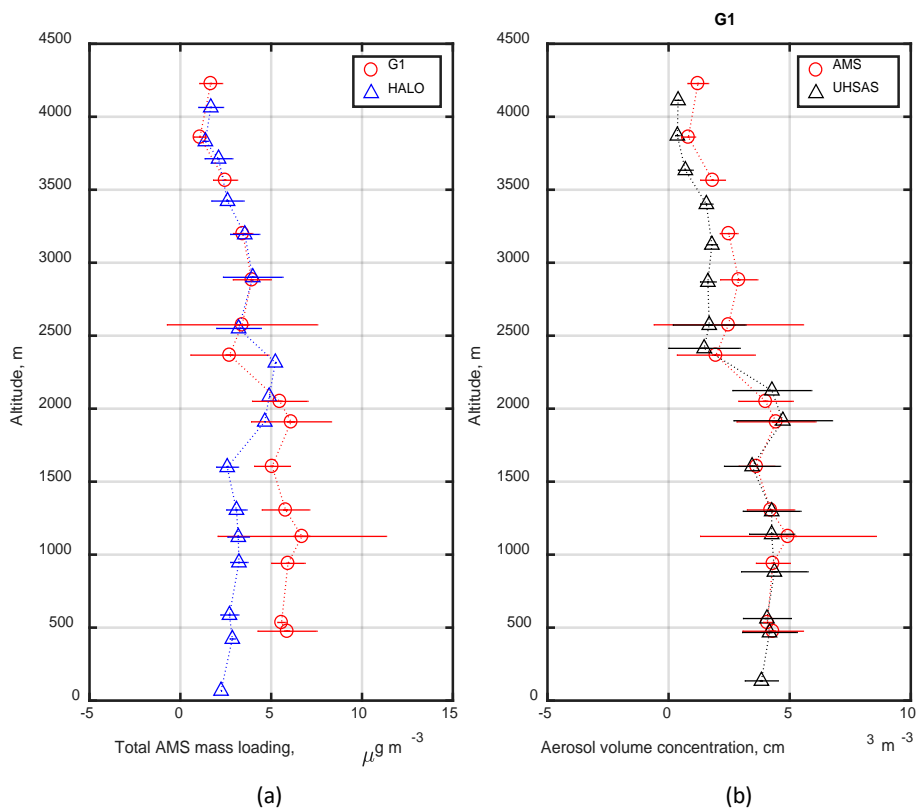
and the 3-hour warmup time we have is long enough for sufficient stability to be achieved, but not for the instrument to completely stabilize. (This is the reason behind my reluctance to have less warmup time, even though it means we all have to get up earlier on flight days). The particle collection efficiency (CE) was determined by comparing AMS data to UHSAS and FIMS data. We also confirmed the CE=0.5 by comparing mass loadings observed at the T3 site to the G1 data.

The HALO-AMS was calibrated before, during (twice) and after the campaign for (relative) ionization efficiencies of nitrate, ammonium and sulfate (Schulz et al., 2018). For organics, the default relative ionization efficiency of 1.4 was assumed. The inlet flow ~~was~~ kept constant by the CPI and was measured before and during the campaign. A collection efficiency of 0.5 was applied, as recommended by Middlebrook et al. (2012) for low nitrate conditions. Further details on the operation of the C-ToF-AMS are given in Schulz et al. (2018).

Figure S6(a) shows vertical profiles of the total mass concentrations measured by the two AMS instruments on September 21. Above 2500 m altitude, the agreement between the two instruments is excellent (mean difference less than 5%). Between 2000 and 2500 m, the agreement is within the uncertainty range. Below 2000 m altitude, however, the aerosol particle mass concentrations measured by the AMS operated on HALO are lower than the concentrations measured by the AMS on the G1. To compare AMS data to UHSAS data, the aerosol mass concentrations of the G1 AMS were converted to the aerosol volume concentration assuming an organic compound density of  $1.5 \text{ g cm}^{-3}$  (Pöschl et al., 2010). The converted aerosol volume concentration agreed well with the volume concentration calculated based on UHSAS data, especially below 2500 m, as shown in Figure S6(b). The agreement at lower altitudes suggests that the lower concentration measured by the HALO AMS is due to the transmission efficiency issue in the constant pressure inlet used by the HALO AMS. This inlet was a prototype, designed and built at MPIC Mainz, and works by changing the size of the critical orifice that regulates the flow into the aerodynamic lens. The design and transmission characteristics will be described in an upcoming publication (Molleker, S., in prep.). The AMS aboard the G-1 used a constant pressure inlet based on the design in Bahreini et al., 2008. Thus, we conclude that data above 2500 m altitude measured by the AMS aboard HALO in 2014 are valid, while data below 2500 m need to be corrected using correction factors derived from laboratory characterization before further study.

139 After 2014, the HALO AMS inlet design was improved to address the inlet transmission issues  
140 specific to this field campaign.

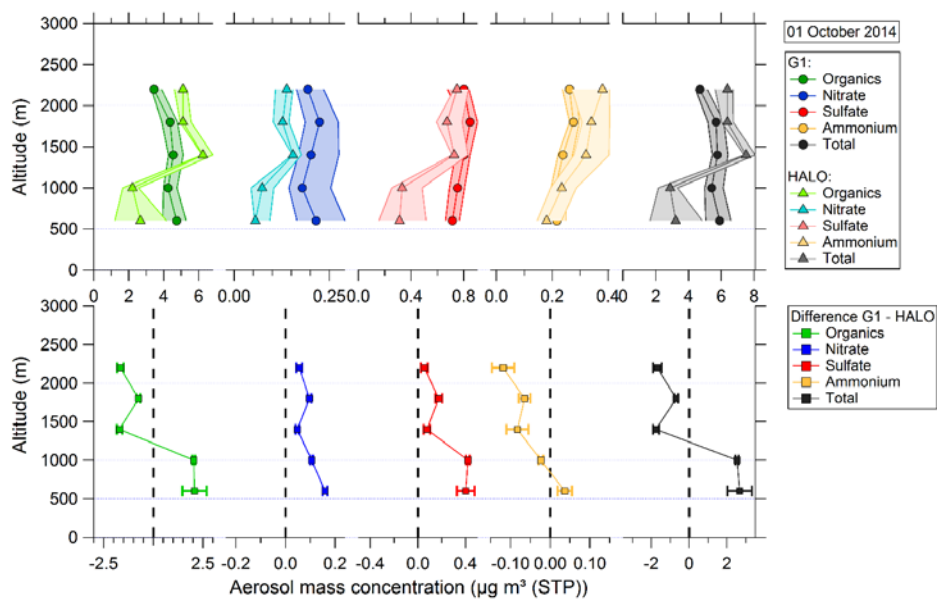
141 The second comparison between the two AMS conducted on October 01 is shown in  
142 Figures S6 and S7. The findings are basically in agreement with those of September 21, although  
143 the underestimation of aerosol mass concentration due to the inlet in the HALO AMS appears here  
144 to be restricted to altitudes lower than 1500 m.



145  
146 Figure S6. (a) Comparison of aerosol mass loading measured by the G1 and HALO AMS on  
147 September 21; (b) aerosol volume concentration comparison from AMS and the integrated  
148 UHSAS on the G1.  
149

Formatted: Justified, Indent: First line: 0.5", Line spacing: 1.5 lines

150



151

152 Figure S7. The vertical profiling of the aerosol mass concentration observed by the G1 and

153 HALO during October 1.

154

155



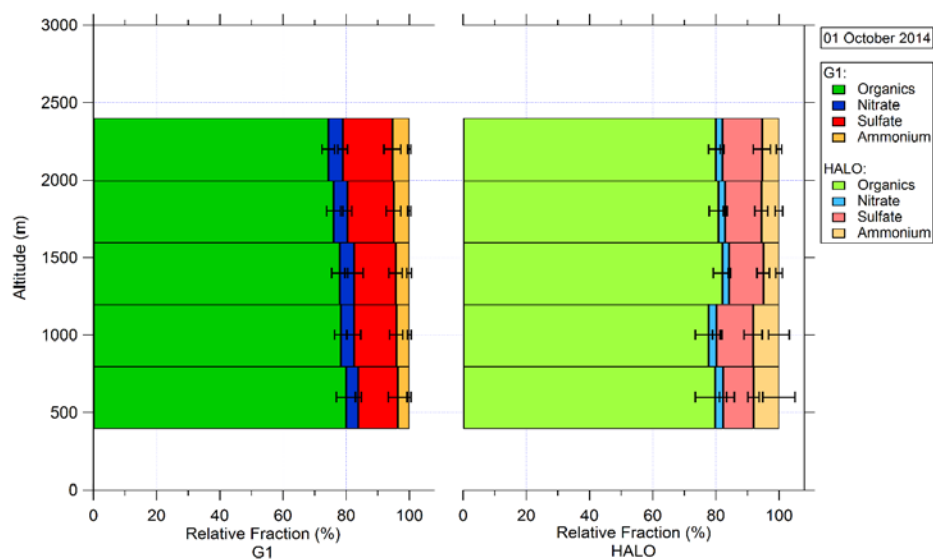
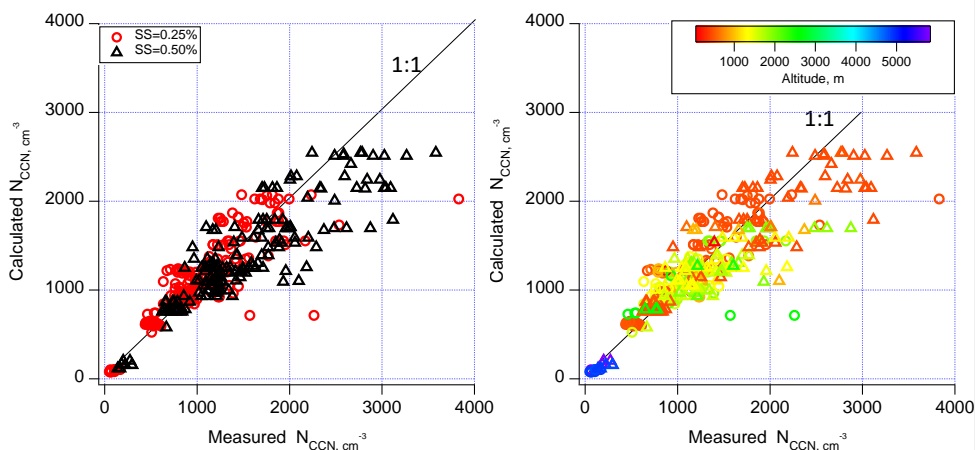


Figure S8. The vertical profiling of the relative fractions for the chemical species observed by the G1 and HALO during October 1.

### 3. CCN closure

To further examine the relative importance of mixing state and chemical composition, the CCN concentrations were calculated from aerosol particle size distribution, and chemical composition measured onboard the G1. The calculation was based on  $\kappa$ -Köhler parameterization (Köhler, 1936; Petters and Kreidenweis, 2007, 2008, 2013) and the detail of the approach was described by Mei et al. (2013b). For the flight on September 9, 2017, the CCN number concentration calculated from the G1 UHSAS size distribution and chemical composition exhibits underestimation at a supersaturation of 0.5% (Fig. S9(a)) and when the altitude is below 1000 m (Fig. S9(b)). This underestimation suggests that the UHSAS size range (90-500 nm) did not fully cover the aerosols with the critical activation diameter ( $D_{p,50}$ ) at high supersaturation. Thus, the FIMS measurements onboard the G1 was the more appropriate size distribution for both the CCN closure study. The CCN concentration calculated using the size distribution from FIMS agrees

well with the measurement (Fig. S10). The scattering of the comparison data in Figure 15 is likely due to the chemical composition and mixing state effect on aerosol hygroscopicity.



(a) (b)

Figure S9. Comparison of calculated CCN with measured CCN using the averaged 1 min measurements from the G1: (a) colored by different supersaturations. (b) colored by different altitude. (Note that both plots used the calculated CCN number concentration from UHSAS size distribution.)

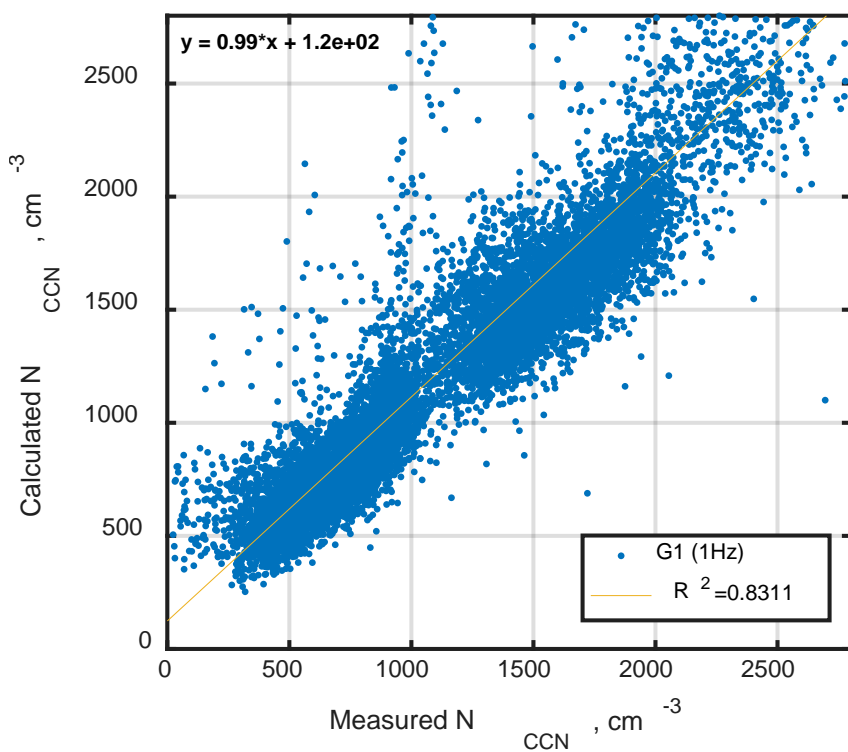
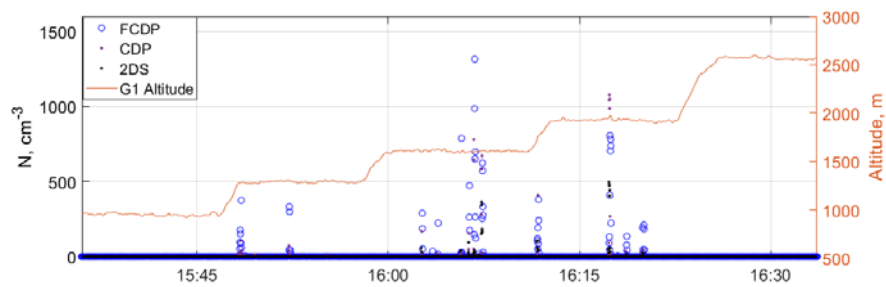
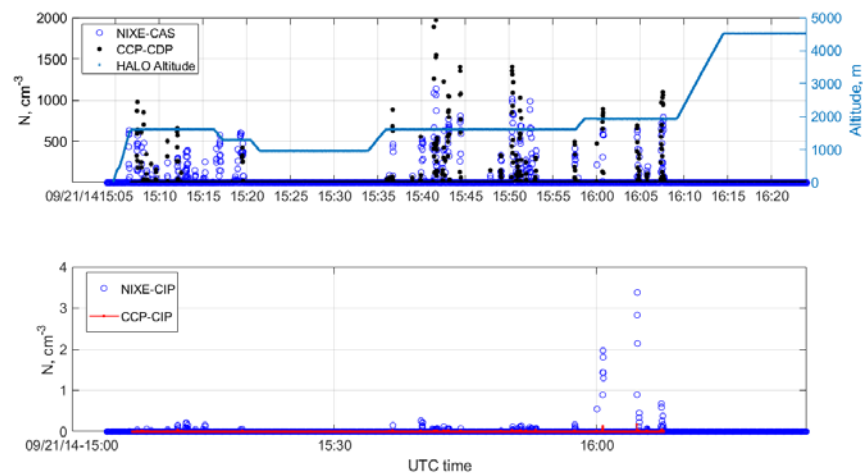


Figure S10. The scatter plot of the calculated CCN number concentration using FIMS size distribution compared with the measured CCN number concentration



187 Figure S118. The cloud droplet number concentration from the G1 aircraft on September 21.

188



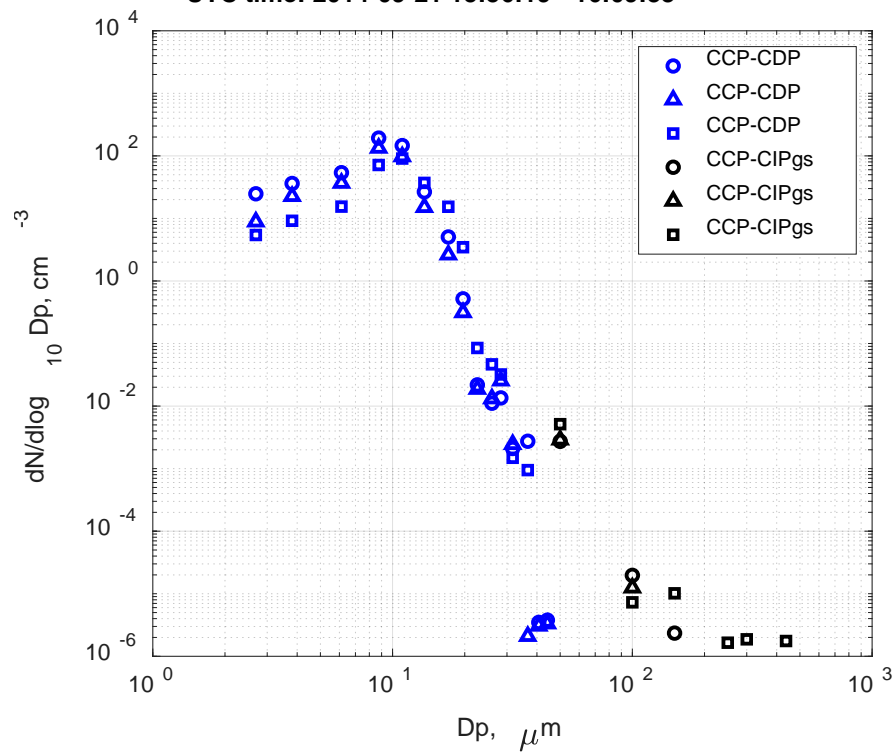
189

190 Figure S129. The cloud droplet number concentration from HALO on September 21.

UTC time: 2014-09-21 15:35:41 - 15:45:19

UTC time: 2014-09-21 15:46:35 - 15:54:46

UTC time: 2014-09-21 15:56:19 - 16:09:33

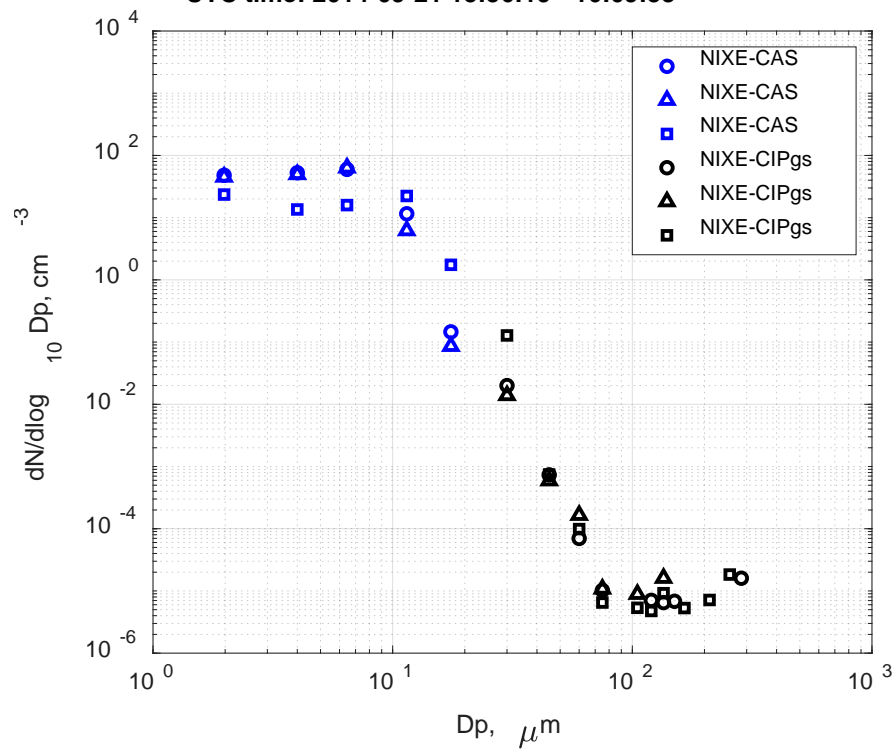


(a)

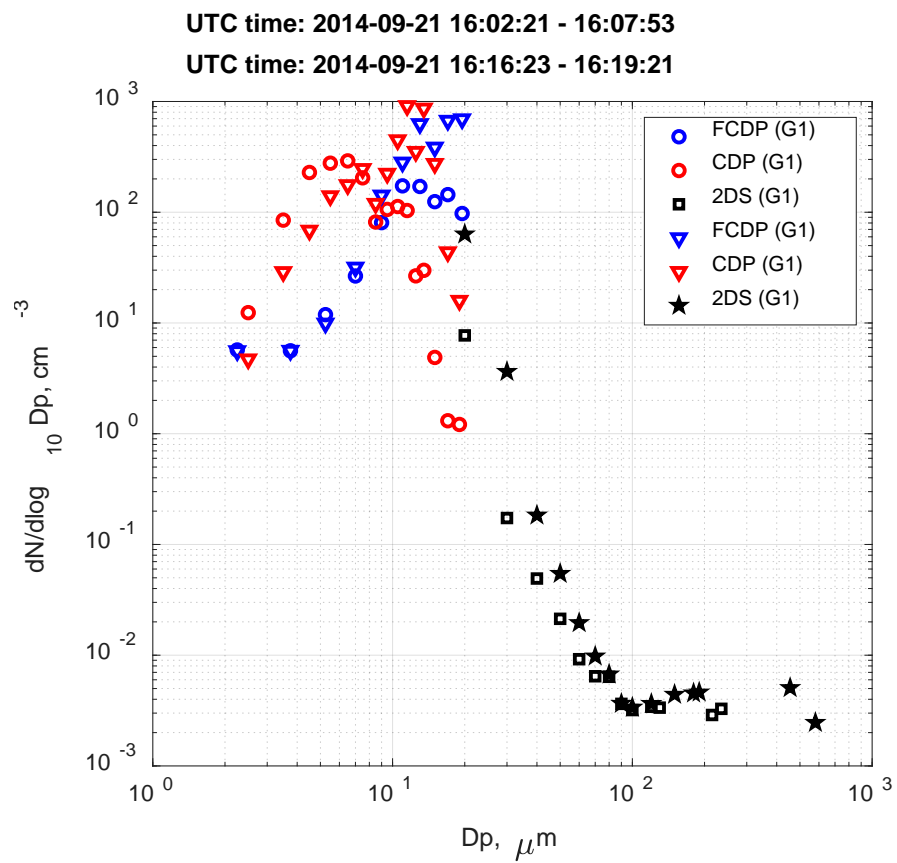
UTC time: 2014-09-21 15:35:41 - 15:45:19

UTC time: 2014-09-21 15:46:35 - 15:54:46

UTC time: 2014-09-21 15:56:19 - 16:09:33



(b)



(c)

Figure S130. The averaged cloud droplet size distributions from HALO on September 21, (a) CCP probes; (b) NIXE-CAPS probes; (c) Cloud probes on board the G1.

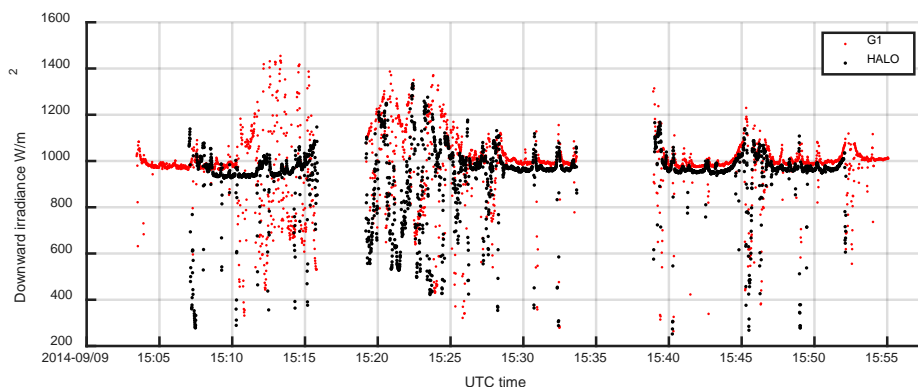


Figure S143. Time series comparison of the G1 (SPN-1) and HALO (SMART-Albedometer) radiation measurements on September 9.

Table S1. Calibration and maintenance for the instruments deployed on G1

Measurement Variables	Instruments deployed on the G1 (Martin et al., 2016; Schmid et al., 2014)	Calibration/Maintenance
Static Pressure	Rosemount (1201F1), 0-1400 hPa	Calibrated before/after each field campaign
Static air temperature	Rosemount E102AL/510BF -50 to +50 °C	Calibrated before/after each field campaign
Dewpoint temperature	Chilled mirror hygrometer 1011B -40 to +50 °C	Calibrated before/after each field campaign
3-D wind	Aircraft Integrated Meteorological Measurement System 20 (AIMMS-20)	Calibrated with Special flight pattern before each field campaign. Inter-comparison with other GPS/INS during deployment.
Particle number concentration	CPC, cut off size ( $D_p$ ) = 10 nm	Calibrated before/after each field campaign. Weekly calibration of sample and sheath flow rates and inter-comparisons with similar counters during deployment.
Size distribution*	UHSAS-A, 60-1000 nm.	Calibrated before/after each field campaign. Weekly check of sizing with PSL
FIMS	10 nm – 500 nm	Calibrated before/after each field campaign. Weekly calibration of sample and sheath flow rates and checks with one size PSL
Non-Refractory particle chemical composition	HR-ToF-AMS: Organics, Sulfate, Nitrate, Ammonium, Chloride, 60-1000 nm	Weekly calibrations.



208

209 Table S2. Calibration and maintenance for the instruments deployed on HALO

CCN concentration	CCN-200, SS= 0.25, 0.5%	Calibrated before/after each field campaign. Biweekly calibration with ammonium sulfate particles.
Gas phase concentration	N2O/CO and Ozone Analyzer, CO, O <sub>3</sub> concentration, precision 2 ppb	Calibrated before/after each field campaign with calibration gas mixture.
CDP	2-50 $\mu\text{m}$ , $\Delta D_p=1-2 \mu\text{m}$	Calibrated before/after each field campaign by the vendor. Weekly check of sizing with glass beads of several sizes
FCDP	2-50 $\mu\text{m}$ , $\Delta D_p=1-2 \mu\text{m}$	Calibrated before/after each field campaign by the vendor. Weekly check of sizing with glass beads of several sizes
2DS	10-1000 $\mu\text{m}$	Calibrated before/after each field campaign by the vendor.
Radiation	SPN1 downward irradiance, 400-2700 nm	Calibrated before/after each field campaign

Measurement Variables	Instruments deployed on HALO (Wendisch et al., 2016)	Calibration/Maintenance
Static Pressure	Instrumented nose boom tray (DLR development), 0-1400 hPa	Calibrated before/after each field campaign
Static air temperature	Total Air Temperature (TAT) inlet (Goodrich/Rosemount type 102) with an open wire resistance temperature sensor (PT100), -70 to +50 °C	Calibrated before/after each field campaign
Dewpoint temperature	Derived from the water-vapor mixing ratio, which is measured by a tunable diode laser (TDL) system (DLR development), 5-40000 ppmv	Calibrated before/after each field campaign
3-D wind	Instrumented nose boom tray (DLR development) with an air data probe (Goodrich/Rosemount) 858AJ and high-precision Inertial Reference System (IGI IMU-IIe)	Calibrated before/after each field campaign
Particle number concentration	CPC, cut off size ( $D_p$ ) =10 nm	Calibrated before/after each field campaign. Weekly inter-comparisons with similar counters during deployment.
Size distribution*	UHSAS-A, 60-1000 nm.	Calibrated before/after each field campaign. Weekly check of sizing with PSL
Non-Refractory particle chemical composition	C-ToF-AMS: Organics, Sulfate, Nitrate, Ammonium, Chloride, 60-1000 nm	<del>Weekly calibrations.</del> Calibrated before and after the campaign and twice during the campaign
CCN concentration	CCN-200, SS= 0.13-0.53%	Calibrated before/after each field campaign. Weekly calibration with ammonium sulfate particles.

Formatted Table

Gas phase concentration	N2O/CO and Ozone Analyzer, CO, O <sub>3</sub> concentration, precision 2 ppb	Calibrated before/after each field campaign with calibration gas mixture.
Cloud properties*	CCP-CDP, 2.5-46 $\mu\text{m}$ , $\Delta D_p=1\text{-}2\ \mu\text{m}$	Calibrated before/after each field campaign. Weekly check of sizing with glass beads of several sizes
	NIXE-CAS: 0.61 -52.5 $\mu\text{m}$	Calibrated before/after each field campaign. Weekly check of sizing with glass beads of several sizes
	NIXE-CIPgs, 15-960 $\mu\text{m}$	Calibrated before/after each field campaign. Weekly check of sizing flight with a spinning disk.
	CCP-CIPgs: 15-960 $\mu\text{m}$	Calibrated before/after each field campaign. Weekly check of sizing flight with a spinning disk.
Radiation	SMART Albedometer, downward spectral irradiance, 300-2200 nm	Weekly calibrations.

Table S3. List of compared measurements ranges and measurement variances caused by the spatial variation during the field campaign.

Measurement Variables	Measured Range during the Field Campaign	Measurement Variances between the Two Aircraft
Static Pressure	500 – 1010 hPa	< 1 %
Static air temperature	272 – 310 K	< 1%
Dewpoint temperature	230 -300 K	Without clouds, <1% With clouds, the measurement from the G1 can be up to 5% lower than that of HALO
3-D wind	1-15 m/s	< 40%
Particle number concentration	500 – 15,000 $\text{cm}^{-3}$	< 20% for CPC, <50% for UHSAS (size dependent)
Non-Refractory particle chemical composition	< 10 $\mu\text{g}\cdot\text{m}^{-3}$	< 10% above 2500 m Up to 50% below 2500 m
CCN concentration	SS=0.25%, 100 – 2000 $\text{cm}^{-3}$	< 10% above 2500 m Up to 50% below 2500 m
Gas phase concentration	Ozone: 15-75 ppb CO: 50-200 ppb	Ozone: < 25% CO: < 15%
Cloud droplet number concentration	3- 20 $\mu\text{m}$	<50 %
Downward irradiance	200 -1500 $\text{W}\cdot\text{m}^{-2}$	< 10%

## 216 Reference

- 217 Fan, J., Rosenfeld, D., Zhang, Y., Giangrande, S. E., Li, Z., Machado, L. A., Martin, S. T., Yang, Y., Wang, J.,  
218 and Artaxo, P.: Substantial convection and precipitation enhancements by ultrafine aerosol particles,  
219 Science, 359, 411-418, 2018.
- 220 Kohler, H.: The nucleus in and the growth of hygroscopic droplets, Transactions of the Faraday Society,  
221 32, 1152-1161, 1936.
- 222 Kotchenruther, R. A. and Hobbs, P. V.: Humidification factors of aerosols from biomass burning in Brazil, J  
223 Geophys Res-Atmos, 103, 32081-32089, 1998.
- 224 Moran-Zuloaga, D., Ditas, F., Walters, D., Saturno, J., Brito, J., Carbone, S., Chi, X. G., de Angelis, I. H., Baars,  
225 H., Godoi, R. H. M., Heese, B., Holanda, B. A., Lavric, J. V., Martin, S. T., Ming, J., Pohlker, M. L.,  
226 Ruckteschler, N., Su, H., Wang, Y. Q., Wang, Q. Q., Wang, Z. B., Weber, B., Wolff, S., Artaxo, P., Poschl, U.,  
227 Andreae, M. O., and Pohlker, C.: Long-term study on coarse mode aerosols in the Amazon rain forest with  
228 the frequent intrusion of Saharan dust plumes, Atmos Chem Phys, 18, 10055-10088, 2018.
- 229 Petters, M. D. and Kreidenweis, S. M.: A single parameter representation of hygroscopic growth and cloud  
230 condensation nucleus activity, Atmos Chem Phys, 7, 1961-1971, 2007.
- 231 Petters, M. D. and Kreidenweis, S. M.: A single parameter representation of hygroscopic growth and cloud  
232 condensation nucleus activity - Part 2: Including solubility, Atmos Chem Phys, 8, 6273-6279, 2008.
- 233 Petters, M. D. and Kreidenweis, S. M.: A single parameter representation of hygroscopic growth and cloud  
234 condensation nucleus activity - Part 3: Including surfactant partitioning, Atmos Chem Phys, 13, 1081-1091,  
235 2013.
- 236 Pöschl, U., Martin, S., Sinha, B., Chen, Q., Gunthe, S., Huffman, J., Borrmann, S., Farmer, D., Garland, R.,  
237 and Helas, G.: Rainforest aerosols as biogenic nuclei of clouds and precipitation in the Amazon, Science,  
238 329, 1513-1516, 2010.
- 239 Schulz, C., Schneider, J., Amorim Holanda, B., Appel, O., Costa, A., de Sá, S. S., Dreiling, V., Fütterer, D.,  
240 Jurkat-Witschas, T., Klimach, T., Krämer, M., Martin, S. T., Mertes, S., Pöhlker, M. L., Sauer, D., Voigt, C.,  
241 Weinzierl, B., Ziereis, H., Zöger, M., Andreae, M. O., Artaxo, P., Machado, L. A. T., Pöschl, U., Wendisch,  
242 M., and Borrmann, S.: Aircraft-based observations of isoprene epoxydiol-derived secondary organic  
243 aerosol (IEPOX-SOA) in the tropical upper troposphere over the Amazon region, Atmos. Chem. Phys.  
244 Discuss., 2018, 1-32, 2018.
- 245 Shilling, J. E., Pekour, M. S., Fortner, E. C., Artaxo, P., Sá, S. d., Hubbe, J. M., Longo, K. M., Machado, L. A.,  
246 Martin, S. T., and Springston, S. R.: Aircraft observations of the chemical composition and aging of aerosol  
247 in the Manaus urban plume during GoAmazon 2014/5, Atmos Chem Phys, 18, 10773-10797, 2018.
- 248 Wang, J., Krejci, R., Giangrande, S., Kuang, C., Barbosa, H. M., Brito, J., Carbone, S., Chi, X., Comstock, J.,  
249 Ditas, F., Lavric, J., Manninen, H. E., Mei, F., Moran-Zuloaga, D., Pohlker, C., Pohlker, M. L., Saturno, J.,  
250 Schmid, B., Souza, R. A., Springston, S. R., Tomlinson, J. M., Toto, T., Walter, D., Wimmer, D., Smith, J. N.,  
251 Kulmala, M., Machado, L. A., Artaxo, P., Andreae, M. O., Petaja, T., and Martin, S. T.: Amazon boundary  
252 layer aerosol concentration sustained by vertical transport during rainfall, Nature, 539, 416-419, 2016.
- 253 Williamson, C., Kupc, A., Wilson, J., Gesler, D. W., Reeves, J. M., Erdesz, F., McLaughlin, R., and Brock, C.  
254 A.: Fast time response measurements of particle size distributions in the 3-60 nm size range with the  
255 nucleation mode aerosol size spectrometer, Atmos Meas Tech, 11, 3491-3509, 2018.